THE UNIVERSITY
of EDINBURGH

Theory and Lattice Boltzmann simulation of Active Fluids

Giulio De Magistris

Doctor of Philosophy
The University of Edinburgh
August 2019

Abstract

Active fluids are far from equilibrium systems, nominally highly dense suspensions of elongated elements that confer to the liquid orientational order, similar in nature to the one found in liquid crystals, and an internal stirring that they exert through the consumption of some fuel reservoir – typically AdenosineTriPhosphate(ATP).

The interplay between the orientational order and the active behaviour gives rise to non-trivial dynamics, order-disorder out-of-equilibrium transitions, and dynamical transitions to non-equilibrium steady states.

In this work we will discuss active fluids in the framework of the hydrodynamic theory of active nematics and active polar fluids, where the structural order is characterised by an elastic formalism drawn from the theory for liquid crystals, and the activity is obtained from the coarse graining of the microscopics. Our aim was to analyse and characterize large scale behaviours in multi-phase systems.

We studied the dynamics of water phases embedded in active polar fluids, or rather 'inverse droplets', and considered how these move by effect of the surrounding active medium. We found two types of motile transitions, depending on the specifics of the boundary conditions of the orientation profile at the interface between the passive and the active phase.

We also considered quenches of disordered mixtures of active nematic and passive isotropic fluids. In these systems we observed cases of arrested phase separation, with the coarsening saturating at finite length scales depending on the strength of the activity. We characterized this behaviour in terms of an active capillary number, resulting from the relative strength of active interface effects and surface tension.

Declaration

I declare that this thesis was composed by myself, that the work contained herein is my own except where explicitly stated otherwise in the text, and that this work has not been submitted for any other degree or professional qualification except as specified. Parts of this work have been published in [1] and [2].

(*Giulio De Magistris, August 2019*)

Acknowledgements

This work was financially supported by studentship funding from EPSRC under grant no. EP/G03673X/1.

First and foremost, I would like to thank Prof. Davide Marenduzzo, my supervisor, for his infinite patience, invaluable guidance, and constant dedication to his job.

I would also like to thank Prof. Mike Cates, Dr. Adriano Tiribocchi, Dr. Oliver Henrich, Dr. Benno Liebchen, Dr. Matthew Blow. Thanks to their helpful conversations and teachings, I've acquired much of the knowledge and the skills the I needed to put this work together.

I thank Dr. Chris Hooley, for being a most understanding director of the CM-CDT. I would also like to thank the rest of the administrative staff of CM-CDT for the invaluable and constant support provided. Thanks Julie, Debra and Christine.

I am grateful to my family: my father Elio, my mother Maddalena, my brother Claudio, and all my other relatives who, either directly or indirectly, supported me and motivated me in pursuing my studies.

I am grateful Maria, who gave me shelter and offered me support, love and joy, through the good and the bad.

Last but not least, I would like to thank all the people that I had the luck to meet while in Edinburgh, who made the time of this *Ph.D.* infinitely more valuable. In (more or less) chronological order, thanks to Dario, Erik, Bartosz, Giovanni, Adriano, Oliver, Matt, Alex, Tom, James, Chay, Toby (Samuels), Greg, Cat, Toby (Searle), Joshua, Xanthe, Tasha, Jennifer, Victor, Stephen, Martina, and many other more, to whom I offer my deepest apologies for them not being mentioned here. To me you have been, and still are, my extended Scottish family.

Contents

List of Figures

List of Tables

Chapter 1

Introduction

In thermodynamics, a system is said to be in equilibrium when no mass or energy flow occurs, and it minimizes some thermodynamic potential, or free energy; such states have a spatially uniform temperature, are mechanically at equilibrium (all the forces sum to zero), and no macroscopic change can be observed in time. Such a system, once subject to external forces - generated by chemical potential or temperature gradients, for example - will be driven away from equilibrium, for as long as these forces persist, and for some time after that, until dissipative forces will maximize the entropy of the system to bring it into at a new state of equilibrium.

Most systems found in the natural world are rarely at equilibrium; and while in many cases the forcing may be regarded as 'external', there as many other situations where a system is inherently not in equilibrium, having some internal energy storage to draw from to perform all sorts of work, for instance to move. This is typically the case of biological systems, which store large quantities of energy to be used for motion, growth, replication, chemical synthesis, and much more.

Living matter, in the forms as complex as a collection of animals such as a school of fish or a flock of birds, or as 'simple' as a collection of swimming bacteria, offers an immense variety of realisations of systems very far from equilibrium. A vast class of non-equilibrium condensed matter systems such as these biological example, as well as their synthetic biomimetic counterparts [11]. Including artificial replications of living organisms in the count, a vast class

of non-equilibrium condensed systems has come to be known as *active matter*. While the nature, as well as the resulting dynamics, of these systems might wildly differ, they all share the common characteristic of being composed by 'self-driven' units capable of absorbing energy from their surroundings or from an internal fuel tank, to dissipate it in the process of carrying out some sort of motion [12–22].

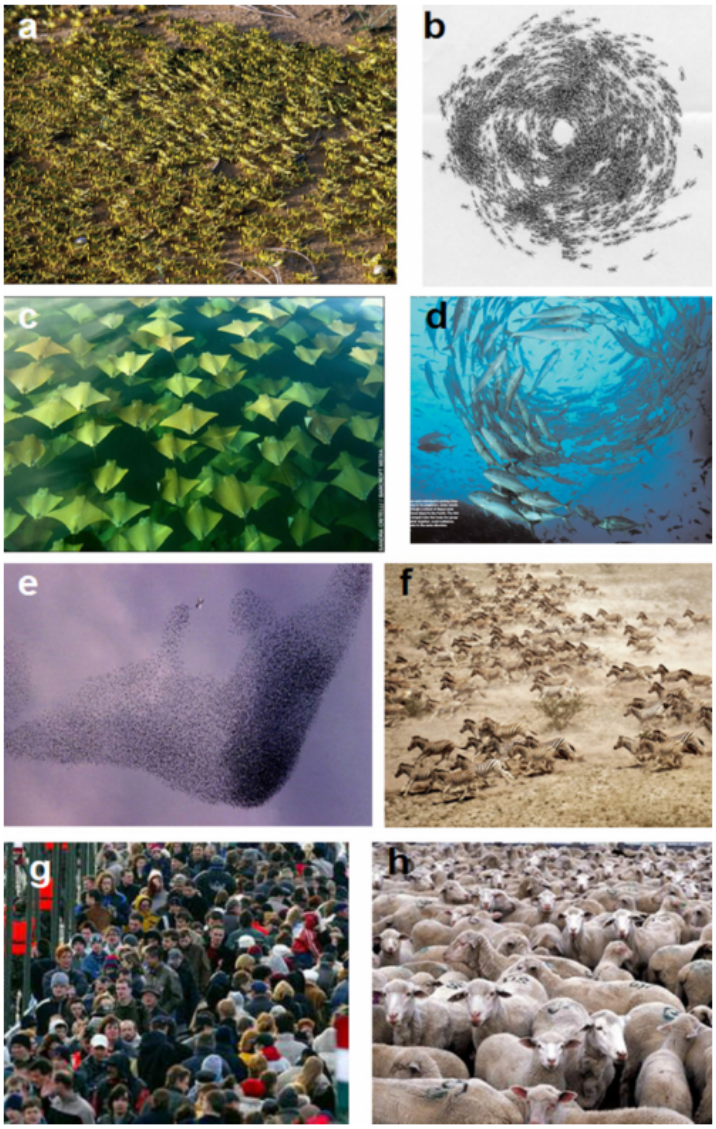

Figure 1.1 *A gallery of images related to collective motion of different animal species. While the single organisms each have their individual orientation, different degrees of overall polar order can be observed from case to case, ranging from uniform motion in a single direction (a,c,e,f), vortices (b,d), to more disordered states in which the different orientations average to zero (g,h). Adapted from [3].*

1.1 Disordered or ordered, polar or nematic

A key feature of active systems is orientational order: active constituents are in general anisotropic, which sets a favoured direction for their self-propulsion, or for the generation of forces in general [4, 6, 23–27]. This is usually the case with groups of moving animals, which can be characterized by an orientation (typically defined by the direction they are facing), figure (1.1); at smaller scales, one can find polymerising eukaryotic cellular filaments, such as actin, have asymmetric ends dubbed 'head' and 'tail' [28].

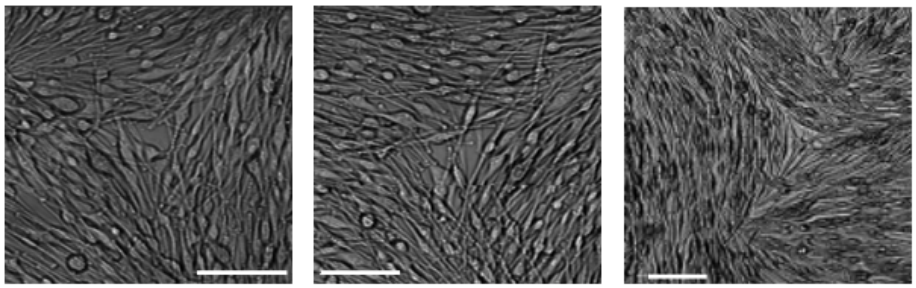

Figure 1.2 *Three different examples of human melanocytes forming nematic structures, with $s = -1/2$ disclinations. Adapted from [4].*

The type of order found is not always necessarily polar: for example, a number of different eukaryotic cell type can form orientationally ordered structures [4] analogous to nematic liquid crystal phases (see figure (1.2)), if the interaction between the active constituents is apolar in nature.

What makes active matter exciting from a purely theoretical point of view is its tendency to form patterns and display collective organized behaviour [29], present long-range order transitions [17], and have giant density fluctuations that scale up even as fast as the system size [21]; at the same time, active systems are characterized by non-equilibrium properties that do not always find an equivalent in standard externally driven non-equilibrium systems; one of the key differences can be found in the injection of energy at small scales (*i.e.* the size of the active agents) rather than having a forcing that acts on the scales of what is typically the whole system. This leads to developing hydrodynamic instabilities that generate turbulent-like behaviours even at small Reynolds numbers, where no classic turbulence can be accounted for [30–34].

On the practical side, the complex features of active matter can be exploited to

craft *in vitro* living materials with non-trivial topological properties, as in the experiment by Sanchez *et al.* [5], where microtubule filaments were made 'active' by the addition of kinesins, molecular motors converting chemical energy from ATP hydrolysis into mechanical motion along the microtubules they bind at; for high filament concentrations, hydrodynamic instabilities driven by a internally sustained flows could be observed; furthermore, the filament network displays a strong nematic order, characterized by half-integer $s = \pm 1/2$ topological defects, as in figure (1.3).

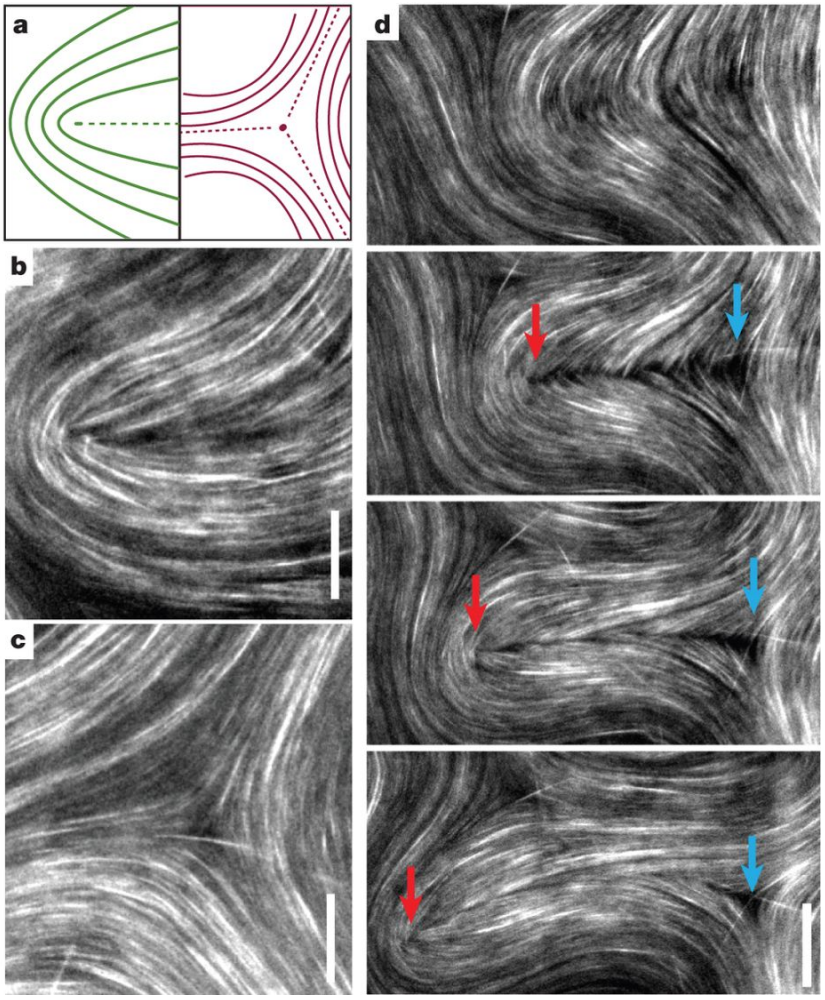

Figure 1.3 **(a)** *Schematic illustration of nematic* $s = +1/2$ *and* $s = -1/2$ *disclination charges;* **(b,c)** *Microtubules under the effect of active stress from molecular motors (kinesins) exhibiting nematic order;* **(d)** *Sequence of images showing the generation of defect charges from an originally defect free nematic domain. Adapted from [5].*

1.2 'Dry' model for self-motile units

A number of different theoretical approaches have been used to tackle the problems that describing active matter poses. One of the simplest and earliest examples is the model proposed by - and later named after - Vicsek [3, 6], which offers a simple theory of flocking of self-motile 'particles'. Originally defined in two dimensions, it aimed to capture the collective motion of various organisms like the flocking of birds, or swimming schools of fishes, motion of herds and migration of bacteria. Without taking into account the internal state of all the different self-motile units, the model reduces every particle to be a point in space, with an orientation defined by an angle θ, along which it moves with a fixed velocity v_0. Time is discretized into steps, and at every succesive step every ith particle re-aligns along the average direction of the other particles in a circle $S_i(t)$ centred on the particle i, plus some noise $\delta\theta_i$, which plays the role of a rotational diffusion.

As the total momentum of the N self-motile particles is not conserved, Vicsek model falls into a class of models known as 'dry' active models, as in opposed to 'wet' models, where the exchanges of momentum between the active constituents and their surroundings (typically a fluid) are accounted for by an additional equation for momentum conservation (typically Navier-Stokes). The key feature of the model is a discontinuous transition from disorder to order as the noise is reduced, observed in the total average velocity of the particles $\langle|\boldsymbol{v}|\rangle = |\sum_{i=1,N} \mathrm{e}^{\mathrm{i}\theta_i}|/N$. At low noise, particles aggregate in bands, which travel along the direction perpendicular to their 'axis'.

While the Vicsek model is agent based, one can derive a set of continuum equation to describe the 'hydrodynamics', that is the macroscopic behaviour of the collection of motile particles. A coarse graining procedure similar to the Chapman-Enskog expansion of velocity moments [35–38] can be carried out to obtain equations for the mean fields of the density ρ and 'velocity' $\boldsymbol{w} = \rho v_0 \boldsymbol{P}$, where the polarisation field $\boldsymbol{P}$ denotes the average direction the self-propelled particles are moving along.

$$\partial_t \rho + \nabla \cdot (v_0 \rho \boldsymbol{P}) = 0, \tag{1.1}$$

$$\partial_t \boldsymbol{w} + A\boldsymbol{w} \cdot \nabla \boldsymbol{w} = \alpha \boldsymbol{w} - \beta |\boldsymbol{w}^2| \boldsymbol{w} - \frac{1}{2}\nabla(\rho v_0^2) + k\nabla(|\boldsymbol{w}^2|) + \tilde{\eta}\nabla^2 \boldsymbol{w}, \tag{1.2}$$

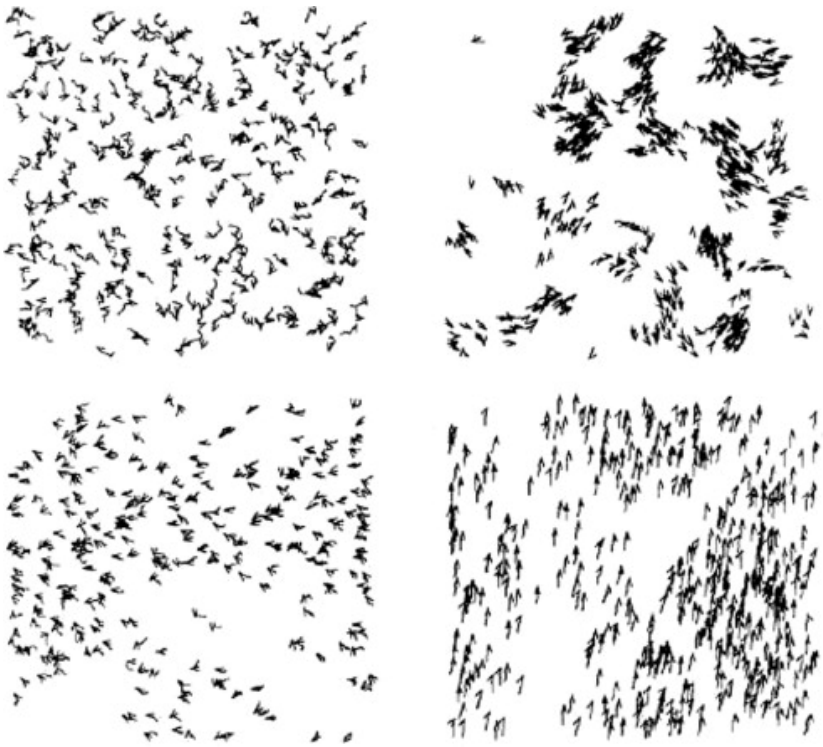

Figure 1.4 *Patterns found by evolving the rule-based Vicsek model, for different values of density and noise. The top left panel shows the initial condition; the bottom left panel shows a pattern typical of the disordered phase; finally the right columns shows two phases where there is local (top) and global (bottom) order. In all cases there are* $N = 300$ *self-propelled particles. Figure adapted from [6].*

where $A, \alpha, \beta > 0, k, \tilde{\eta}$ are functions of the parameters of the 'microscopic' model. Equation (1.1) represents continuity, while (1.2) resembles a Navier-Stokes-like equation which does not satisfy Galilean invariance, as $A \neq 1$ in general. Equation (1.2) is also a simplified version for the Toner and Tu model of flocking [17]. It is interesting to note that for spatially uniform states where gradients are neglible, equation (1.2) reduces to

$$\partial_t \boldsymbol{w} = \alpha \boldsymbol{w} - \beta |\boldsymbol{w}^2| \boldsymbol{w}, \tag{1.3}$$

which is equivalent to a time dependent Landau-Ginzburg theories for phase separation [39], which predicts a disordered phase for $\alpha < 0$, with a steady state value for the velocity $\boldsymbol{w} \simeq 0$; and an ordered aligned phase for $\alpha > 0$, characterised by non-vanishing steady state $|\boldsymbol{w}| \simeq \sqrt{\beta/\alpha}$ corresponding to the flocking transition of the Vicsek model. This simple example will be instructive, as in the following chapters we will make an extensive use of time dependent

Landau-Ginzburg theories for description of active matter as a continuum.

1.3 'Wet' model, stirring particles and spontaneous flows

In many situations, it is worth considering that active particles do not only interact with each other, but also with their surrounding medium. This arises, for instance, when self-motile particles swim in a fluid: in order to move, such particles need to exert some force on, or to stir, the surrounding fluid. In the case of bacteria, for example, the movement is typically propelled by flagella on their back. If we consider a neutrally buoyant active particle, the total force acting on it needs to be zero (there is no external force on it), hence the simplest force distribution which an active particle can exert on its surrounding fluid is a force dipole. Consequently, active 'stirrers' are naturally associated with a direction, that of their force dipole. The forces then can either be directed 'outwards' (from the centre of mass of the particles towards the fluid) or 'inwards'. In the first case the active particle is 'extensile', or a pusher [12, 21]; in the second case it is called 'contractile', or a puller. Examples of pushers and pullers can be found among unicellular organisms: bacteria such as *E. Coli* can be approximated to be 'pushers', pushing the fluid back with their flagella, whereas algae such as *Chlamydomonas* swim by 'pulling' the fluid towards them [40]. Cellular filamentous networks constitute another notable example: when cross-linked by the appropriate molecular motors (myosins), filamentous actin behaves as under the effect of a contractile force [41, 42]; while the microtubules in [5], when bound to kinesins, experience extensile stresses.

When a large collection of stirrers is considered, it is easier to consider the macroscopic effect that activity has on hydrodynamic scales, by computing a stress distribution on the continuum, rather than the sum of all the single forces. As we will discuss in Chapter 2, a derivation in d dimensions for an active stress tensor $\sigma_{ij}^{\mathrm{act}}$ $(i, j = 1, ..., d)$ - first proposed in [16] - can be obtained starting from a 'microscopic' simplified picture for the swimmers. Here we anticipate the derivation of the stress tensor to discuss the emergence of a type of spontaneous flows that arise for polar (and apolar) active fluids. As we will see in equation (2.36), the stress distribution exerted by a large collection of pushers/pullers

reads:

$$\sigma_{ij}^{\text{act}} = -\zeta\phi p_i p_j, \tag{1.4}$$

where ζ is the intensity of the activity, and has the dimensions of a force dipole, with $\zeta > 0$ corresponding to extensile activity; changing the sign of ζ turns the activity contractile; ϕ is the local concentration field for the pushers/pullers; and the vector p_i, $i = 1, ..., d$ is the swimmers local averaged orientation.

We can consider some of the consequences of the active stress by studying an extremely simplified set of linearised equations of motion, which are instructive to understand what instabilities to expect in an active fluid. We restrict to a quasi-one dimensional geometry, of an active slab confined between two planes, perpendicular to the x axis, at $x = 0$ and, say $x = L$. We also assume that the dipoles lie in the xy plane at all times, and that the density is constant, and equal to $\phi = 1$ for simplicity. We consider an active fluid initially in the quiescent (passive) disordered phase, where both the velocity, v_i, $i = x, y$, and the polarisation field p_i, are initially zero. Due to the quasi-one dimensional geometry, for an incompressible active gel the only potentially non-zero velocity component is v_y, $\boldsymbol{v} = (0, v(x), 0)$; the corresponding component of σ_{ij}^{act} to consider is then $\sigma_{xy}^{\text{act}} = q(x)$. We can write a set of hydrodynamic equations for the active gel (the fluid plus the active dipoles) as follows:

$$\partial_t v = \eta\partial_x\partial_x v - \zeta\partial_x q, \tag{1.5}$$

$$\partial_t q = K\partial_x\partial_x q - aq + \xi\partial_x v. \tag{1.6}$$

These equations are effectively a simplified version of the ones illustrated in table (2.1). In equation (1.5), η is an effective viscosity and ζ is the active stress contribution from (1.4). In equation (1.6), K is a diffusive term with the physical meaning of elastic constant (which penalises changes in orientational order), $a > 0$ ensures that the baseline steady state with $v = 0$ is isotropic ($q = 0$), while the last term proportional to $\zeta > 0$ describes the fact that anisotropic particles (that is, the swimmers in the fluid) in general align under shear.

While oversimplified, equations (1.5,1.6) are instructive, as the minimal flow-ordering coupling which they contain (via ζ and ξ) is enough to trigger a non-equilibrium phase transition to a spontaneously flowing state. To show this, we

first rewrite the equations in Fourier space as follows,

$$\partial_t \tilde{v} = -k^2 \eta \tilde{v} - \mathrm{i}k\zeta\tilde{q}, \tag{1.7}$$

$$\partial_t \tilde{q} = -k^2 \tilde{q} - a\tilde{q} + \mathrm{i}k\xi\tilde{v}, \tag{1.8}$$

or, equivalently,

$$\partial_t \begin{pmatrix} \tilde{v} \\ \tilde{q} \end{pmatrix} = \underbrace{\begin{pmatrix} -\eta k^2 & -\mathrm{i}k\zeta \\ \mathrm{i}k\xi & -a - k^2 K \end{pmatrix}}_{\mathrm{A}} \begin{pmatrix} \tilde{v} \\ \tilde{q} \end{pmatrix}. \tag{1.9}$$

In order to evaluate the stability of the quiescent disordered state, $v = q = 0$, we need to follow the evolution of the velocity and order parameter fields, starting from small fluctuations around the baseline state. As the equation of motion is linear, this problem is equivalent to finding the eigenvalues of the operator A, λ_1 and λ_2: if they are both negative, then the quiescent disordered state is stable as any fluctuation from it decays exponentially with time; if at least one of them is positive, the state is unstable, and the system starts to flow. Instead of computing the eigenvalues explicitly, we can observe that the determinant and trace of A, which are respectively the product and sum of its two eigenvalues, are

$$\det \mathrm{A} = \eta k^2 (a + k^2 K) - k^2 \xi\zeta \tag{1.10}$$

$$tr\, \mathrm{A} = -a - k^2(K + \eta) < 0 \tag{1.11}$$

As the trace is negative, either both eigenvalues are negative, or $\lambda_1 < 0$ and $\lambda_2 < -\lambda_1$; the latter case means that the quiescent state is unstable to small perturbations. This condition is equivalent to detA < 0. For large scale perturbations, *i.e.* $k \to 0$, the instability condition becomes

$$\det \mathrm{A} \simeq \eta a k^2 - \zeta\xi k^2 < 0, \tag{1.12}$$

which is equals $\zeta > \frac{\eta a}{\xi}$, which can occur only for extensile systems ($\zeta > 0$).

This instability is a simple example of the so-called 'generic instability' [12, 21, 22, 43], also known as spontaneous flow, which is much more general in active gels and has been discussed by several groups, both analytically [44, 45] and numerically [46–49]. Note that our discussion only proves that there is an instability, the final

pattern of course requires the introduction of non-linear stabilising terms which are absent in the linearised (1.5,1.6).

While we have shown that there is an instability in the disordered phase, a similar situation arises in the orientationally ordered case, as we will discuss in Section 3.3; in this case the instability is present for both contractile and extensile swimmers.

Chapter 2

Dynamic model for active fluids

In the present chapter, we will present the theoretical model we considered for the dynamics of active fluids. Our intention is to reproduce with a minimal model a generic biological anisotropic fluid that generates non-thermal forces at the scale of its constituents which result in active stress distributions on larger scales. Here, by 'constituents', we mean the biological elements suspended in the fluid that, by stirring the fluid around them, can give rise to interesting structures and dynamics. Typical examples we have in mind are microtubules and molecular motors suspensions [5] and dense bacterial suspensions [50].

There is a plethora of models that qualitatively and quantitatively describe the dynamics of active matter, ranging from agent-based models [6, 29, 51–54] that track individual self-propelled particles, to continuum theories [17, 44, 55–57], which focus on the large scale behaviours and the hydrodynamics of active systems; further distinctions can be made between momentum conserved (wet) and non-conserved (dry) models, and oriented (polar) and non-oriented constituents (nematic). A more comprehensive summary can be found in [22].

We will consider here mainly wet systems, both polar and nematic. The main ingredients for such models are the following: *(i)* the 'fluid physics', which will be accounted for by a momentum (and density) equation, such as the Navier-Stokes equation; *(ii)* the possibility for the constituents of the active fluids to arrange in ordered structures, which will be described by an equation for a nematic (or polar) director field - borrowed from the continuum theories for liquid crystals; *(iii)* and finally the energy input at small scales, and how does this affect the fluid

on larger scales. Here by 'large scale' we mean length-scales such as to include a large number of elementary constituents, so that they can be regarded to a good approximation as a continuum.

We will start from presenting the dynamic equations for a generic conserved or non-conserved field model. These describe the time evolution of the concentration field and of the orientational order parameter, together with the equation for momentum conservation. We will see how these couple, and we will discuss the role of activity, and how this can be consistently introduced in the dynamics from a coarse-graining of the underlying microscopic dynamics. Finally, we will introduce the Hybrid Lattice Boltzmann Model as a numerical solver for the dynamics.

2.1 Field theory for conserved and non-conserved dynamics

As we seek to analyse active fluids from a coarse-grained point of view that ignores the microscopic details and focuses on the dynamics on the hydrodynamic scales, we will consider equations for the dynamics of continuous fields rather than attempting to build a particle-based theory. In this continuum framework, the system can be suitably described with a free energy functional approach.

In the following, we will first briefly introduce the background for the active fluids models that has been extensively used in the literature [30, 36, 46, 49, 58], and that has been the basis for our work. We will start from summarising the equations that are know in the classification by Hohenberg and Halpin [59] as model A and model B equations; we will then make use of these for the dynamics of a nematic/polar director $\boldsymbol{n}/\boldsymbol{p}$ and concentration ϕ order parameters respectively, and include the hydrodynamics through the extension to model H, which couples the order parameters to a hydrodynamic flow field $\boldsymbol{u}$ that conserves momentum. A more extensive discussion on phase field dynamics can be found in [39].

Given a generic field $\phi(\boldsymbol{x}, t)$, we will call free energy the functional

$$\mathcal{F}[\phi](t) = \int_{\Omega} f\big(\phi, \nabla\phi\big)\mathrm{d}\boldsymbol{x}, \tag{2.1}$$

where f and Ω are respectively the free energy density and the spatial extension

of the system; we will assume that $\mathcal{F}$ can be minimised by some equilibrium field ϕ_{eq}. The free energy that functionals we will use in this dissertation will be of phenomenological nature: f will be constructed so that it keeps into account the relevant symmetries of the system. These are examples of the Landau-Ginzburg theory, which can be useful to approach multiple phases systems, and phase separation phenomena.

The evolution of ϕ will be dictated by some equation that will tend to minimise $\mathcal{F}$. In doing this, we need to consider whether the field ϕ is or is not conserved, that is, whether the quantity

$$\int_{\Omega} \phi \mathrm{d}\boldsymbol{x}, \tag{2.2}$$

is or is not a constant in time over any volume Ω. In both cases, we are considering cases in which the dynamics leads to steady statesfor which the free energy $\mathcal{F}$ reaches a variational minimum, *i.e.* that any small variation in the field $\delta\phi$ will correspond to no change in the free energy, or $\delta\mathcal{F} = 0$.

If the field ϕ is not conserved, a suitable way to describe its dynamics is through the Time-Dependent-Ginzburg-Landau equation, also known as Model A [59]:

$$\partial_t \phi = -\Gamma \frac{\delta \mathcal{F}}{\delta \phi}, \tag{2.3}$$

where Γ is a relaxation constant, and $\frac{\delta\mathcal{F}}{\delta\phi}$ is the functional derivative of the free energy:

$$\frac{\delta \mathcal{F}}{\delta \phi} = \frac{\partial f}{\partial \phi} - \partial_i \frac{\partial f}{\partial(\partial_i \phi)}. \tag{2.4}$$

Equation (2.3) tends to minimise $\mathcal{F}$ with a steepest descent method, by moving the field down gradients of $\mathcal{F}$. The reason why we introduced this model is to treat the dynamics of the nematic (or polar) orientation field: as it will be discussed later, this order parameter doesn't need to be conserved, and it relaxes to reduce the elastic free energy of the system.

We will also need an equation for the time evolution of conserved order parameters such as, for instance, the mass of the active constituents[1]. In this case, model A does not apply, and we need to consider a dynamical equation that is intrinsically

[1]This assumption is not always valid, as one might consider birth/death processes. However, here we will continue under the assumption that the total mass of the constituents stays the same over the time scales considered.

a conservation equation in d dimensions, hence written as:

$$\partial_t \phi = -\partial_i j_i, \tag{2.5}$$

where j_i $(i = 1, ..., d)$ is some diffusive flux for field ϕ. In kinetic processes, j_i can be usually written by Fick's law as a gradient of some density of chemical potential $\mu(\phi)$; here the natural choice μ is once again the functional derivative of the free energy with respect to ϕ, where the latter can be understood as a concentration order parameter - which is how we are going to intend it. Thus:

$$j_i = -M\partial_i \mu = -M\partial_i \frac{\delta \mathcal{F}}{\delta \phi}, \tag{2.6}$$

where M is a diffusive mobility coefficient, that could in principle depend on the order parameter itself, such as it is the case in some phase separating or non-homogeneous systems [60]. In the following M will be assumed for simplicity to be constant. Equation (2.6) leads to what is known as the Cahn-Hilliard equation, or model B

$$\partial_t \phi = M\partial_i \partial_i \frac{\delta \mathcal{F}}{\delta \phi}. \tag{2.7}$$

Unlike model A from equation (2.3), stationary states of equation (2.7) do not correspond to stationary points of the free energy $\mathcal{F}$. However, from equations (2.6), (2.7), we can immediately obtain that the variation in time of the free energy is given by:

$$\frac{\mathrm{d}\mathcal{F}}{\mathrm{d}t} = -M \int_\Omega |\nabla \mu|^2 \mathrm{d}\boldsymbol{x}, \tag{2.8}$$

which implies that the free energy decays to zero, as the integrand is positive defined. We can then carefully choose the zeroes of $\mathcal{F}$ to be stationary points to recover the results of model A.

One typical example of model B dynamics is represented by spinodal decomposition, for which the free energy reads:

$$\mathcal{F} = \int_\Omega \left(\frac{a}{4}\phi^2(\phi - \phi_0)^2 + \frac{k}{2}(\nabla \phi)^2 \right). \tag{2.9}$$

The first term in equation (2.9) represents the bulk energy of a binary system, which can separate in two phases corresponding to $\phi = 0$ and $\phi = \phi_0$; the second term corresponds is the interfacial contribution, that creates a transition region in which ϕ varies smoothly between the bulk value of the two phases. Effectively, it provides a surface tension, and regularises the corresponding model B equation

by ensuring the continuity of ϕ.

So far we have not introduced the fluid character of the system. Effectively, equation (2.7) is a diffusion equation; however, the order parameter ϕ can be coupled to a momentum, or flow, field $\boldsymbol{u}$ which 'advects' the field along its course. This can be simply done by slightly changing model B to the following form:

$$\partial_t \phi + \partial_i (u_i \phi) = M \partial_i \partial_i \frac{\delta \mathcal{F}}{\delta \phi}, \tag{2.10}$$

where $\boldsymbol{u}$ is in turn evolved by an incompressible Navier-Stokes equation, namely

$$\rho(\partial_t u_i + u_j \partial_j u_i) = \eta \partial_j \partial_j u_i - \partial_i P + \partial_j \sigma_{ij}(\partial_l u_m, \phi), \tag{2.11}$$

$$\partial_i u_i = 0. \tag{2.12}$$

Equations (2.10) and (2.11) are known altogether as model H.

In equation (2.11), η is the dynamic viscosity, P is the hydrodynamic pressure[2]; and finally, σ_{ij} is the stress distribution acting on the fluid. The latter can depend on the order parameter ϕ. What we have in mind is that the configuration of the active material suspended in a fluid will exert some feedback on the fluid itself, which will be expressed in the constitutive law giving the explicit form for σ_{ij} in terms of the director $\boldsymbol{n}/\boldsymbol{p}$ and concentration ϕ fields. In what we are going to consider in the following, the stress tensor will contain terms originating from the elastic properties of the order parameter fields, terms denoting flow-aligning/tumbling regimes of the director fields, and most importantly the expression for the active forces that the biological constituents exert on the fluid, *i.e* the *active stresses*.

Finally, note that we could add an advection term to equation (2.3) in the same way, to introduce transport effect from a fluid. For example, for a polarization field $\boldsymbol{p}$, the non-conserved dynamics will read:

$$\partial_t p_i + \partial_j (u_j p_i) = -\Gamma \frac{\delta \mathcal{F}}{\delta p_i}. \tag{2.13}$$

Equation (2.13) can be further generalized by including the effects of alignment or tumbling in a shear flow [62–64], as it will be discussed for the dynamics of polar suspensions in the following sections.

[2]Being the fluid incompressible, this is effectively a Lagrange multiplier, and can be expressed in terms of the velocity gradients through the mass conservation equation; see Landau [61].

2.2 Nematic and polar models for microbiological elongated bodies

To choose one model for the dynamics of active suspensions, we will have to consider what are the archetypical, or the most common examples of active fluids. By saying 'active fluid', we want to try and encircle a large and varied number of possible realizations. A bacterial suspension [65], or the actin-myosin networks in the cytoskeleton of a cell [66], or even 'artificial' active model-toy active fluids [15], such as highly packed self-phoretic colloids, are all valid realizations of a fluid that transforms chemical energy from some *reservoir* of 'fuel' in non-thermal stresses. There are several models that construct the dynamics of the aforementioned examples by considering the motion of the single constituents. Constitutive equations on the hydrodynamic scale can be obtained from coarse graining the microscopics, as in [36, 37].

How does an active fluid differ structurally from an isotropic Newtonian passive fluid? The active constituents introduce some orientational order, as there will be preferential directions set by the elongated axis of the *E. Coli* bacteria, or by the F-actin, or by the head-tails asymmetry of self-phoretic particles. Furthermore, the constituents might coexist in systems where their orientation is random, but because of steric and hydrodynamic interactions, they tend to align forming ordered states that can give rise to interesting and non-trivial collective dynamics.

The elongated character, or more generically the presence of a preferred direction for the constituents, can be well summarised in a coarse grained approach by the elastic theory for nematic liquid crystals and polar rods [67, 68]. For this purpose, we will briefly summarise the continuum theory of nematic/polar rods that we are going to use in the following.

Given a fluid volume element large enough so as to contain numerous active constituents, that in first approximation we consider to be rod-like particles, but small enough to be considered as a point $\boldsymbol{x}$ in a continuum, the average direction of alignment of the nematogen may be encoded by a vector field $n_i(\boldsymbol{x})$, $(i = 1, ..., d)$, namely:

$$\boldsymbol{n}(\boldsymbol{x}) = \frac{1}{\phi(\boldsymbol{x})} \left\langle \sum_{\alpha=1}^{N} \hat{\boldsymbol{\nu}}^{\alpha} \delta(\boldsymbol{x} - \boldsymbol{x}^{\alpha}) \right\rangle, \tag{2.14}$$

where $\langle \cdot \rangle$ denotes a local average, $\hat{\boldsymbol{\nu}}^{\boldsymbol{\alpha}}$ $(\alpha = 1, ..., N)$ are the directions of the

elongated axis of the N individual elongated nematic constituents, or *nematogens*, and $\phi(\boldsymbol{x}) = \langle \sum_\alpha \delta(\boldsymbol{x} - \boldsymbol{x}^\alpha) \rangle$ is their concentration.

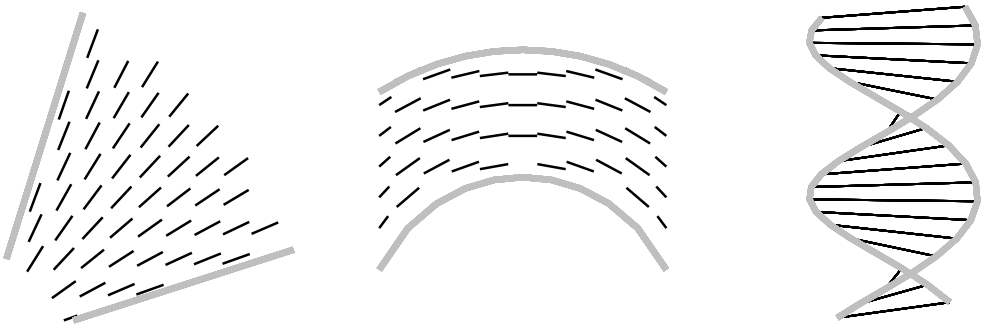

(a) **(b)** **(c)**

Figure 2.1 **(a)** *Splay,* **(b)** *bend* **(c)** *and twist.*

If one considers the ground state of a nematic to be of uniform orientation along one axis, the contributions to the free energy will be from the distortions of $\boldsymbol{n}$, expressed in terms of gradients of $\boldsymbol{n}$, namely $\partial_i n_j$. Furthermore, nematic liquid crystals are made of rod-like particles with head-tail symmetry, which implies the symmetries $\boldsymbol{n} \to -\boldsymbol{n}$ and $\boldsymbol{x} \to -\boldsymbol{x}$; all contributions to a Landau free energy functional have to respect this symmetries. The easiest way to achieve this goal is to have terms even in n_i and in the derivatives ∂_j. To the second order in the derivatives, the independent allowed terms are of the form [68]:

$$\begin{array}{cc} (\nabla \cdot \boldsymbol{n})^2 & (splay), \\ (\boldsymbol{n} \times (\nabla \times \boldsymbol{n}))^2 & (bend), \\ (\boldsymbol{n} \cdot (\nabla \times \boldsymbol{n}))^2 & (twist). \end{array} \tag{2.15}$$

These three modes of deformations correspond to the ones shown in figure (2.1). Thus a Landau elastic free energy would read

$$\mathcal{F}[\boldsymbol{n}] = \int_\Omega \mathrm{d}^d\boldsymbol{x} \left\{ \frac{k_1}{2}(\nabla \cdot \boldsymbol{n})^2 + \frac{k_2}{2}(\boldsymbol{n} \times (\nabla \times \boldsymbol{n}))^2 + \frac{k_3}{2}(\boldsymbol{n} \cdot (\nabla \times \boldsymbol{n}))^2 \right\}, \tag{2.16}$$

where $k = k_1, k_2, k_3$ are known as Frank's elastic constants. Note that by the single elastic constant $k_1 = k_2 = k_3$ approximation, equation (2.16) reduces to

$$\mathcal{F}[\boldsymbol{n}] = \int_\Omega \mathrm{d}^d\boldsymbol{x} \frac{k}{2} \partial_i n_j \partial_i n_j. \tag{2.17}$$

In the following chapters, we will be working solely in the single constant

approximation, which is a common choice in theoretical or simulation work.

Another way to describe nematic symmetries in $\mathcal{F}$ is to drop the vector description, and consider a tensorial approach, by using the nematic tensor:

$$Q_{ij}(\boldsymbol{x}) = S(\boldsymbol{x}) \left(\hat{n}_i(\boldsymbol{x}) \hat{n}_j(\boldsymbol{x}) - \frac{\delta_{ij}}{d} \right), \tag{2.18}$$

where $\hat{n}_i(\boldsymbol{x})$ $(i = 1, ..., d)$ are the components of the unit vector in the direction of $\boldsymbol{n}(\boldsymbol{x})$, and $S(\boldsymbol{x})$ is the 'strength' of the nematic order. We can give a microscopic definition of Q_{ij} similarly to the one for $\boldsymbol{n}$

$$Q_{ij}(\boldsymbol{x}) = \frac{1}{\phi(\boldsymbol{x})} \left\langle \sum_{\alpha=1}^{N} \left(\hat{\nu}_i^\alpha \hat{\nu}_j^\alpha - \frac{\delta_{ij}}{d} \right) \delta(\boldsymbol{x} - \boldsymbol{x}^\alpha) \right\rangle. \tag{2.19}$$

The nematic tensor Q_{ij} is even in $\hat{\boldsymbol{n}}$, symmetric and traceless. Scalar terms to appear in a free energy invariant by rotations can be constructed by taking the trace of powers of Q_{ij}. Up to the fourth order in $\mathrm{Tr}(\mathbf{Q})$:

$$\mathcal{F}[\mathbf{Q}] = \int_\Omega \mathrm{d}^d \boldsymbol{x} \left\{ \frac{A}{2} Q_{ij} Q_{ji} + \frac{B}{3} Q_{ij} Q_{jk} Q_{ki} + \frac{C}{4} Q_{ij} Q_{jk} Q_{kl} Q_{li} + e(\mathbf{Q}, \nabla \mathbf{Q}) \right\}, \tag{2.20}$$

where the A, B, C can be function of external parameters, such as temperature or pressure, or the concentration ϕ of the nematic constituents [8]. C has to be positive so that $\mathcal{F}$ has minima for finite values of Q_{ij}; as for A and B, depending on their value and sign, $\mathcal{F}$ will have minima for finite Q_{ij}. As the tensor Q_{ij} itself is traceless, there is no linear term[3], ensuring that there can be minima of $\mathcal{F}$ corresponding to a disordered isotropic state with $S = 0$. Using the definition of Q_{ij} (2.18), equation (2.20) can also be written in the form:

$$\mathcal{F}[\mathbf{Q}] = \int_\Omega \mathrm{d}^d \boldsymbol{x} (d-1) \left\{ \frac{A}{2d} S^2 + \frac{B(d-2)}{3d^2} S^3 + \frac{C(d-1)}{4d^2} S^4 + f_d(\mathbf{Q}, \nabla \mathbf{Q}) \right\}. \tag{2.21}$$

Here the term $f_d(\mathbf{Q}, \nabla \mathbf{Q})$ contains the contributions given by the elastic deformations that will correspond to the Frank elastic free energy. Note that a term of the third order in the order parameter is allowed for tensors, while it's not for vector order parameters. This is necessary for the isotropic-nematic transition to be first order. Note that the cubic term is identically null in two-dimensions.

[3] In the absence of an external field.

If one wants to obtain the Frank elastic free energy from equation (2.21), then we need to assume uniform $S = S_0$, so that the the elastic term f_d must read [69]

$$f_d(\mathbf{Q}, \nabla\mathbf{Q}) = \frac{L_1}{2}\partial_i Q_{jk}\partial_i Q_{jk} + \frac{L_2}{2}\partial_j Q_{ij}\partial_k Q_{ik} + \frac{L_3}{2}Q_{ij}\partial_i Q_{kl}\partial_j Q_{kl}, \tag{2.22}$$

where $L_1 = \frac{k_3+2k_2-k_1}{9S_0^2}$, $L_2 = 4\frac{k_1-k_2}{9S_0^2}$, $L_3 = 2\frac{k_3-k_1}{9S_0^2}$. In the single elastic constant approximation, only the term in $L_1 = L$ survives in the elastic energy (2.22):

$$\mathcal{F}[\mathbf{Q}] = \int_\Omega \mathrm{d}^d\boldsymbol{x} \left\{ \frac{A}{2}\operatorname{Tr}\mathbf{Q}^2 + \frac{B}{3}\operatorname{Tr}\mathbf{Q}^3 + \frac{C}{4}\operatorname{Tr}\mathbf{Q}^4 + \frac{L}{2}(\nabla\mathbf{Q})^2 \right\} \tag{2.23}$$

This will be the form of the nematic free energies we will use from now on.

One of the building blocks for constructing (2.23) is the inversion symmetry. However, active fluids do not necessarily have nematic symmetry. For example, swimming *E. Coli* and self-phoretic particles usually swim in the preferential direction of their head: they are inherently polar. The definition of the vector $\boldsymbol{p}$ is identical to equation (2.14)

$$\boldsymbol{p}(\boldsymbol{x}) = \frac{1}{\phi(\boldsymbol{x})}\left\langle \sum_{\alpha=1}^{N} \hat{\boldsymbol{\nu}}^\alpha \delta(\boldsymbol{x} - \boldsymbol{x}^\alpha) \right\rangle, \tag{2.24}$$

but its symmetries in the free energy $\mathcal{F}[\boldsymbol{p}]$ will be different. Up to fourth order:

$$\mathcal{F}[\boldsymbol{p}] = \int_\Omega \mathrm{d}^d\boldsymbol{x} \left\{ \frac{A}{2}\boldsymbol{p}^2 + \frac{B}{4}(\boldsymbol{p}^2)^2 + \frac{\kappa}{2}(\nabla\boldsymbol{p})^2 \right\}, \tag{2.25}$$

where this time third order terms in $\boldsymbol{p}$ are not allowed because of rotational symmetry; κ is equivalent to the elastic constant k for nematics, and we are implicitly assuming the single constant approximation.

The difference between considering a system polar or nematic ultimately lies in the nature of the interaction between its constituents. In most of the biologically relevant cases, the suspended particles are anisotropic and asymmetric in nature, but unless their density is high enough for excluded volume effect to count, or unless the particles have a preferred direction of motion, the long range interactions between the constituents have in first approximation the same expression, and form the same flow field in the surrounding fluid. We will discuss this further in Section 2.2.3.

2.2.1 Topological defects

We here briefly consider topological defects in polar and nematic fields. A topological defect, or disclination, is a point or a line (dubbed 'defect core') around which the director field – either $\boldsymbol{p}$ or $\boldsymbol{n}$ – is poorly defined and varies discontinuously, as shown by some examples in figure (2.2). A topological defect can be characterized by its 'charge' [8], defined as the winding number around its core, namely

$$s = \frac{1}{2\pi} \oint_C \mathrm{d}\theta \tag{2.26}$$

where the line integral defined above is carried out along any not-self-crossing closed contour C around the defect core, and θ is the angle defining the director profile orientation in a polar coordinates system with the z axis going through the defect core.

A more down to earth and intuitive definition of the topological charge is by counting in how many $2s\pi$ rotations the director profile incurs along any circuit around the core; the sign of s can be negative if the director profile rotates in the opposite sense to the one set by the contour.

Topological defect contribute significantly to the total energy of the system, as they cannot be made to disappear by any continuous deformation of the director profile. While defects such as the ones shown in figure (2.2) can be shrunk down to regions with no volume, they effectively alter the configuration of the whole system at very large distances, up to the size of the system itself. For example if we were to try to bring a vortex defect as in (2.2A) to a completely aligned state, we would have to alter not only the director profile in proximity of the core, but we would necessarily have to consequently adjust $\boldsymbol{p}$ or $\boldsymbol{n}$ everywhere else as we move away from the defect. This is a direct consequence of non-zero winding number s.

An argument based on energetics can be given on why topological defects are stable, and do not relax to aligned state, despite being associated with high distortion energies [8]. Let us, for example, consider a vortex defect around a point in two dimensions; it can be argued that this kind of defect is associated with a distortion energy that scales with the size of the system L as $k \log L$, where $k = k_1 = k_2 = k_3$ is the relevant elasticity under the one-constant approximation. If we were to perform a set of small deformations to try to align the director profile around the core, we would end up with a region of perimeter $\sim L$ with

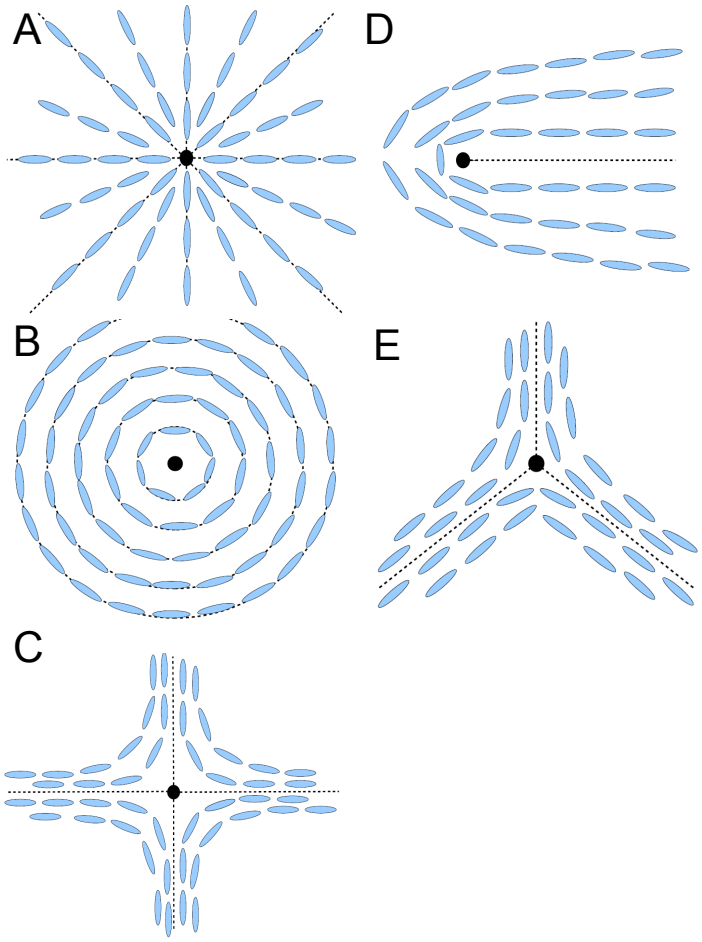

Figure 2.2 *A few configurations of topological defects of different charges.* **(A,B)** *two 'vortex' defects, both of topological charge* $+1$*;* **(C)** -1 *charge disclination, also known as 'hyberbolic hedgehog', with charge sign opposite to A,B, as the director profile rotates around the defect in the opposite sense;* **(D)** $+1/2$ *charge defect;* **(E)** $-1/2$ *charge disclination. Note that half-interger charges are topologically stable in nematic materials, but not in polar media, as a continuous deformation could turn said disclinations into a completely aligned region. Adapted from [7], with permission.*

sharp gradients, such as the one shown in (2.3).

This new configuration is characterized by a distortion energy scaling as $\sim kL$, hence the system will unlikely turn to this state as a result of fluctuations. Another possible route would involve changing $\boldsymbol{p}$ or $\boldsymbol{n}$ everywhere, but this present an even higher energy barrier that would scale with the system size, namely $\sim kL^2$.

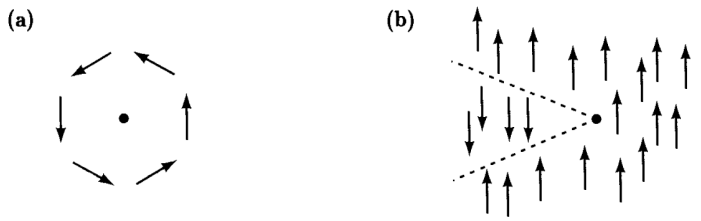

Figure 2.3 **(a)** *Schematics of a vortex defect and* **(b)** *a (poor) attempt to align the director profile around it, resulting in the formation of a boundary wall with a region with orientation opposite to the rest of the bulk. Adapted from [8].*

2.2.2 Dynamics for polar and nematic fields

The concentration ϕ will follow a model B (2.7) type of equation, where the dynamics is driven by gradients of the chemical potential $\mu = \frac{\delta \mathcal{F}}{\delta \phi}$, where $\mathcal{F}[\phi, \boldsymbol{p}]$ is the free energy of the system

$$\partial_t \phi + \partial_j(\phi u_j) = M \partial_j \partial_j \frac{\delta \mathcal{F}[\phi, \boldsymbol{p}]}{\delta \phi}. \tag{2.27}$$

The director field is evolved by a model A (2.3) type of equation, as there is no reason for the total orientation to be conserved: the field just relaxes to the minima of the free energy. For the polar field $\boldsymbol{p}$:

$$\partial_t p_i + u_j \partial_j p_i = \xi \Lambda_{ij} p_j - \Omega_{ij} p_j - \Gamma h_i. \tag{2.28}$$

Here $h_i = \frac{\delta \mathcal{F}}{\delta p_i}$ is the molecular field, $\Lambda_{ij} = \frac{1}{2}(\partial_j u_i + \partial_i u_j)$ and $\Omega_{ij} = \frac{1}{2}(\partial_j u_i - \partial_i u_j)$ are the symmetric (shear) and antisymmetric (vorticity) parts of the gradients of the velocity field u_j. The shear term is proportional to ξ: this parameter is related to the eccentricity of the constituents, being positive for rod-like elements and negative for disc-like ones [44]. Its absolute value determines whether particles will tumble in a shear flow, or align to it at the Leslie angle[4], respectively for $|\xi| < 1$ and $|\xi| > 1$. The diffusive coefficient M and Γ are referred to as chemical mobility and rotational viscosity [70].

For a nematic fluid, the concentration equation for ϕ is the same as in (2.27), while the equation for Q_{ij} reads [71]:

$$\partial_t Q_{ij} + u_k \partial_k Q_{ij} = -\xi \Sigma_{ijkl} \Lambda_{kl} - T_{ijkl} \Omega_{kl} - \Gamma H_{ij}, \tag{2.29}$$

[4] θ_{Les} is such that $\sec \theta_{\text{Les}} = \xi$

where H_{ij} is the molecular field for a free energy $\mathcal{F}[\phi, \mathbf{Q}]$ of the form in equation (2.23), namely

$$H_{ij} = \frac{1}{d}\delta_{ij}\frac{\delta \mathcal{F}}{\delta Q_{kk}} - \frac{1}{2}\frac{\delta \mathcal{F}}{\delta Q_{ij}} - \frac{1}{2}\frac{\delta \mathcal{F}}{\delta Q_{ji}} \tag{2.30}$$

and the two tensors $\mathbf{\Sigma}$ and $\mathbf{T}$ that couple to the shear $\mathbf{\Lambda}$ and vorticity $\mathbf{\Omega}$ tensors can be written in terms of Q_{ij} [71]

$$\begin{aligned} \Sigma_{ijkl} &= Q_{ij}Q_{kl} + \delta_{ij}\left(Q_{kl} + \frac{\delta_{kl}}{d}\right) - \delta_{ik}\left(Q_{lj} + \frac{\delta_{lj}}{d}\right) - \delta_{kj}\left(Q_{il} + \frac{\delta_{il}}{d}\right) \\ T_{ijkl} &= Q_{ik}\delta_{jl} - \delta_{ik}Q_{jl} \end{aligned} \tag{2.31}$$

2.2.3 Active stress and Navier-Stokes

So far we have considered the equations of motion for the nematic/polar orientational order parameters, but we have not introduced the activity. Being the active forces of non-thermal nature, they cannot be obtained as derivatives of a free energy [72]. We will focus on those models that are momentum conserving, and consider the dynamics of both the constituents and the surrounding fluid. The latter is described by a Navier-Stokes equation, in which forces can be expressed as the divergence of a stress tensor.

The stress generated by the activity can be derived from the 'microscopics' of the model through a coarse graining of the forces, following the approach of Hatwalne *et al.* [2, 16]. The fluids we want to describe are dense collections of 'swimmers' suspended in a flow. Their presence enriches the hydrodynamics not only with the orientational order and the consequent macroscopic elastic properties; they also exert 'activity' by constantly converting some form of fuel (typically ATP) into some force distribution that 'stirs' the fluid. If we consider a buoyant 'swimmer' suspended in a fluid, when subject to no external forces, the total force acting on it has to be zero. This can be achieved with a zero net force distribution over the microscopic swimmer, of which the simplest example is a dipolar force.

Let us consider a simplified model of a suspension of N identical dipolar 'swimmers'. As a first approximation, we will consider the swimmers to be thin cylindrical rods of length b along their central axis $\hat{\boldsymbol{\nu}}^\alpha$ ($\alpha = 1, ..., N$), with center of mass is in $\boldsymbol{x}^\alpha$. Let $f\hat{\boldsymbol{\nu}}_\alpha$ be the force acting at $\boldsymbol{x}^\alpha + \frac{b}{2}\hat{\boldsymbol{\nu}}^\alpha$, *i.e.* at the head of the rod, and $-f\hat{\boldsymbol{\nu}}^\alpha$ the force acting at $\boldsymbol{x}^\alpha - \frac{b}{2}\hat{\boldsymbol{\nu}}^\alpha$.

The total force that the swimmers exert on the surrounding fluid is:

$$\boldsymbol{F} = f \sum_{\alpha=1}^{N} \hat{\boldsymbol{\nu}}^{\alpha} \left(\delta \left(\boldsymbol{x} - \boldsymbol{x}^{\alpha} - \frac{b}{2} \hat{\boldsymbol{\nu}}^{\alpha} \right) - \delta \left(\boldsymbol{x} - \boldsymbol{x}^{\alpha} + \frac{b}{2} \hat{\boldsymbol{\nu}}^{\alpha} \right) \right). \tag{2.32}$$

For $b \to 0$, we can expand the latter to be

$$\boldsymbol{F} = -fb \sum_{\alpha=1}^{N} \hat{\boldsymbol{\nu}}^{\alpha} \nu_i^{\alpha} \partial_i \delta(\boldsymbol{x} - \boldsymbol{x}^{\alpha}) + \mathcal{O}(b^3), \tag{2.33}$$

which can be rearranged to be a divergence of tensor

$$F_j = \partial_i \left(-fb \sum_{\alpha=1}^{N} \hat{\nu}_i^{\alpha} \hat{\nu}_j^{\alpha} \delta(\boldsymbol{x} - \boldsymbol{x}^{\alpha}) \right). \tag{2.34}$$

Defining the dipolar strength $\zeta = fb$ to be the 'intensity' of the activity, equation (2.34) can be rewritten using the definition of the nematic tensor:

$$F_j = -\partial_i \left(\zeta \phi \left(Q_{ij} + \frac{\delta_{ij}}{d} \right) \right) = \partial_i \sigma_{ji}^{\mathrm{act}}. \tag{2.35}$$

The force f and the activity ζ do not have a defined sign. The dipole forces can either be pointing towards the centre of mass of the rod, or outwards from it; these two cases divide the active constituents in two categories, respectively the 'contractile' and 'extensile'. These are usually referred to as being 'pullers' and 'pushers', figure (2.4).

In the derivation of equation (3.9), there is no assumption on the symmetry of the swimmers; $\sigma_{ij}^{\mathrm{act}}$ can also be written in terms of p_i instead of Q_{ij}:

$$\sigma_{ij}^{\mathrm{act}} = -\phi \zeta p_i p_j \tag{2.36}$$

Here we want to remark that this stress distribution, despite being slightly different at a first look from the nematic to the polar case, is exactly the same, independently of the type of symmetry. Therefore, the hydrodynamic interaction does not, in first approximation, characterise the symmetry of the system; for this reason, if purely hydrodynamic interactions are present between the constituents, even intrinsically asymmetric swimmers might give rise to a nematic type of order.

Equations (3.9, 2.36) define the *'active stress'* $\sigma_{ij}^{\mathrm{act}}$. This will be the source of the non-thermal forces at small scales by which the active constituents drive the

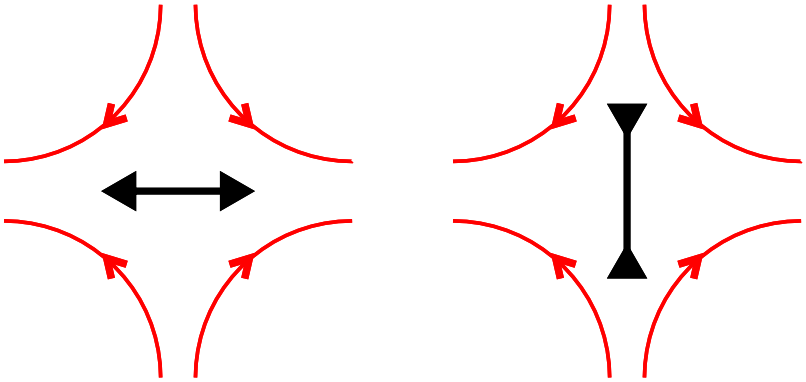

(a) **(b)**

Figure 2.4 *Force dipoles (***black arrows***) and corresponding flow field (in red) for a* **(a)** *'pusher' and a* **(b)** *'puller'. A rotation by $\frac{\pi}{2}$ accompanied by changing the sign of the dipole $\zeta \to -\zeta$ transforms the extensile system in a contractile with the same velocity field, and viceversa. Note that the force 'stresslet' generated is independent of the symmetry of the particle, that is, it is the same in the polar and nematic case.*

system out of equilibrium. Furthermore, being the active force in terms of a stress divergence, which is appropriate for an internal force in a fluid. It can be plugged into the Navier-Stokes equation (2.11) for the fluid to give:

$$\partial_t u_i + u_j \partial_j u_i = \eta \partial_j \partial_j u_i - \partial_i P + \partial_j \sigma_{ij}^{\text{act}} + \partial_j \sigma_{ij}^{\text{pass}}, \tag{2.37}$$

where σ^{pass} is the elastic stresses generated by the liquid-crystalline nature of the fluid. For a system with polar symmetry:

$$\begin{aligned} \sigma_{ij}^{\text{pass}} = \; & \frac{1}{2}(p_i h_j - p_j h_i) - \frac{\partial f}{\partial(\partial_j p_k)}\partial_i p_k - \frac{\xi}{2}(p_i h_j + p_j h_i) \\ & - \frac{\partial f}{\partial(\partial_j \phi)}\partial_i \phi + (f - \mu\phi)\delta_{ij}. \end{aligned} \tag{2.38}$$

The first two terms of (2.38) are the elastic stresses arising from distortions in the polar field, from the theory of liquid crystals [67, 73]. The term proportional to ξ arises from the aligning or tumbling of the director profile $\boldsymbol{p}$ in response to shear flow [44]. The fourth and fifth terms are interfacial terms, characterizing the stress contribution from surface tension arising between domains with different density [39, 74].

For a nematic fluid, $\sigma_{ij}^{\text{pass}}$ is a function of the nematic tensor, and reads [71]:

$$\sigma_{ij}^{\text{pass}} = \xi\Sigma_{ijkl}H_{kl} + T_{ijkl}H_{kl} - \frac{\partial f}{\partial(\partial_j Q_{kl})}\partial_i Q_{kl} + (f - \mu\phi)\delta_{ij} - \frac{\partial f}{\partial(\partial_j\phi)}\partial_i\phi, \quad (2.39)$$

where H_{ij} is the molecular field (2.30) and the two tensors $\mathbf{\Sigma}$ and $\mathbf{T}$ are defined in (2.31). Similarly to the polar case, the first term is the aligning/tumbling contributions to the stress, the second and third terms keep track of nematic distortions, while the fourth and the fifth are the interface contributions.

2.3 Lattice Boltzmann Method

We have laid down the set of equations for the hydrodynamic theory of an active fluid, which consist of a concentration, an orientation and a momentum equation, as show in Table 2.1. In addition to these, one should include the mass

Table 2.1 *Equations of motion for the concentration ϕ, the director profiles $\boldsymbol{p}$ or $\mathbf{Q}$, and the fluid momentum $\boldsymbol{u}$.*

polar	nematic
$\partial_t\phi + \partial_j(\phi u_j) = M\partial_j\partial_j\frac{\delta\mathcal{F}[\phi,\boldsymbol{p}]}{\delta\phi}$	$\partial_t\phi + \partial_j(\phi u_j) = M\partial_j\partial_j\frac{\delta\mathcal{F}[\phi,\mathbf{Q}]}{\delta\phi}$
$D_t p_i = (\xi\Lambda_{ij} - \Omega_{ij})p_j - \Gamma h_i.$	$D_t Q_{ij} = -\xi\Sigma_{ijkl}\Lambda_{kl} - T_{ijkl}\Omega_{kl} - \Gamma H_{ij}$
$(\partial_t + u_j\partial_j)u_i = \partial_j\sigma_{ij}^{\text{act}}(\boldsymbol{p}) + \partial_j\sigma_{ij}^{\text{pass}}$	$(\partial_t + u_j\partial_j)u_i = \partial_j\sigma_{ij}^{\text{act}}(\mathbf{Q}) + \partial_j\sigma_{ij}^{\text{pass}}$

conservation equation for the density ρ

$$\partial_t\rho + \partial_i(\rho u_i) = 0, \quad (2.40)$$

If the fluid is considered to be incompressible, this reduces the dynamics for the density to equation (2.12), namely the incompressibility constraint:

$$\partial_i u_i = 0. \quad (2.41)$$

The most common liquids have a bulk moduli in the order of magnitude of $10^9 \div 10^{11} N/m^2$, which makes them to most effects incompressible.

Numerically integrating the coupled equations for $\boldsymbol{u}, \phi$ and $\mathbf{Q}$ or $\boldsymbol{p}$ can be a challenging computational task; furthermore, a brute-force discretisation of the equations will not, in general, satisfy the incompressibility condition (2.41) at all

times[5], and more sophisticated iterative and computationally expensive schemes are required [75].

The Lattice Boltzmann Method provides a reasonable compromise by slightly relaxing the incompressibility condition, allowing very small variations of the density ρ. The trade-off is a non-iterative, simple and efficient scheme, that in addition lends itself to treating efficiently multiphase fluids. The Lattice Boltzmann Method, or LBM, is based on the evolution of a set of probability distribution functions f_α on a suitable discrete lattice. The change in f_α is local, and can be defined by a Boltzmann-like collision operator with the neighbouring f_α's. The averages of the f_α's define hydrodynamic fields ρ and $\boldsymbol{u}$, which can be shown to satisfy the continuity and momentum equations for a fluid (2.40),(2.11). What LBM effectively does is "solving the Navier-Stokes equation by playing billiard on a chequerboard" [76].

We will present the constitutive equations and some features of the LBM; more details can be found in [77–82]. In our work, we made an extensive use of a Hybrid Lattice Boltzmann (HLB) scheme for active fluids; the HLB was originally developed by Swift *et al.* [77, 78] to include the thermodynamics of a two-phase non-ideal fluid, by defining a suitable free-energy, from which a non-ideal equation of state for the pressure P follows. This treatment can be extended to a generic free energy $\mathcal{F}$ defined by some order parameter ϕ that evolves in time with a suitable equation, such as the ones defined by model A and B, namely equations (2.3),(2.7). The dynamics for the phase field order parameters are then integrated separately, and coupled to the LBM via their contribution to the stress tensor.

2.3.1 Lattice Boltzmann Equation

Boltzmann kinetic equation describes the time evolution for the density distribution function $f(\boldsymbol{x}, \boldsymbol{v}; t)$ of a diluted gas:

$$\partial_t f + v_i \partial_{x_i} f + \frac{F_i}{m} \partial_{v_i} f = \mathcal{L}_{\text{coll}}[f, f]. \tag{2.42}$$

The distribution f is defined on the phase space of the system, and it denotes the number density of particles of mass m with velocity $\boldsymbol{v}$ at position $\boldsymbol{x}$ at time t;

[5]This issue is also referred to as the 'pressure-velocity coupling problem'.

here $\boldsymbol{F}$ is the force acting on the gas particles. The explicit form of the bilinear collision operator $\mathcal{L}_{\text{coll}}$ keeps into account the variations of f from elastic binary collisions that 'bounce' particles from neighbouring regions in the phase space. $\mathcal{L}_{\text{coll}}$ can be shown to have a zero for an equilibrium distribution $f = f^{eq}$, this being the Maxwell-Boltzmann distribution:

$$f^{eq}(\boldsymbol{x}, \boldsymbol{v}; t) = \left(\frac{m}{2\pi k_B T(\boldsymbol{x}, t)} \right)^{\frac{3}{2}} \frac{\rho(\boldsymbol{x}, t)}{m} \mathrm{e}^{-\frac{m(\boldsymbol{v}-\boldsymbol{u}(\boldsymbol{x},t))^2}{2k_B T(\boldsymbol{x},\boldsymbol{v};t)}}, \tag{2.43}$$

where the $\rho, \boldsymbol{u}$ and T are density, velocity and temperature fields, defined as the zeroth, first and second order moments of f in $\boldsymbol{v}$:

$$\rho(\boldsymbol{x}, t) = m \int \mathrm{d}\boldsymbol{v} f(\boldsymbol{x}, \boldsymbol{v}; t), \tag{2.44}$$

$$\boldsymbol{v}(\boldsymbol{x}, t) = \frac{1}{\rho(\boldsymbol{x}, t)} \int \mathrm{d}\boldsymbol{v} f(\boldsymbol{x}, \boldsymbol{v}; t) \boldsymbol{v}, \tag{2.45}$$

$$T(\boldsymbol{x}, t) = \frac{2}{3k_B \rho(\boldsymbol{x}, t)} \int \mathrm{d}\boldsymbol{v} f(\boldsymbol{x}, \boldsymbol{v}; t) \boldsymbol{v} \cdot \boldsymbol{v}. \tag{2.46}$$

The distribution (2.43) is also known as local Maxwell distribution, and it does not generally satisfy equation the Boltzmann equation, if not in the case of constant and homogeneous $\rho, \boldsymbol{v}, T$. The latter case corresponds to the Maxwell equilibrium distribution. Effectively, equation (2.42) relaxes the system to the equilibrium distribution.

A linearised version of $\mathcal{L}_{\text{coll}}$ is made in the Bhatnagar-Gross-Krook (BGK) approximation, where equation (2.42) reduces to:

$$\left(\partial_t + v_i \partial_{x_i} + \frac{F_i}{m} \partial_{v_i} \right) f = -\frac{f - f^{eq}}{\tau}, \tag{2.47}$$

where f^{eq} is the local Maxwell distribution in equation (2.43); here τ is the characteristic relaxation time of the gas molecules. It is possible to obtain the Navier-Stokes equations (2.11),(2.40) from a Chapman-Enskog expansion of the moments in $\hat{v}$ of equation (2.47) in the low Mach number limit [35, 83]:

$$\partial_t \rho + \partial_i (\rho u_i) = 0, \tag{2.48}$$

$$\rho(\partial_t + u_j \partial_j) u_i = -\partial_i P + \partial_j (2\eta \Lambda_{ij}) + \boldsymbol{F}, \tag{2.49}$$

with $\Lambda_{ij} = \frac{\partial_i u_j + \partial_j u_i}{2}$ being the shear rate. These are the equations for a compressible fluid; the pressure obeys the equation of state for an ideal gas,

with $P = \frac{\rho k_B T}{m}$. The fluid viscosity is found to be:

$$\eta = \frac{\tau \rho T}{m}. \tag{2.50}$$

One must note that, in general, compressible fluids would have an isotropic term $\delta_{ij}\mu\partial_k u_k$ in the viscous stress, with known as bulk viscosity. However, this does not emerge from the BGK model, as there is one single relaxation time, which in turn gives only the shear viscosity. Compressive viscosity can be effectively introduced - and independently controlled - by considering a generalization of the BGK model, with multiple relaxation times, as presented by d'Humieres *et al.* [84].

The Lattice Boltzmann equation is obtained from discretising (2.47) in the phase space: every point in the space is on a lattice, and so are the velocities allowed; $f(\boldsymbol{x}, \boldsymbol{v}; t)$ is replaced by a set of f_α's, $(\alpha = 1, ..., Q)$, representing the expected number of particles travelling along the discrete velocity direction $\boldsymbol{e}^\alpha$. In principle one could make use of all the possible connecting the spacial lattice points in the unit of time. However, it can be shown that a handful is more than sufficient to correctly reproduce the correct hydrodynamic behaviour for the moments ρ and $\boldsymbol{u}$, which are now defined as:

$$\rho(\boldsymbol{x}, t) = \sum_{\alpha=1}^{Q} f_\alpha, \tag{2.51}$$

$$\boldsymbol{u}(\boldsymbol{x}, t) = \frac{1}{\rho(\boldsymbol{x}, t)} \sum_{\alpha=1}^{Q} \boldsymbol{e}^\alpha f_\alpha. \tag{2.52}$$

We have not included the temperature as we are mostly interested in isothermal fluids; in such systems the equilibrium distribution f^{eq} is replaced by a quadratic in ρ and $\boldsymbol{u}$, by truncating at the second order its expansion in Hermite polynomials, and evaluating their Gauss-Hermite quadrature. This procedure has been outlined by Shan *et al.* [85], and it guarantees that the equations for the moments resulting from the Chapman-Enskog expansion of the discrete f_α's are exact in the continuum for moments up to the second order. The Shan procedure also sets a minimal number of discrete velocities $\{\boldsymbol{e}^\alpha\}$, thus identifying the lattice on which f_α is defined. In two and three dimensions, $\{\boldsymbol{e}^\alpha\}$ corresponds to the lattices known as[6] D2Q9 and D3Q15, figure 2.5, table 2.2.

[6]Using the nomenclature proposed by Qian [86].

Table 2.2 *D2Q9 and D3Q15 fundamental cells' nodes, in units of the speed of sound in the ideal fluid, defined in Lattice Boltzmann dimensionless units, where $t' = t/\Delta t$, $v' = v/c_s$, $c_s^2 = 1/3$. The speed of sound c_s is set for convenience to $1/\sqrt{3}$.*

D2Q9	D3Q15
$e^0 = (0,0)$	$e^0 = (0,0)$
$\boldsymbol{e}^{1,3} = (\pm 1, 0)$, $\boldsymbol{e}^{2,4} = (0, \pm 1)$	$\boldsymbol{e}^{1,3} = (\pm 1, 0, 0)$, $\boldsymbol{e}^{2,4} = (0, \pm 1, 0)$, $\boldsymbol{e}^{5,6} = (0, 0, \pm 1)$
$\boldsymbol{e}^{5-8} = (\pm 1, \pm 1)$	$\boldsymbol{e}^{7-10} = (\pm 1, \pm 1, 1)$, $\boldsymbol{e}^{11-14} = (\pm 1, \pm 1, -1)$

Truncations at higher order in the Shan procedure do not contribute significantly to lattice models for single component isothermal ideal fluid. However, higher orders - and correspondingly bigger sets of lattice vectors $\{\boldsymbol{e}^\alpha\}$ - can be required for the Thermal Lattice Boltzmann [87], or for higher precision in multiphase schemes [88]. In this thesis, we will consider isothermal LBM's, where T is constant.

It is convenient to consider dimensionless quantities: we redefine times in terms of the integration step Δt, $t' = \frac{t}{\Delta t}$, speeds in term of the speed of sound $c_s = \sqrt{\frac{k_B T}{m}}$, $v' = v/c_s$, and take the mass of the fluid's particles m to be unitary. Once the Boltzmann equation is expressed in dimensionless units, and discretized on an

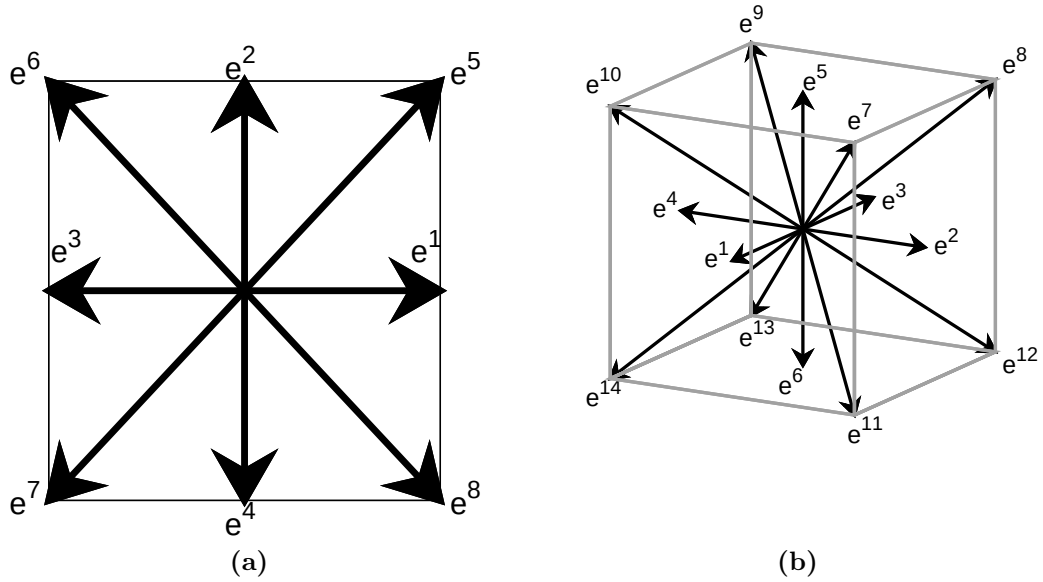

Figure 2.5 **(a)** *D2Q9 lattice velocities.* **(b)** *D3Q15 lattice velocities. See table (2.2) for reference.*

appropriate lattice $\boldsymbol{e}^\alpha$, the Lattice-Boltzmann equation reads:

$$f_\alpha(\boldsymbol{x}+\boldsymbol{e}^\alpha, t+1) - f_\alpha(\boldsymbol{x}, t) = -\frac{1}{\tau}(f_\alpha(\boldsymbol{x}, t) - f_\alpha^{eq}(\rho, \boldsymbol{u})) + g_\alpha(\boldsymbol{x}, t). \tag{2.53}$$

The discrete equilibrium distributions read:

$$f_\alpha^{eq} = w_\alpha \rho \left(1 + \frac{u_i e_i^\alpha}{c_s^2} + \frac{u_i u_j (e_i^\alpha e_j^\alpha - c_s^2 \delta_{ij})}{c_s^4}\right). \tag{2.54}$$

Here w_a are the weights resulting from the Gauss-Hermite quadrature, ρ and $\boldsymbol{u}$ are the local density and velocity, and c_s is the speed of sound in the fluid. Altogether with the LB time step Δt, c_s defines the units of lattice. For D2Q9 and D3Q15 lattices, it is convenient to defice $c_s = 1/\sqrt{3}$, as the zero of the Hermite polynomials for the construction of this lattices are $\sqrt{3}$ away from the origin; thus, with this choice of c_s, the lattice spacing becomes unitary.

The term g_α on the right hand side of equation (2.53) accounts for the effect of volume forces acting on the the fluid, and its is determined by the constraints imposed by the Chapman-Enksog expansion, as discussed by Guo *et al.* [89]:

$$g_\alpha = \left(1 - \frac{1}{2\tau}\right) w_\alpha \left(\frac{e_i^\alpha - u_i}{c_s^2} + \frac{e_j^\alpha u_j u_i}{c_s^4}\right) F_i, \tag{2.55}$$

It has to be noted that g_α introduces a shift in the Chapman-Enskog expansion for the hydrodynamics velocity field, thus resulting in the macrodynamic fluid equations being satisfied by $\boldsymbol{u}'$, defined by:

$$\begin{aligned} \rho \boldsymbol{u}' &= \sum_{\alpha=1}^{Q} f_\alpha \boldsymbol{e}^\alpha + \frac{\Delta t}{2}\boldsymbol{F} \\ &= \rho \boldsymbol{u} + \frac{\Delta t}{2}\boldsymbol{F}. \end{aligned} \tag{2.56}$$

The link to the hydrodynamics comes, just as for the BGK continuum equation (2.47), from the moments in the discrete velocities $\boldsymbol{e}^\alpha$ of equation (2.53). Summing over α equation (2.53) times $\boldsymbol{e}^\alpha$ leads to the Navier-Stokes equation (2.49), up to order $\mathcal{O}(\mathrm{Ma}^3)$. The resulting dynamic viscosity reads:

$$\eta = \rho c_s^2 \left(\tau - \frac{1}{2}\right), \tag{2.57}$$

which is equivalent to equation (2.50), except for the extra $\frac{1}{2}$ term that arises from

the discretization. The pressure is once again the one for an ideal gas, $P = \rho c_s^2$.

2.3.2 Hybrid Lattice Boltzmann

In this thesis we considered the LBM as a tool for numerically integrating the hydrodynamics of polar and nematic suspensions. However, the original LBM arises from an approximation valid for disperse mono-atomic gases, and not for elongated bodies. Furthermore, we have the need to describe situation in which there is more than one phase, which is a situation far from the ideal gas. Fortunately, several Lattice Boltzmann schemes exist that present different techniques to deal with non-idealities, multiple phases, or recovering correct thermodynamic behaviours at equilibrium.

Non-ideal interactions can be engineered in equation (2.53) in different fashions: by rewriting phenomenologically the collision operator [90]; by considering a mean-field inter-particle interaction [91, 92]; or by defining a thermodynamically consistent free-energy approach in the body-force term g_α in equation (2.53) [77, 78, 93, 94]. Of these approaches, we considered the latter, as it is of great convenience to deal with, as we already rely on a free-energy approach for defining the dynamics of the directional order parameters.

In our works, the free energy $\mathcal{F}$ will be in general a functional of a concentration parameter ϕ and an order parameter, this being $\boldsymbol{p}$ for polar systems or $\mathbf{Q}$ for nematic. We will consider the specific form that $\mathcal{F}$ takes in the following chapters.

While the LBM is versatile enough to obtain an equation for heat transport in thermal hydrodynamics [79, 95], there is not a simple and efficient 'recipe' for constructing a lattice kinetic theory in the fashion of equation (2.53) that, in the macroscopic limit, is equivalent to an arbitrary set of partial differential equations. Therefore, in the most efficient existing LB algorithrms, equations that are not related to the kinetics of the underlying microscopic Boltzmann gas must be integrated separately with a different scheme – hence the resulting scheme being known as Hybrid LB.

In our work, we solved numerically equations (2.27),(2.28) and (2.29) with an explicit Euler scheme; again, in terms of the dimensionless Lattice Boltzmann units for times $t' = t/\Delta t$ and lengths $l' = l\Delta t/c_s$, the nematic/polar concentration

and order parameter discrete equations are given by:

$$\begin{aligned}
\phi(\boldsymbol{x}, t+1) &= \phi(\boldsymbol{x}, t) - (u_j \partial_j)_{\text{upw.}} \phi + M(\partial_j \partial_j)_{\text{discr}} \frac{\delta F}{\delta \phi}, && (2.58)\\
p_i(\boldsymbol{x}, t+1) &= p_i(\boldsymbol{x}, t) - (u_j \partial_j)_{\text{upw.}} p_i - p_j (\Omega_{ij})_{\text{upw.}} + \xi p_j (\Lambda_{ij})_{\text{upw.}} && (2.59)\\
&\quad -\Gamma h_i && (2.60)\\
Q_{ij}(\boldsymbol{x}, t+1) &= Q_{ij}(\boldsymbol{x}, t) - (u_k \partial_k)_{\text{upw.}} Q_{ij} - T_{ijkl} (\Omega_{kl})_{\text{upw.}} \\
&\quad -\xi \Sigma_{ijkl} (\Lambda_{kl})_{\text{upw.}} - \Gamma H_{ij} && (2.61)
\end{aligned}$$

were we have replaced the laplacian with its discrete equivalents; the choice of discretization can be made sensible by picking the derivatives on a lattice that minimize the spurious currents that plague non-ideal LBM's (see [96]). The advective terms streaming the order parameters along $\boldsymbol{u}$ can be appropriately discretized with a third order upwind scheme for all the $\partial_i u_j$ contributions: this choice ensures a correct treatment of advective terms and minimises numerical diffusion [97].

Chapter 3

Spontaneous motility of inverse passive droplets in polar fluids in two dimensions

The entirety of eukaryotic cells contains a large number of different proteic filaments, of different shapes and sizes. They constitute a large part of the cytoskeleton, provide the cell with a structural support that affects its shape and rigidity. Furthermore, they take part in many cellular processes, ranging from cell division, endocytosis and exocytosis, and they are functional for the transport of cellular material such organelles and vesicles through the inside of the cell.

In the general framework of active matter, the dynamics of filamentous networks have been considered to be crucial for the understanding of several biophysical processes. The reason why filaments have attracted this much interest is due to a few important factors: on one hand, they are omnipresent in every eukaryotic cell, and they are considered to be a prototypical example of anisotropic active fluid; their dynamics are qualitatively and quantitatively fairly well described by a liquid-crystal-like hydrodynamic theory, that captures several essential features, such as defects formation and dynamics [98–100], active turbulence [30, 31, 101], and that at the same time can be considered a general enough theory to be suitable to describe the physics of other biological systems, such as cell ordering in bacterial suspensions [102]. On the other hand, filamentous networks dynamics seem to have a key role in cell motility [70, 103–107], and constitute a possible

vast class of building blocks for potential man-made biological active materials, as it has been shown that their dynamics can be controlled to form non-trivial flow patterns [98, 108, 109]. The possibility of crafting biological micromachines is fascinating, as it could possibly open routes to creating a whole new class of materials, whose potential is still to be explored [33, 110].

Actin represents a large part of the filaments that can be found in the cell. It consists of oriented globular protein monomers (G-actin) that can polymerise in flexible thread-like structures, known as F-actin; these filaments are a double helical polymer of a length typically in the order of the μm. F-actin has two distinct (+) and (-) end, effectively making the filament polar. Filamentous actin can be found in high concentration in proximity of the cellular membrane, where it assembles in bundles cross-linked by myosins, a family of protein motors. Myosins have a binding site for actin, and they can 'tread' along filaments with their 'head' by ATP hydrolysis. This process effectively exerts a force on the actin filaments connected to the myosin, which start sliding along their axis; effectively myosin contracts the bundles, exerting a contractile stress; extensile effects can be neglected, as the filaments can bend, as discussed by [41].

The actin and myosin networks, also known as acto-myosin, take part in the formation of pseudopia, tendril-like extensions of the cell that allow it to adhere to substrates and later contract, thus allowing a crawling motion. They have been identified as one of the prime agents in cell migration, through either a rapid actin polymerisation [111] dubbed 'treadmilling', or by just exploiting the contractile stresses to break the symmetry of the cell shape, thus creating a non-symmetric stress distribution that effectively polarises the cell, that allows the cell to move in a favoured direction [106]. The latter mechanism can be translated mathematically into a model that can give rise to different types of motions in two or three dimensions [70, 112].

Microtubules are another class of proteic filaments; compared to F-actin, they are stiffer than myosin, and can be up to 50μm in length. Their building blocks are tubulins, and just as their actin equivalents, they are polar, with a (+) and (-) end. They take part in cell division, and provide a support for pseudopodia to contract on, effectively cooperating with actin; and similarly to actin, they have binding sites for kinesin and dyneins, two different superfamilies of protein molecular motor that can tread along the filaments, exerting an overall extensile stress.

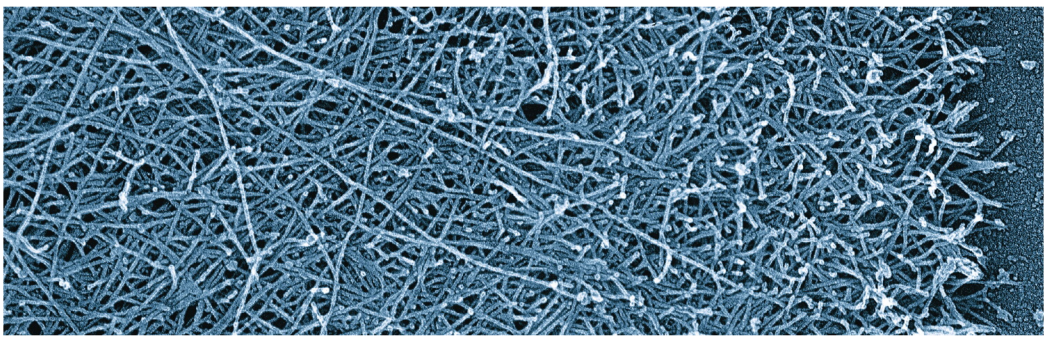

Figure 3.1 *Micrograph of an actin network extracted from a Triton keratocyte, adapted from Pollard et al., Cell, 2003.*

Actin and microtubules take part in several other processes, such as muscle fiber contraction, or cilia and flagella formation; however, we are principally interested in the transport phenomena to which they are associated; intracellular movement of organelles and vesicles happens prevalently along cytoskeletal filaments, allowing the motion to be faster compared to diffusive motion, and more efficient and well coordinated thanks to the defined polarisation of the filaments [103, 113–115].

In this part of our work, we have considered networks of filaments and molecular motor to be a continuum polar contractile or extensile fluid, for acto-myosin and microtubules, respectively. This minimal model relies on the filaments being characterized by a defined orientation, having a plus end (head) and a minus end (tail); including the effects of the motors as an active contractile/extress stress distribution can give rise to spontaneous motile states, both in the filamentous network and in the surrounding medium. In our model, we consider a mixture of two distinct phases in two dimensions: the first is a droplet of isotropic passive fluid, embedded in the second, a polar extensile or contractile fluid, prevalently in a nematically ordered state. We hypothesise that, if an asymmetric stress distribution configuration is achieved at the surface of the droplet, the latter can be 'spontaneously' moved in a favoured direction. What we propose is a potential mechanism for active filaments to give rise to motile steady states in passive media. In the following, we will discuss how droplets of a non-active fluid can be transported by surrounding active polar fluids. We investigated different cases of 'inverse-droplets', allowing the stress to be both contractile, as it is for acto-myosin, or extensile, for kinesins/dyneins and microtubules. We also considered the effect of the boundary conditions at the interface between the active and the passive medium; as we observed in numerical simulations,

orientation of the polar field at the interface changes dramatically the dynamics, making the droplets more susceptible to either contractile or extensile stresses when the polarisation is respectively perpendicular or parallel to the droplet.

3.1 Microfilaments as a polar active fluid

F-actin is a polar filament, having two distinct ends that can both polymerise and de-polymerise; depending on the concentration of actin monomers in the cell cytoskeleton, the rate at which either end gains or loses monomers can be tuned. Similarly, microtubules polymerise at both their ends, and it prevalently does so at its (+) end. This is an essential aspect in tread-milling mechanics; however, as we are interested in an entirely different process (that effect of contractile and extensile stresses on filament suspensions), we will neglect this aspect, considering just the bulk of the filamentous network of very long filaments; in this case, we can consider the net polymerisation and de-polymerisation rates to be null. We make the further assumption, for the sake of simplicity, that the concentration of bound molecular motors is on average the same along the filaments, so that the concentration of myosin/kinesin-dyneins can be in first approximation considered to be proportional to the concentration of the filaments. In this way, we can use equation 2.36 as a reasonable approximation for the contractile stress exerted by the motors.

In the following we will denote the concentration of the polar filaments as ϕ, the average orientation as $\boldsymbol{p}$, and the hydrodynamic fields with the conventional ρ and $\boldsymbol{u}$ for the density and the momentum, respectively.

From now on, we will describe the free energy of the active and the passive fluids as $\mathcal{F}$, namely:

$$\begin{aligned}\mathcal{F}[\phi,\boldsymbol{p}] \;=\; & \int\Bigg\{\frac{a}{4}(\phi-\phi_0)^2\phi^2+\frac{k}{2}\partial_i\phi\partial_i\phi+\frac{\kappa}{2}\partial_k p_i\partial_k p_i \\ & +\alpha\left(\frac{\boldsymbol{p}^4}{4}-\left(\phi-\frac{\phi_0}{2}\right)\boldsymbol{p}^2\right)+\beta_\perp p_i\partial_i\phi+\beta_\parallel(p_i\partial_i\phi)^2\Bigg\}\mathrm{d}^2\boldsymbol{x}\end{aligned} \tag{3.1}$$

This free energy combines two principal contributions: the first two terms, which stem from a typical binary fluid formalism, and the remaining part which is

borrowed from liquid crystal theory. In particular, the first term of equation (3.1) is a double well potential allowing bulk phase separation into a dense and dilute phases of filaments, corresponding to bulk of the network ($\phi \sim \phi_0$) and to the passive medium devoided of the filaments ($\phi \sim 0$). The second term creates an interfacial tension between these phases, whose strength depends on k.

The remaining terms in the free energy (the ones taken from liquid crystals) are made up of three different contributions: the term quadratic in the gradients of p_i creates an elastic penalty for local distortions of the polar order, within the 'one constant' approximation, with κ the resulting single elastic constant. The terms multiplied by the factor α are the bulk free energy associated with the polar phase, which contains terms in the polarisation $\boldsymbol{p}$ up to the fourth order. In the quadratic contribution, which also depends on ϕ_0, $\phi_0/2$ is the critical concentration for the transition from isotropic ($|\boldsymbol{p}| = 0$) to polar ($|\boldsymbol{p}| > 0$) states. This ensures that orientational order only arises in the bulk of the filamentous network, once equilibrium values of the concentration and polarisation are obtained by minimizing the free energy.

Finally, the last two terms take into account the boundary conditions for the polarisation at the interface between the dense and dilute phase. We will refer from now on to these as the anchoring terms. The term in $\beta_\perp$ favours the orientation of the filaments to be perpendicular (*homeotropic*) to the interface with the isotropic fluid: at the interface between the polar and the isotropic fluid, $\boldsymbol{p}$ will point towards the former if $\beta_\perp < 0$ and towards the latter if $\beta_\perp > 0$. A second term, quadratic in $\boldsymbol{p}$ and in the gradient of ϕ, needs to be included when tangential (planar) anchoring is required. Such anchoring arises when $\beta_\perp = 0$ and $\beta_\parallel$ is positive. The magnitude of $\beta_\perp$ and $\beta_\parallel$ controls the anchoring strength; we assume strong alignment throughout this chapter.

It has to be noted that the two anchoring terms are proportional to gradients of ϕ, thus making them contribute to the surface tension of the droplet. For a standard binary fluid described by a free energy that consists only of the first two terms of equation (3.1), the surface tension can be found to be proportional to $\sqrt{ka}$ [116], sometimes also expressed in the form k/ξ_I, where $\xi_I = \sqrt{k/a}$ is the "thickness" of the diffuse interface. Adding the third and fourth term leads to a slightly different result, with the surface tension scaling[1] as $\gamma \sim (k + \kappa/8)/\xi_I$. However, the addition of the terms in $\beta_\perp$ and $\beta_\parallel$ can potentially lead to some changes if

[1]This result can be obtained assuming a strong coupling α, hence $p_i p_i \simeq (\phi - \phi_0/2)$.

these coefficients are not positive, as that could contribute as an effective negative surface tension, leading to instabilities in the integrity of the two phases, and to changes in the effective value of the equilibrium value of the concentration and of the polar fields; this effect can be controlled by opportunely tuning the other parameters, ensuring that the overall surface remains stable.

The dynamics for the fields follow equations (2.10), (2.28) and (2.11): the concentration field ϕ is therefore conserved, and altogether with the polarisation field $\boldsymbol{p}$, it is advected by the overall velocity field of the fluid mixture. Once again, these equations read:

$$\partial_t \phi + \partial_k(\phi u_k) = M \partial_k \partial_k \mu, \tag{3.3}$$

$$\partial_t p_i + u_k \partial_k p_i = -\Omega_{ij} p_j + \xi \Lambda_{ij} p_j - \frac{1}{\Gamma} h_i, \tag{3.4}$$

These equations describe the dynamics of the polar active fluid concentration and orientation. Here M is the a mobility coefficient for the concentration, μ is the chemical potential, once again:

$$\mu = \frac{\delta \mathcal{F}}{\delta \phi} = \frac{\partial f}{\partial \phi} - \partial_i \frac{\partial f}{\partial(\partial_i \phi)}, \tag{3.5}$$

where f is the free energy density. Ω_{ij} and Λ_{ij} are the anti-symmetric and symmetric velocity gradients tensors, ξ is the shear-aligning parameter, Γ is the rotational viscosity, h_i is the molecular field, which reads similarly to the chemical potential:

$$h_i = \frac{\delta \mathcal{F}}{\delta p_i} = \frac{\partial f}{\partial p_i} - \partial_k \frac{\partial f}{\partial(\partial_k p_i)}. \tag{3.6}$$

Alongside the latter, some equations for the density and momentum are required, in the form of the standard incompressible Navier-Stokes equations, which in addition include the effects of the elastic properties of the polar phase, interface contributions to the stress tensor, and active stresses altogether;

$$\rho(\partial_t u_i + u_k \partial_k u_i) = -\partial_i P + \eta \partial_k \partial_k u_i + \partial_j \sigma_{ij}^{\text{act}} + \partial_j \sigma_{ij}^{\text{pass}}, \tag{3.7}$$

$$\partial_i u_i = 0. \tag{3.8}$$

Here the active stress σ_{ij}^{act} is:

$$\sigma_{ij}^{\text{act}} = \zeta \phi p_i p_j, \tag{3.9}$$

where ζ is the strength of contractile/extensile dipolar force operated by the motors. The passive stress $\sigma_{ij}^{\text{pass}}$ contains all the elastic contributions from the anisotropic nature of the fluid, as well as the interfacial tension terms. See Chapter 2 for more detail.

Table 3.1 *Correspondence between simulations and typical values of the physical units. This choice of parameters is made to be consistent with physical estimates from literature [9, 10].*

Model parameters (actomyosin)	Simulation units	Physical units
Shear viscosity η	1	1 kPa s
Elastic constant κ	$0.01 \div 0.02$	1-2 nN
Effective diffusivity $D = Ma$	0.004	$0.4\mu\text{m}^2 s^{-1}$
Rotational viscosity Γ	1	1 kPa s
Activity ζ	$0 \div 0.001$	$(0 \div 0.1)$ kPa

3.2 Inverse droplet at equilibrium

Before discussing how an active fluid can transport passive droplets, we are going to briefly summarise the state of such systems at equilibrium, in the absence of activity, that is $\zeta = 0$. What we have in mind is embedding an isotropic passive droplet in a mostly nematically ordered polar phase, that is a polar bulk characterized by a polar vector parallel to the x.

In a polar-isotropic mixture, the two phases coexist divided by a smooth interface, an extended spatial region in which the density profile varies smoothly between the two bulk values of the concentration ϕ_{pol} and ϕ_{iso} characterizing the two fluids. At equilibrium the chemical potential has to be constant across the interface:

$$\mu(\phi_{pol}, \boldsymbol{p}_{pol}) = \mu(\phi_{iso}, \boldsymbol{p}_{iso}) \tag{3.10}$$

In addition, equilibrium implies stationary conditions, therefore all the time derivatives and the flow field $\boldsymbol{u}$ have to be null, which in equation (3.4) leads to:

$$h_i(\boldsymbol{p}_{iso/pol}, \phi_{iso/pol}) = 0 \tag{3.11}$$

The latter equation effectively reads $p_i p_i|_{bulk} \simeq (\phi - \phi_0/2)|_{bulk}$. Provided that the polarisation/concentration coupling α is strong enough, we can assume this to hold at the interface too, thus allowing to evaluate the concentration profile in the region in which changes from one bulk value to the other. It can be found that the presence of the coupling slightly shifts the minima of the double well potential term in equation (3.1) from $\phi = 0, \phi_0$; the bulk values for the density field effectively correspond to the zeroes of the chemical potential μ, namely:

$$\phi_{pol/iso} \simeq \frac{\phi_0}{2}\left(1 \pm \sqrt{1 + \frac{2\alpha}{\phi_0^2 a}}\right) \tag{3.12}$$

Thus the concentration profile across an interface centred on $g = 0$ - where g is the coordinate normal to the interface itself - varies approximately as:

$$\phi(g) \simeq \phi_{iso} + (\phi_{pol} - \phi_{iso}) \tanh(g/\xi_I), \tag{3.13}$$

where $\xi_I = \frac{4}{\phi_0^2}\sqrt{\frac{k}{a}}$ is the interface thickness. The parameters a and k can be tuned appropriately in order to minimize finite size effects; at the same time, stability demands that ξ_I should be, in Lattice Boltzmann units, larger than the computational grid spacing.

While the bulk we consider a uniform polar director along the x axis in the bulk of the polar phase, distortions are expected to arise in proximity of the interface in order to satisfy the strong anchoring condition [7, 117, 118]. For homeotropic anchoring ($\beta_\perp < 0, \beta_\parallel = 0$) the aster configuration of the polar field p_i at the interface corresponds to a $+1$ hedgehog topological defect; to match a defect free pattern in the bulk of the polar phase, an additional defect of topological charge -1 needs to be present in proximity of the passive droplet; figure (3.2) shows this can be realised numerically for a droplet of isotropic fluid immersed in an initially uniform state with $\boldsymbol{p} = (p_x, p_y) = (1, 0)$. The system is intrinsically asymmetric, and in absence of activity ($\zeta = 0$ in equation (3.9)), the defect persists stably at the rear of the droplet; the existence of the defect also generates a region of positive splay ($\nabla \cdot \boldsymbol{p} > 0$) behind the -1 hyperbolic hedgehog defect.

An analytical form for the director profile in figure (3.2) can be given [118]. As the director profile is a unit vector field, it's form can be specified by a single angle field variable $\alpha(\boldsymbol{x})$, such that $(p_x, p_y) = (\cos(\alpha), \sin(\alpha))$. For a passive droplet centred in the origin it is convenient to use polar coordinates; the angle field then

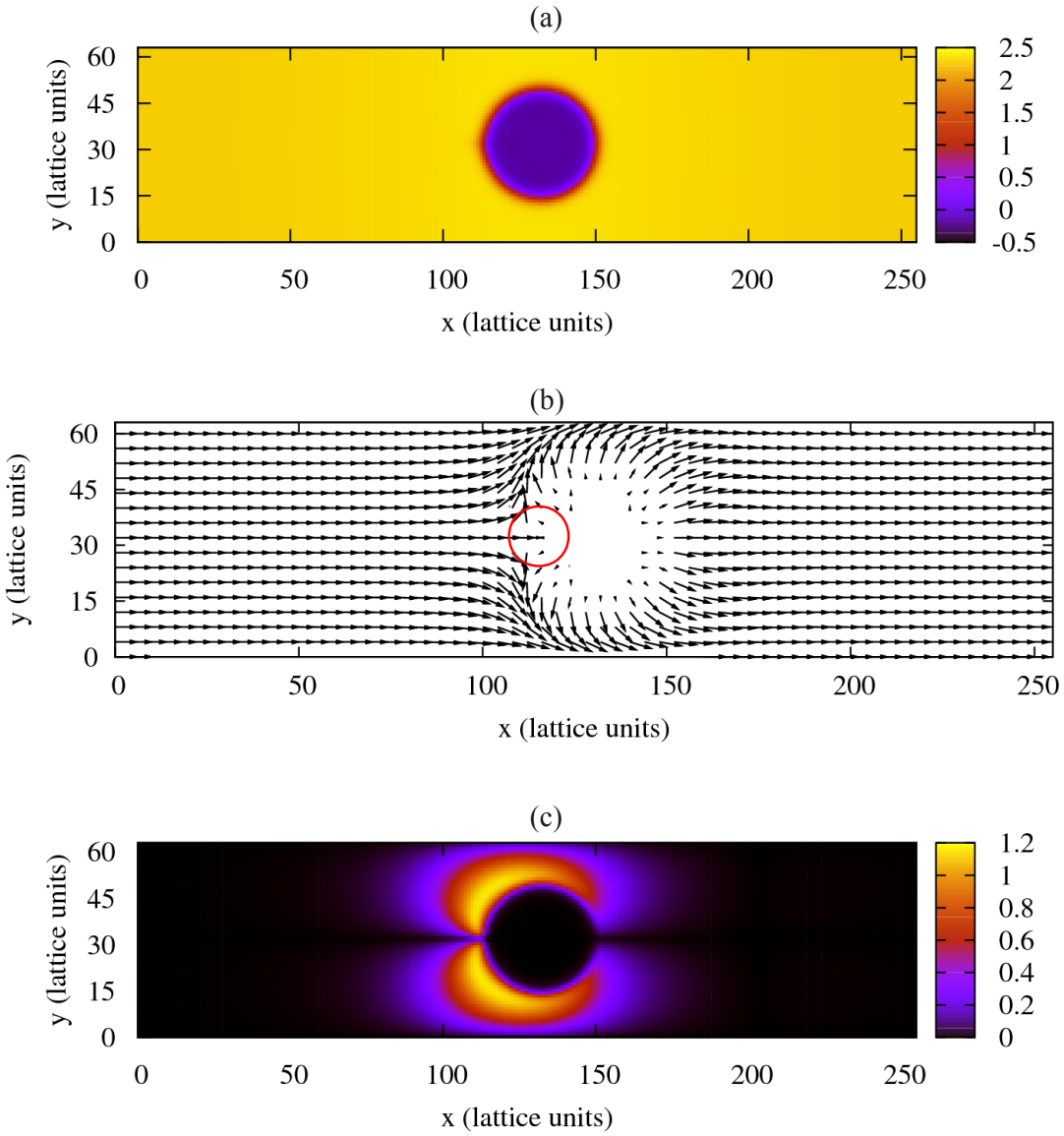

Figure 3.2 **(a)** *Equilibrated concentration field of an isotropic droplet (dark-/purple) in a passive polar liquid crystal (bright/yellow).* **(b)** *Polarisation field outside the droplet. Strong homeotropic (normal) anchoring is set on its surface; a defect of topological charge* -1 *is visible on the left (circled).* **(c)** *Density plot of the absolute value of the y-component of* $\boldsymbol{p}$*. Two bright (yellow) stripes, close to the droplet's surface, identify regions where its value is around 1. We initialised the system with a circular droplet, and with the bulk polarisation in the liquid crystal along the x-direction,* $\boldsymbol{p} = (1, 0)$*, on a lattice of dimensions* $L_x = 256$*,* $L_y = 64$*. The elastic constant is* $\kappa = 0.01$*. In equilibrium, the droplet attains a radius of* $R \simeq 17$*. To ensure strong normal anchoring of* $\boldsymbol{p}$ *at the droplet surface, we chose* $\beta_\perp = 0.01$ *and* $\beta_\parallel = 0$ *in equation (3.1). The remaining parameters are* $a = 0.04$*,* $k = 0.06$*,* $\Gamma = 1$*,* $M = 1$*,* $\phi_0 = 2$*,* $\alpha = 0.1$*,* $\eta = 1$*.*

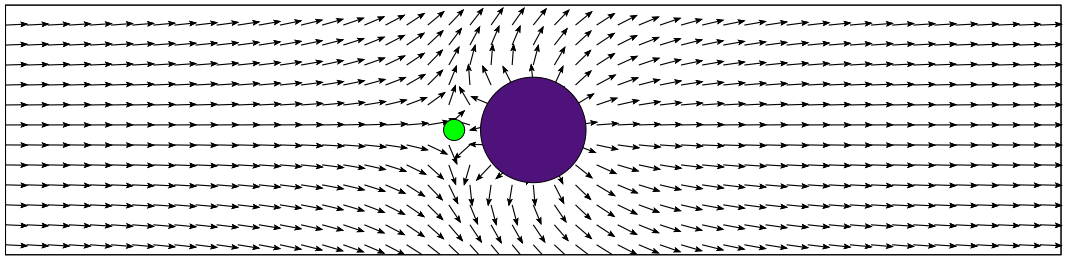

(a)

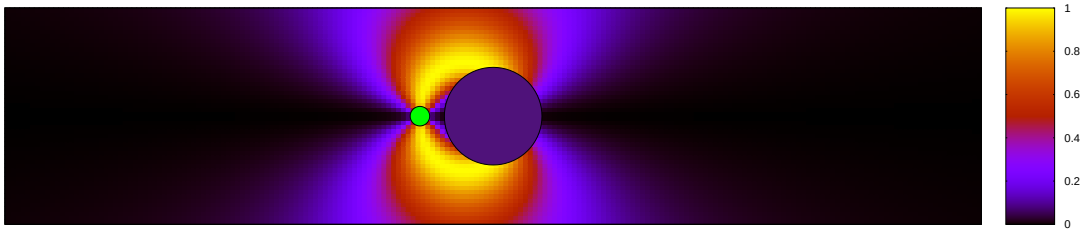

(b)

Figure 3.3 **(a)** *Polarisation* $(p_x, p_y) = (\cos\alpha, \sin\alpha)$ *around a passive droplet (large violet circle), with* $\alpha(r,\theta)$ *defined by equation (3.14). A defect of charge* -1 *emerges at* $(-Rc_0, 0)$ *(small green circle); the angular field* $\alpha(r,\theta)$ *satisfies the homeotropic anchoring, being* $\alpha(r = R, \theta) = \theta$*; compare to figure (3.2b).* **(b)** *Density plot of the absolute value of the* p_y*; compare to figure (3.2c).*

reads:

$$\alpha(r,\theta) = 2\theta - \tan^{-1}\left(\frac{r\sin\theta}{Rc_0 + r\cos\theta}\right) - \tan^{-1}\left(\frac{r\sin\theta}{R/c_0 + r\cos\theta}\right), \qquad (3.14)$$

where R is the radius of the droplet, and Rc_0 is the distance of the -1 defect from the origin; the actual value of c_0 in simulations depends on the elastic properties, these being specified by κ and $\beta_\perp$. The director profile defined by $(\cos(\alpha), \sin(\alpha))$ is shown in figure (3.3a, 3.3b), and compares fairly well to the one obtained from simulations. In addition, $\alpha(r,\theta)$ satisfies the right boundary conditions for the inverse droplet, both at the surface, where $\alpha(r = R, \theta) = \theta$ and far away from the droplet, $\alpha(r \to \infty, \theta) = 0$.

When the anchoring is tangential, the configuration of p_i at the interface between the polar and the passive phase is compatible with a defect free polar phase, as in figure 3.4. This holds only in two dimensions: in three dimensions this configuration would generate two *boojum* defects at the front and the rear of the droplet, as observed by Poulin *et al.* [117, 119] for water droplet in a nematic solution; it has to be noted that for a nematic solvent it is also possible to develop

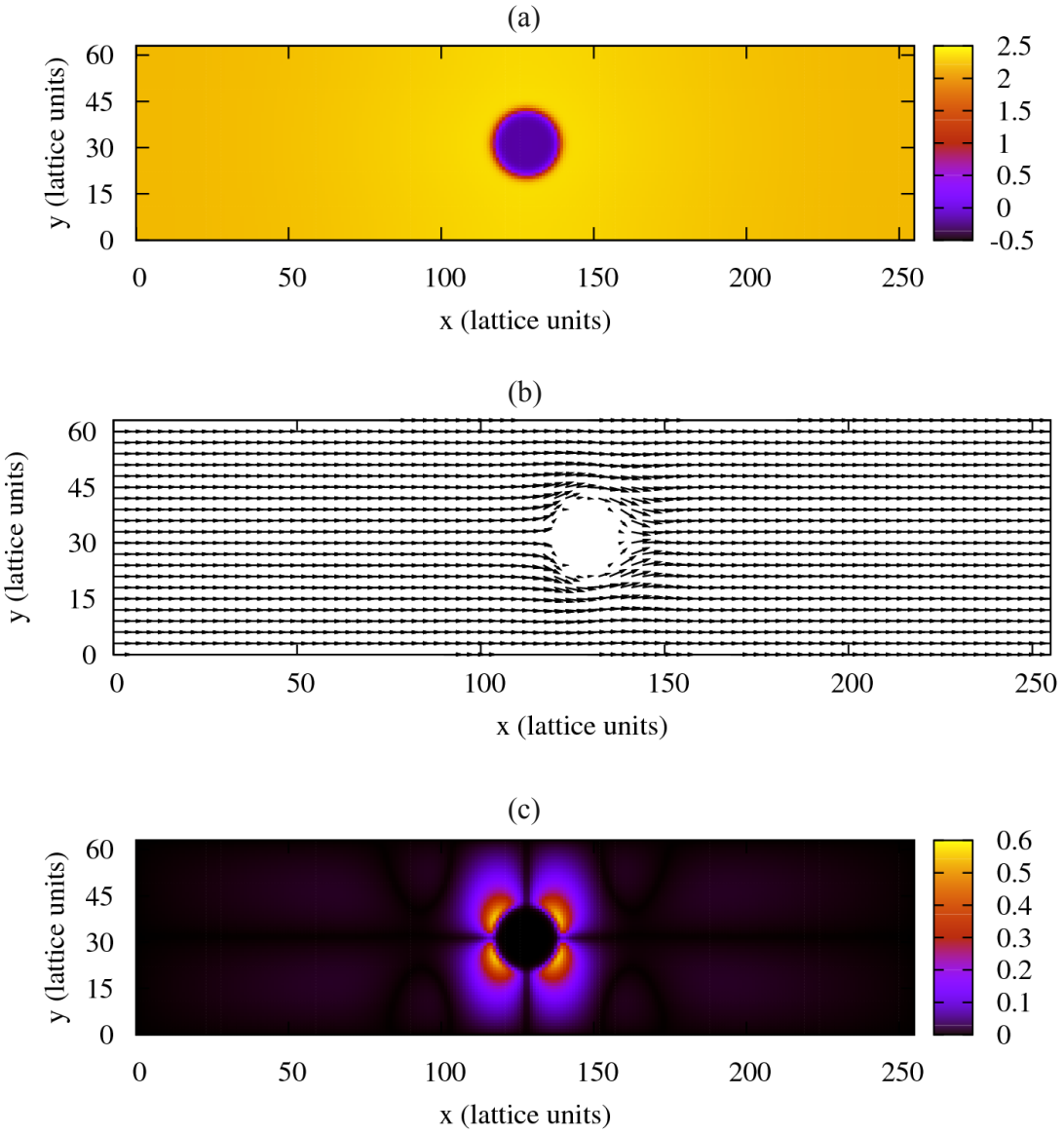

Figure 3.4 **(a)** *Equilibrium density field of an isotropic droplet (dark/purple) in a passive polar liquid crystal (bright/yellow).* **(b)** *Polarisation field outside the droplet. Strong tangential anchoring is set on its surface.* **(c)** *Density plot of the absolute value of the y-component of P. Four almost symmetric bright spots, close to the droplet's surface, identify regions where the polarisation deviates the most from the totally aligned state of the bulk. To set up the simulation, we initialized the droplet as in figure (3.2), with the bulk polarisation in the liquid crystal initially along x. To ensure tangential anchoring, we set* $\beta_\perp = 0$ *and* $\beta_\parallel = 0.01$. *The elastic constant is* $k = 0.01$. *In equilibrium, the droplet attains a radius of* $R \simeq 11$ *(in simulation units). The remaining parameters are* $a = 0.04$, $k = 0.06$, $\Gamma = 1$, $M = 1$, $\phi_0 = 2$, $\alpha = 0.1$, $\eta = 1$.

four distinct defects of charge $+\frac{1}{2}$. However, in the polar case we intend to consider half-integer defects are not topologically stable, and the director profile gently curves around the passive droplet, in a configuration characterized by a higher degree of symmetry compared to the homeotropic case.

3.3 Spontaneous motility of the passive droplet

When there is no activity, the passive droplet reaches an equilibrium condition corresponding to a minimum of the free energy (3.1); as shown in figures (3.2) and (3.4), the equilibrium configuration of the polar director profile $\boldsymbol{p}$ is drastically changing depending on whether the anchoring is chosen to be tangential or homeotropic. The flow field $\boldsymbol{u}$ is negligible everywhere, and the only currents that can be found are spurious finite size effects that plague the Lattice Boltzmann method for multiphase systems [96]. However, this currents are small in magnitude, vanish quickly moving away from the interface, and sum to zero, producing no effective movement of the droplet.

Switching on the activity will result in currents arising, prevalently around regions where the polar profile $\boldsymbol{p}$ is distorted, as in a completely aligned state all the 'stresslets' from the individual dipole sum to zero. Two instabilities, known as 'generic instabilities' [12, 21, 22, 120], arise in active polar fluids in the presence of bending or splay.

In an aligned polar medium, any small amount of splay (or rather, a splay perturbation), is unstable to contractile stress, that is $\zeta < 0$ in the active stress tensor (3.9); the contractile stirring causes the splay to increase, generating a stronger asymmetry in the flow, thus increasing the splay even further, as schematically shown in figure (3.5a). Similarly, any bending perturbation is unstable to extensile stresses ($\zeta > 0$), figure (3.5b). Eventually, the instabilities will produce non-trivial patterns for the polar director $\boldsymbol{p}$ and the hydrodynamic flow $\boldsymbol{p}$. These patterns have been studied by analytical [44, 45] and numerical means [47–49], and their final structure depends on the interplay between the activity and the elastic properties of the polar medium.

In polar-isotropic mixtures the active stress is usually confined to the polar region, which is still susceptible to the generic instability; the latter can generate a net flow and ordered motion in the active phase, making it effectively 'self-motile'.

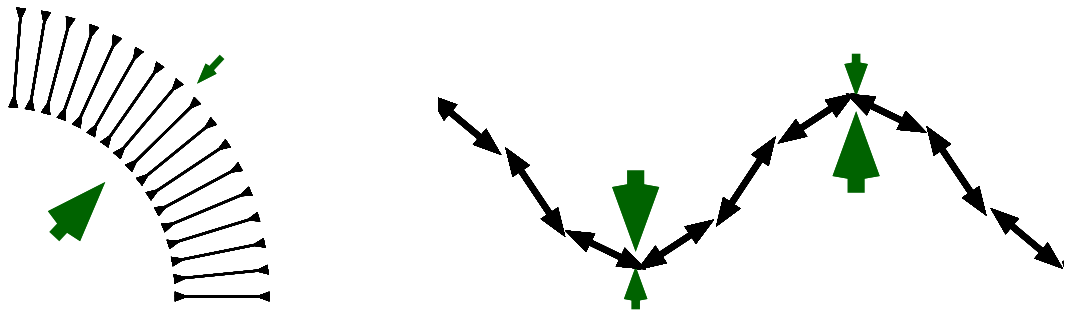

(a) (b)

Figure 3.5 **(a)** *Sketch of how the generic instability works in the active ordered phase, for a contractile active fluid. Splay produces a higher polarisation density - and consequently a higher force density - at one side of the splayed layer. The imbalance between the forces (schematically shown with green arrows) creates a net flow in the direction of the splay, namely* $(\nabla \cdot \boldsymbol{p})\boldsymbol{p}$*; this creates further splay, hence an instability.* **(b)** *A similar mechanism drives the bending instability, generating an imbalance between the force densities and a net flow in the direction of the bend, that being* $\nabla \times (\nabla \times \boldsymbol{p})$*. The two instabilities can be related by noticing that a contractile splayed configuration produces the same flow of an extensile* $(\zeta \to -\zeta)$ *bent polar profile obtained by a* $\frac{\pi}{2}$ *rotation of* $\boldsymbol{p}$*.*

In particular, the generic instability is understood to be a pivotal mechanism to give rise to asymmetric stress distributions that result in spontaneous motile state [106, 121], usually associated with the symmetry breaking of ordered states. When subject to active stresses, the droplets of non-zero polarization field will splay or bend, respectively for contractile or extensile activity, and the net flow generated in the direction of the deformation[2] will effectively move the active material in what seems to be a dynamical transition to a motile steady state. These transitions seems to be continuous in nature, characterized by a critical activity ζ_C for which polar droplets enter motile states [106] or even divide in multiple droplets [121].

Inverse droplets can display similar motile steady states. However, differently from the case of Tjhung *et al.* and Giomi *et al.*, our system is not intrinsically symmetric; the symmetry of the polar phase can be broken by the specific choice of the anchoring, as it is in the homeotropic case, where the polarisation profile around the droplet is highly asymmetric, figure (3.2b). For this reason, we will discuss the tangential and homeotropic boundary conditions separately, and we

[2] $(\nabla \cdot \boldsymbol{p})\boldsymbol{p}$ for splay, $\boldsymbol{p} \times (\nabla \times \boldsymbol{p})$ for bend.

will see how they undergo a significantly different transition when the activity is non-zero.

3.3.1 Homeotropic anchoring, contractile

Our numerical simulations show that for any $\zeta < 0$ the droplet is set in motion by the asymmetric polarisation pattern arising from the presence of the hyperbolic hedgehog at its side. This polarisation pattern sets up an active flow powering the droplet's motion. An analysis of the droplet centre of mass velocity shows that for $|\zeta| < 1.5 \cdot 10^{-4}$ the speed increases linearly with the magnitude of the contractile activity, figure (3.6). We will refer to this as the 'linear regime'. Dimensional analysis and scaling arguments further suggests that the steady state velocity of the droplet should scale as $v_{drift} \sim |\zeta| R/\eta$, where R is the size of the droplet, as noted by Giomi *et al.* [122]. An exhaustive and full numerical validation of this scaling is difficult, as increasing R would require an increase in system size to avoid finite size effects, and this is known to affect the magnitude of bulk active flow [46, 123]. For $|\zeta| > 1.5 \cdot 10^{-4}$ there is a deviation from the linear regime, and for sufficiently negative activity, the spontaneous active flow starts dominating, and the droplet motion becomes eventually chaotic.

In the linear regime, the droplet moves parallel to the positive x-direction, with the defect at its rear, preserving its circular shape, and the hyperbolic hedgehog follows it along during the motion, figure (3.7). The flow field around the propelled droplet is dipolar (*i.e.* is a stresslet far from the droplet [124]), and features vortices, which arise due to the active force distribution in the bulk of the contractile gel. There are forces pushing the droplet to the right due to the polarisation splay which are localised at the right and left boundary; these are balanced by opposing forces to the left, again driven by splay, and localised in the bulk of the active gel, where this deformation is largest.

Effectively, the linear regime corresponds to elastic interactions (due to κ and $\beta_\perp$) dominating over flow induced reorientation. This is quantified by the Ericksen number which measures the ratio between viscous and elastic effects, $\mathrm{Er} \sim \Gamma v_{drift} R/\kappa$, where Γ is the rotational viscosity of the active gel, and v_{drift} is the droplet speed, is small for $|\zeta| < 1.5 \cdot 10^{-4}$.

As the polarisation $\boldsymbol{p}$ seems to 'rigidly' follow the droplet, we can make the assumption that in the linear regime the polar configuration just translates with

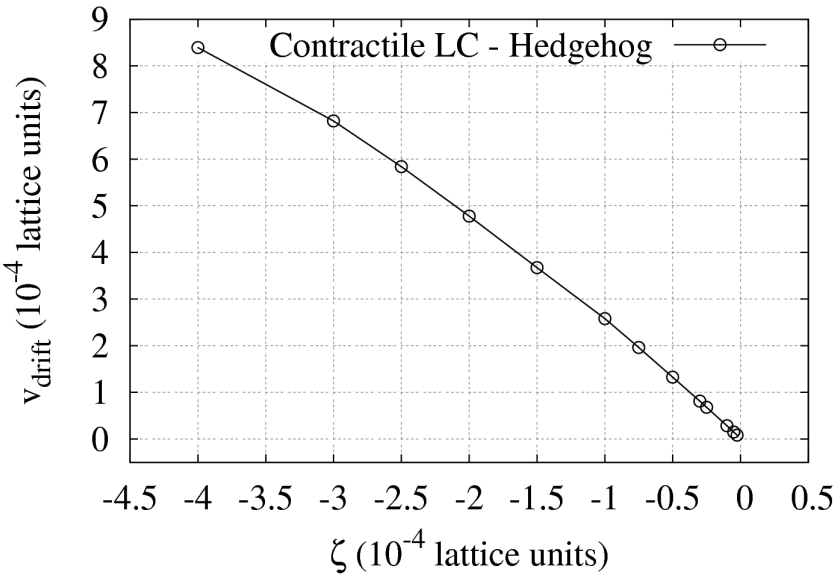

Figure 3.6 *Steady state drift velocity as a function of the activity for a contractile system with homeotropic anchoring on the droplet's surface. For* $|\zeta| < 0.00015$ *(corresponding to a contractile active stress of* $15Pa$*, see mapping in table (3.1)) the dependence is linear, whereas for more strongly negative values there is a deviation. The elastic constant is* $k = 0.02$ *(*$2pN$*).*

the same speed of the droplet, that is $\boldsymbol{p} = \boldsymbol{p}(\boldsymbol{x} - v_{drift}\hat{x}t)$. In this quasi-static, small Ericksen number limit, we can then compute active stress tensor, namely $\sigma_{ij}^{\text{act}} = -\zeta\phi p_i p_j$, by using the definition given in equation (3.14). After some algebra (Appendix B), we can calculate the net force density on the droplet boundary in the x-direction as an integral over θ, as follows:

$$f_x = \frac{1}{2\pi}\int_{-\pi}^{\pi} \hat{x}_i \partial_j \sigma_{ij}^{\text{act}}\Big|_{r=R} \mathrm{d}\theta = -\frac{\zeta\phi_0}{Rc_0} \tag{3.15}$$

Hence, the total active force density on the droplet along the x direction is positive in the contractile case ($\zeta < 0$), which suggests that the droplet will be pushed in the positive x direction, as in our simulations, figure (3.6).

Our droplet becomes motile because of its effect on the bulk polarisation field. In that sense, although it is motile, it is not self-propelled. However, the dipolar (stresslet) fluid flow is indistinguishable from that which would be expected for a self-propelled object which exerts a force distribution around its surface, mirroring that exerted here by the contractile gel. As a result, the exterior flow field

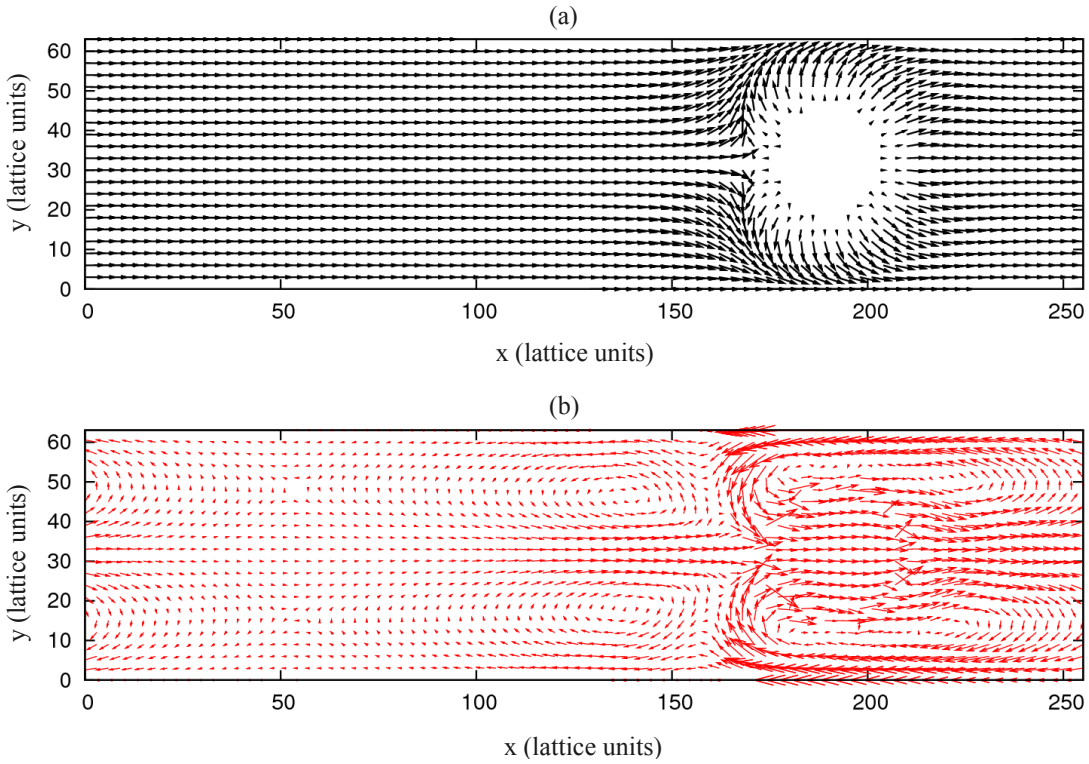

Figure 3.7 **(a)** *Polarisation field outside an isotropic droplet with homeotropic anchoring on its surface, with* $\zeta = -0.0001$ *(corresponding to a contractile stress of* $10Pa$ *according to the mapping in table (3.1)) and* $\kappa = 0.02$ *(*$2nN$*);* $\mathrm{Er} = 0.2$*. The* -1 *hyperbolic hedgehog defect follows the droplet.* **(b)** *Velocity field profile. The flow pushes the droplet forward along the positive* x*-direction and four stretched vortices are generated by the contractile stress, being qualitatively analogous to the far-field of a contractile stresslet.*

strongly resembles that observed in the direct active emulsion case, where active gel droplets self-propel when embedded in an isotropic fluid [106]. An important difference is that in the current case there is no activity threshold below which the droplet is static; this is because the anchoring breaks the symmetry in the polarisation pattern even in the passive limit, due to the creation of the hyperbolic hedgehog, and the consequent dipolar nature of the $\boldsymbol{p}$ field. Intriguingly, this non-trivial velocity field leaves little sign on the polarisation, which is almost unaffected by the flow.

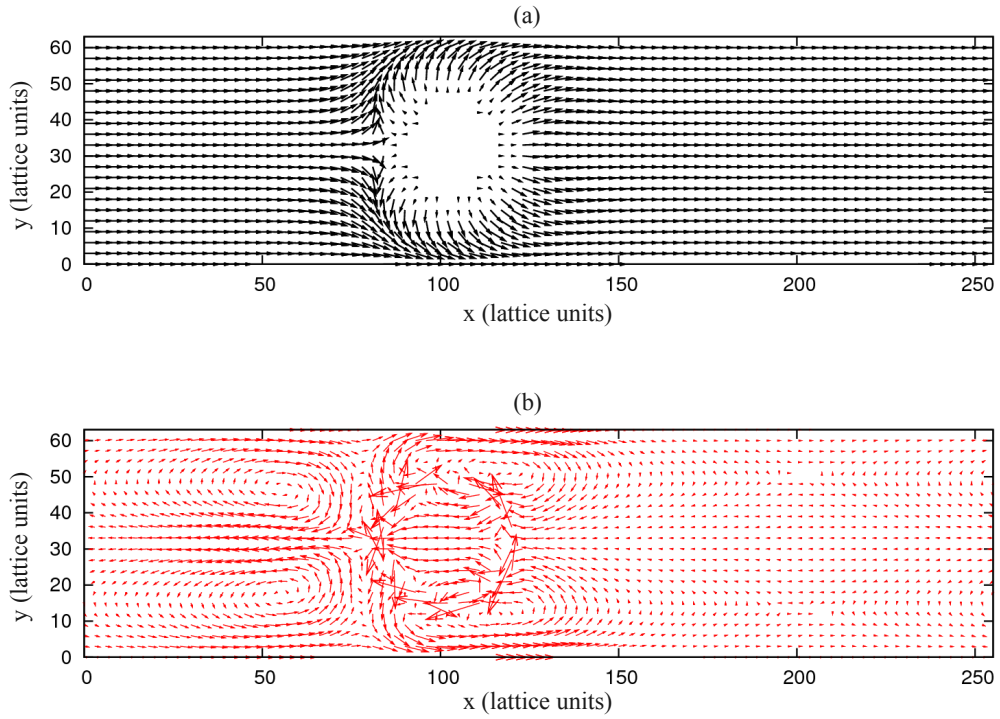

Figure 3.8 *The polarisation field outside an isotropic droplet with homeotropic anchoring on its surface is reported in* **(a)** *for the extensile case, with* $\zeta = 10^{-5}$ *(corresponding to an extensile stress of* $1Pa$ *according to the mapping in table (3.1)) and* $\kappa = 0.02$ *(*$2nN$*). As for the contractile case, a defect is located on the left of the droplet, close to its surface. The corresponding velocity field profile is in* **(b)**. *Now the flow pushes the droplet backward, along the negative* x*-direction and towards the defect. As the flow is much smaller (compare activity values in figure (3.2) and (3.8)), spurious currents due to numerical artifacts in the Lattice Boltzmann scheme show up; the overall pattern of the flow field is still visible.*

3.3.2 Homeotropic anchoring, extensile

Figure (3.8) shows the case in which the active polar liquid crystal is extensile (for $\zeta = 10^{-5}$), again with normal anchoring. The polarisation profile is virtually unchanged if compared to the contractile case; according to our analytical calculation reported above, one would thus expect the active forces to change sign leading to motion in the opposite direction. Simulations confirm this expectation: the droplet now moves with the defect at the front, rather than the rear. At the same time, the force distributions in figure (3.7) and (3.8) are not related by

a simple sign change. This is due in part to the fact that an extensile fluid responds more to bend than to splay deformations (indeed in 1D it is only unstable to bend). On the other hand, presumably as a result of the droplet 'colliding' as it moves towards the region of large deformation located at the defect core, the stability of the linear regime in an extensile environment is much diminished. Chaotic motion starts to occur already for $\zeta = 5 \times 10^{-5}$, which is why a much smaller value is used in figure (3.7). This means however that the flow scale is much smaller in figure (3.8) than in figure (3.7), and indeed small enough to be partly masked by so-called spurious currents [96, 125]. These are small but finite velocity values that arise when using multiphase Lattice Boltzmann simulations, even in the quiescent state, due to the finite precision of the numerics. Therefore our results for the steady motility of an emulsion droplet with homeotropic anchoring in an extensile polar gel should be viewed as qualitative, not quantitative, in character.

3.4 Tangential anchoring

A significantly different dynamics is observed when tangential anchoring is imposed on the droplet surface. For simplicity, we focus here mainly on extensile gels, which leads to more interesting physics in this case. We note that this tangential anchoring may be more easily achieved than normal anchoring in experiments with extensile microtubule bundles such as those in [5] as, due to their high stiffness (or persistence lengths) such bundles would presumably tend to follow the surface of a spherical inclusion.

Because tangential anchoring leads to a symmetric polarisation profile around the droplet (figure 3.4), we would expect any droplet motion to require symmetry breaking, and hence be associated with a non-zero activity threshold. In line with this expectation, we find that for small activity the droplet fails to move (3.9). Interestingly, though, for the activity values in figure (3.9) for which the speed is zero, the droplet is not quite quiescent. Indeed, the values of ζ in figure (3.9) are already large enough for spontaneous flow [45] to set up within the bulk of the extensile fluid: the threshold above which this occurs decreases with system size L as L^{-2} , hence it would be zero in the limit of an infinite system. The associated active flow shears the droplet, and continuously rotates it, figure (3.10a). The direction of this rotation is persistent within a simulation, but varies according

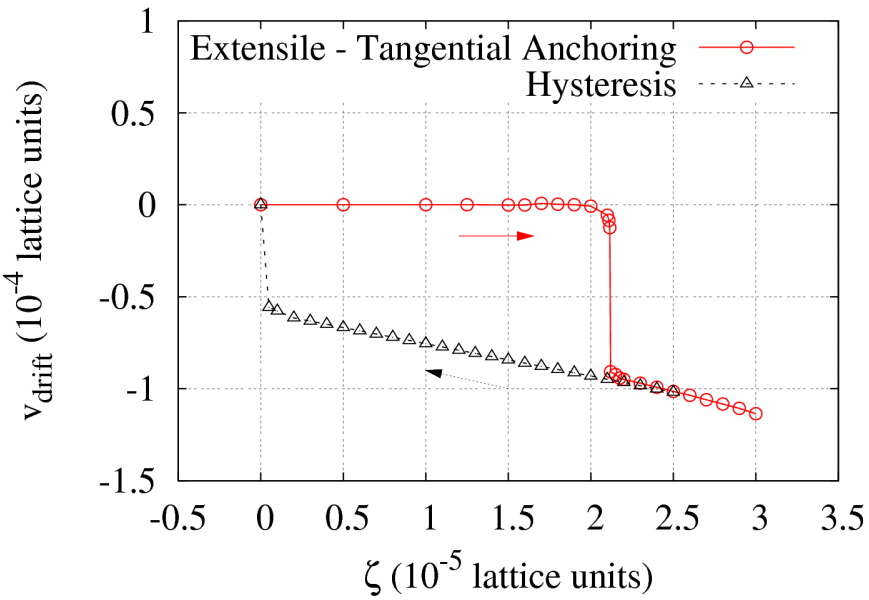

Figure 3.9 *Steady state drift velocity of the isotropic droplet as a function of the activity for an extensile system with tangential anchoring at the polar-isotropic interface. Two different regimes, one in which the droplet is not moving (is at rest or rotates) and another one in which is moving, can be clearly distin- guished before and after* $\zeta_c \simeq 0.000021$ *(or* $2.1Pa$*, see table (3.1)), respectively. For the flow and the polarisation field for the two different regimes, see figure (3.10) Note the strong hysteresis observed on reducing the value of the activity* ζ*.*

to the initial condition from one run to another, consistent with a spontaneous symmetry breaking mechanism.

Figure (3.9) shows also that for large enough ζ the droplet begins to translate, in this case drifting downwards along the negative y-direction; again the direction of motion is selected by spontaneous symmetry breaking. In this regime, the droplet now also stops rotating. Consistent with the change of symmetry, we find a sharp nonequilibrium transition between rotating and translationally motile states of the droplet at around $\zeta \simeq 0.000021$. We observed that there is strong hysteresis associated with this transition, as shown in figure (3.9), which strongly corroborates its discontinuous character.

The motility of the droplet in figure (3.10c) is caused by the bend distortions close to the droplet surface, which lead to extensile active flows within the gel. In the motile state, as expected of a moving droplet, the deformations are asymmetric. As was seen for the contractile droplet with normal anchoring, there are balancing

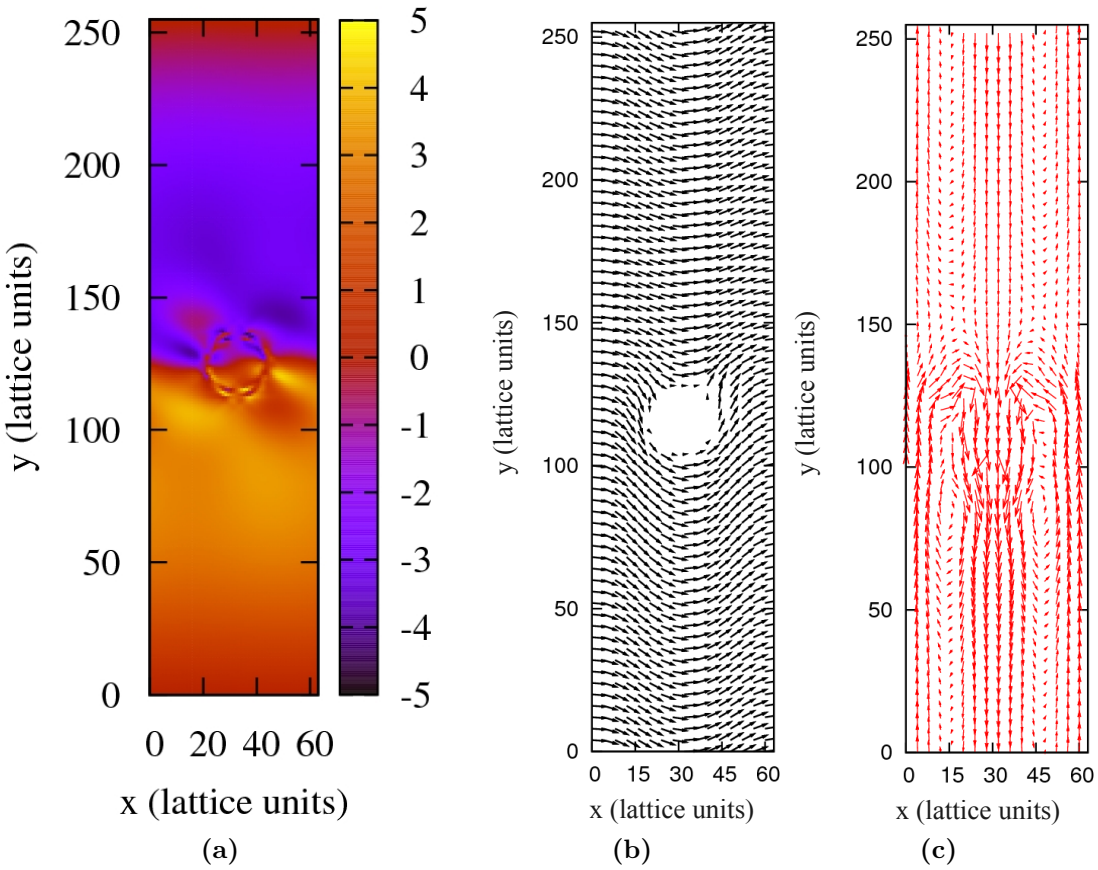

Figure 3.10 **(a)** *Contour plot of the x component of the velocity field for an isotropic droplet with tangential anchoring at the surface, with $\zeta = 10^5 < \zeta_c$, corresponding to $1Pa$, and $\kappa = 0.02$ $(2nN)$. Below the critical threshold, the activity set the polar fluid in a shear-like motion, which in turn makes the droplet rotate. Above the critical activity ζ_c, the symmetry of the system is broken, causing the polar configuration to be asymmetric around the droplet,* **(b)**, *where $\zeta = 10^{-4}$. A more pronounced bend distortion appears at either end (in figure, we show the case where there is more bend at the bottom) of the droplet, thus giving way to a motion in this preferred direction. In* **(c)**, *the velocity field is shown. The simulation box is now $L_x = 64$, $L_y = 256$ to avoid interactions with periodic images along the direction of the droplet's drift.*

currents, now at the sides of the droplet, and due to opposing bend deformation deeper in the active fluid.

Finally, we would like to briefly comment on the result for contractile activity, $\zeta < 0$. The two polar splayed regions on the left and right side of the droplet are the most susceptible to the formation of spontaneous flows, due to the generic instabilities of active fluids. For small activity levels, there seems to be no

significant steady flow that translates into a motion of the droplet. However, stronger activities will lead to a similar instability as seen in the extensile case, where one bent region prevailed on the other, causing the polar profile to shift the bending deformation mostly on one side of the droplet, in the direction that will ultimately define the motion of the droplet. Similarly, for contractile activity one of the two splayed regions develops a stronger flow than the other, thus starting a flow that moves the droplet; however, the onset of this asymmetry immediately develops in a seemingly chaotic flow, and in the consequent erratic unstable motion of the droplet. As a reference, see the videos in the Supplementary Materials in [1]

3.5 Summary

In conclusion, we investigated by computer simulations the dynamics of an isotropic passive droplet embedded in a polar active fluid, either contractile or extensile; these can be seen as minimal coarse grained model for the dynamics of, respectively, actomyosin and microtubule suspensions. Activity renders the physics of this composite material highly non-trivial, and the resulting motile steady states depend strongly on the type of boundary condition, or anchoring, given at the interface between the polar active and isotropic passive media.

We first considered a normal anchoring for the polarisation of the active gel at the droplet surface. In equilibrium and in the absence of activity, this leads to an asymmetric polarisation field, where a hyperbolic hedgehog defect of charge -1 appears at one side of the droplet. In the presence of any contractile activity (even infinitesimal), the polarisation pattern leads to an unbalanced force distribution, in which activity in the polar phase is transduced by splay deformations and propels the droplet along an axis containing the defect and the droplet centre, with the defect at the rear. We identified a regime where the speed of the droplet increases with the activity ζ linearly; in this linear regime, the polarisation field is almost unchanged from the static case, and it translates altogether with the droplet. The motion becomes unsteady for larger activities, and apparently chaotic; this regime is not characterized by neither a steady velocity or directionality.

Extensile activity leads to motility at all activity intensities, once more with no threshold; differently from the contractile case, the active flow pushes the droplet

towards the defect rather than away from it, and this extra interaction leads to a significantly narrower linear regime, leading to unstable and chaotic motions for larger ζ's.

We studied the case of tangential anchoring of the polarisation at the droplet boundary. This boundary condition might possibly be more readily realised experimentally with microtubules [5]. Our computer simulations show that this case leads to different physics, and to an interesting non-equilibrium transition between a droplet which rotates due to the spontaneous active flow in the host, and a steadily moving droplet. In these cases, activity in the surrounding polar medium is transduced by bend deformations into either rotational motion, with a threshold that vanishes at large system sizes), or translational motility along the direction perpendicular to the bulk polarisation. The latter transition occurs via symmetry breaking, and shares some similarities with the self-motile active droplets in an isotropic fluid studied by Tjhung *et al.*. In contrast to the latter case, this transition appears discontinuous, and is associated with a large hysteresis loop, in which a finite propulsion speed can be sustained at a very small activity level by decreasing this from an initially larger value.

The two mechanisms we analysed indicate two possible routes for transport of a passive medium by active fluids. It has to be noted that this mechanisms are unlikely to be responsible for transport *in vivo*, as they rely on a high degree of order for the order parameter; furthermore, transport of 'cargo' inside the cell is understood to happen via the mediation of molecular motors like dyneins, kinesins and myosin, which can grapple to vesicles or other intracellular material with their 'tail' end, while they tread along filaments (actin or microtubules) to which they bind with their 'head' [103, 115]. However, the inverse droplets systems here analysed present us with non-trivial dynamics, and the tangential case in particular offers an example of dynamical phase transition caused by a symmetry breaking mechanism. It is possible, in principle, to realize *in vitro* passive droplets embedded in a microtubule suspension with tangential anchoring, as shown in [5]; this could be an example of active material that is able to transport passive 'cargos', with possible applications of biological and medical relevance.

It is worth noting that, despite being there no realisation of this particular active system to present date, similar experiments have been conducted for colloidal particles embedded in passive liquid crystals with homeotropic anchoring under the effect of external electric fields, by Lazo *el al.* [126]. Most notably, they

obtained a similar scaling for the drift velocity, but with the active stress intensity ζ being replace in their case by the electrostatic energy density $\epsilon\epsilon_0 E^2/2$.

Chapter 4

Active anchoring and arrested phase separation in biphasic active nematics

In the previous chapter, we used a model of mixtures of polar active fluids and passive isotropic fluids to describe the dynamics of eukaryotic cellular filaments; we argued that actin and microtubules can be considered to have a polar symmetry, as they have a distinct 'head-and-tail' orientation. However, we would like to remark how this symmetry was chosen over a nematic one because of the specific boundary conditions we used at the interface; in particular, the homeotropic anchoring type of boundary condition between polar and isotropic fluids made this choice necessary for defining the orientation of the motile droplet with respect to the defect that the anchoring creates. However, in the absence of defects - as it was the case for the tangential anchoring - a nematic symmetry is indistinguishable from a polar one, as they are both are associated with the same 'stresslet', and consequently the same flow. Cellular filaments and, more in general, active fluids can be treated as with both a vector or headless vector field, depending on whether their head orientation is a preferred direction for the dynamics; fast polymerising filaments, dense suspensions of swimming bacteria, and school of fishes have all a tendency to move in the direction of their 'head', and should be considered as being polar; bundles of slow polymerising filaments, bacteria deprived of their cilia and flagella, and vibrated rods all have no preferential 'swimming' direction, but they still exert a stress on their

surrounding fluid and have an orientational order, therefore should be regarded as nematic.

In the present chapter, we will discuss a generic property of binary mixture of ordered and isotropic fluids in two dimensions, and see how the presence of active stress distribution can give rise to a variety of different possible phase structures with non-trivial interfacial properties that cannot be characterized by the thermodynamics (*i.e.* the free energy) of the systems, but have to be regarded as a purely out-of-equilibrium effect emerging from the activity.

Here we will provide qualitative and quantitative description of the dynamics of nematic-isotropic binary fluid mixtures, and show how activity shapes a completely different physics at the interface between the ordered and disordered phases. Unlike we did previously, we will not include any anchoring terms enforcing a given orientation at the interface. It has been observed that, even in the absence of a thermodynamic anchoring terms, nematic active systems experience an effective alignment at interfaces in the presence of activity: in particular, the nematic phase seems to align parallel or perpendicular to the interfaces for extensile or contractile stresses, respectively [71], shown in figure (4.1). This effect has been termed 'active anchoring', and it plays an important role in the generation of defects: point defects of positive topological charge can be ejected into the nematic phase, leaving the interface itself with a diffuse negative charge.

It is also well known that the stirring effect of the activity can disrupt the aggregational tendency of surface tension, causing a finite domain length-scale to persist [22, 30, 32, 58]. The resulting phase structure is typically anisotropic, reflecting the underlying anisotropy of the nematic order, presenting this mixture as a promising candidates for novel types of emulsions and bicontinuous fluids. In this chapter we will present an analysis detailing the structural dynamics of the phases, and propose an 'active capillary number' as a candidate dimensionless parameter to predict the steady state structure of the fluid.

Finally, we will discuss how the active anchoring can be quantified in terms of an opposing thermodynamic anchoring that it can overcome [127], and show how the interfacial dynamics is deeply interconnected with the phase structure. Indeed, active anchoring is produced by shear fields that persist into the bulk, therefore its strength depends not only on the activity but also on the length-scale over which these shear fields act.

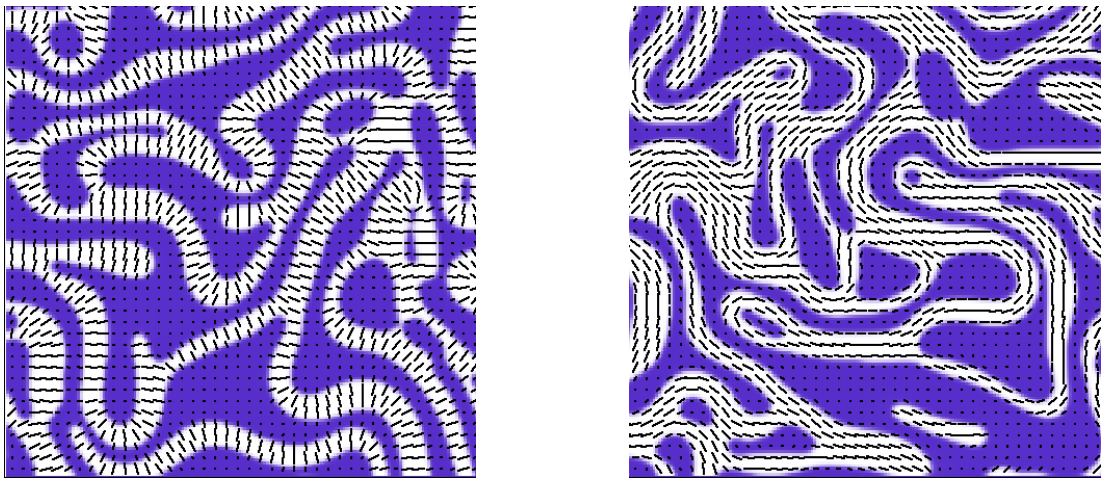

Figure 4.1 *Snapshots of numerical simulations of a mixture consisting of equal proportions of isotropic and nematic fluids, in the presence of contractile (left) and extensile (right) activity. The dynamics of these systems are described via a free energy approach with no thermodynamic anchoring - as it will be presented in equation (4.1) - yet a preferred alignment of the nematic field arises at the interface.*

4.1 Dynamics of nematic-isotropic fluid mixture

In the nematic-isotropic mixture, we will denote the nematogen concentration field as ϕ, with $\phi = 1$ corresponding to the nematic phase, and $\phi = 0$ to the isotropic fluid. The nematic order will be characterized by the traceless tensor $Q_{ij} = S(2n_i n_j - 1)$, as defined by equations (2.18, 2.19), where $n_i, i = 1, 2$ and S respectively are the director and the magnitude of the order.

The thermodynamic free energy of the systems we will consider is:

$$\mathcal{F}[\phi, Q_{ij}] = \int \left\{ \frac{A}{2}\phi^2(\phi-1)^2 + \frac{K}{2}\partial_k\phi\partial_k\phi + \frac{L}{2}\partial_k Q_{ij}\partial_k Q_{ij} + \frac{C}{2}\left(\phi^2 - \frac{Q_{ij}Q_{ij}}{2}\right)^2 \right\} \tag{4.1}$$

The first term is the usual double well bulk potential for the nematic concentration field ϕ, which ensures that two phases have the correct bulk values $\phi = 0$ and $\phi = 1$. The term in the gradients of ϕ represents the energy at the boundary between the two phases, with K characterizing the strength of the surface tension. The third term is the elastic part of the free energy, expressing the contribution from the distortions of the nematic director, with L being the effective elastic

constant; once again, we work under the assumption of the one elastic constant approximation. The fourth and final term couples the nematic order $S = 2Q_{ij}Q_{ij}$ to the nematic concentration ϕ, so as to favour isotropic order ($S = 0$) in regions with low nematic concentration ($\phi \sim 0$) and nematic order ($S = 1$) where high nematic concentration ($\phi = 1$).

The free energy has no terms coupling $\partial_k\phi$ with Q_{ij}, which would correspond to a thermodynamic anchoring, as seen in Chapter 3. These types of terms act on the fluid through two dynamical pathways: a force difference between regions of interface with different orientations, which tends to lengthen those with the favoured alignment and shorten those with the unfavoured alignment; and a torque on the director at the interface, which tends to rotate it into the preferred alignment. In the following, we will discuss that an analogous effect takes place in the presence of activity, which we characterize once again through a dipolar stress distribution of intensity ζ. This effective alignment tendency cannot be regarded as a thermodynamic effect, as it emerges from a purely out of equilibrium term. To fully understand the implications of this active interfacial physics, we have analysed through numerical simulations the dynamics of the mixture, and the way in which non-equilibrium forces compete with the thermal ones, namely the surface tension and the elasticity.

The dynamical equations for the evolution of the fields ϕ and Q_{ij}, altogether with the ones for the fluid density and momentum, are (2.27, 2.29, 2.37), once again:

$$\partial_t\phi + \partial_k(\phi u_k) = M\partial_k\partial_k\mu, \tag{4.2}$$

$$\partial_t Q_{ij} + u_k\partial_k Q_{ij} = -\xi\Sigma_{ijkl}\Lambda_{kl} - T_{ijkl}\Omega_{kl} - \Gamma H_{ij}, \tag{4.3}$$

$$\partial_t u_i + u_k\partial_k u_i = \eta\partial_k\partial_k u_i - \partial_i P + \partial_k\sigma^{\text{act}}_{ik} + \partial_k\sigma^{\text{pass}}_{ik}, \tag{4.4}$$

where M is the chemical mobility coefficient; μ the chemical potential defined as $\mu = \frac{\delta\mathcal{F}}{\delta\phi}$; Λ_{ij} and Ω_{ij} the symmetric and antisymmetric parts of the shear tensor $\partial_i u_j$; Σ_{ijkl} and T_{ijkl} the shear-alignment coupling tensors as defined in equation (2.31); ξ is the shear aligning parameter, which determines if the nematogens tumble ($\xi < 1$) or align to a shear flow ($\xi \geq 1$); Γ is an effective rotational viscosity; H_{ij} is the molecular field, as defined in equation (2.30); η is the hydrodynamic viscosity; and P is the hydrodynamic pressure.

The stress tensors σ_{ik}^{act} and $\sigma_{ik}^{\text{pass}}$ encapsulate, respectively, the active and passive stress contributions; the former being characterized by being a non-equilibrium term, since it depends on the activity ζ, defined by equation (2.36) ; the latter including all the thermodynamics descending from the free energy (4.1), and the flow-aligning coupling counterparts to the terms in ξ in equation (4.3), as seen in equation (2.38).

We note that when $\xi = 0$, equations (4.2, 4.3, 4.4) are invariant under the transformation $Q \to -Q, \zeta \to -\zeta$. Such transformation corresponds to a rotation $\theta \to \theta - \pi/2$ of the director field, and to a change from contractile to extensile systems (and viceversa). Therefore, the evolution of extensile and contractile systems with the same magnitude $|\zeta|$ should differ only by a local rotation of the director by $\pi/2$ everywhere. Any property of the system that is independent of orientation (*e.g.* isotropic lengthscale, interfacial length, kinetic energy), should be equivalent for the two systems, while any orientation-dependent property (*e.g.* active anchoring, domain anisotropy) should change sign. Thus we can infer properties of the contractile system by studying only the extensile system. We should bear in mind that this symmetry is specific to two-dimensional systems.

4.2 Active anchoring

An interface nematic aligning effect has been first documented qualitatively by Blow *et al.* [71]. Examples from numerical simulations are shown in figure (4.1) for fifty-fifty mixtures of isotropic and nematic extensile/contractile fluids. While the presence of a planar/homeotropic alignment for the extensile/contractile system is clear from visual inspection, we here confirm it quantitatively. The angle of the nematic director relative to the interface can be obtained from:

$$\theta_{int} = -\frac{1}{2}\arccos\left(\frac{-(\partial_i\phi)Q_{ij}(\partial_j\phi)}{S\partial_k\phi\partial_k\phi}\right). \tag{4.5}$$

A histogram of the angle θ_{int} can be obtained, figure (4.2), weighting each simulation node by $\partial_i\phi\partial_i\phi$ and normalising. For an extensile system, it can be seen that there is a strong prevalence of tangential alignment, with approximately 70% of the weighted nodes with an orientation within 10 degrees from the tangent to the interface. A similar result in figure (4.3), where a perpendicular anchoring dominates.

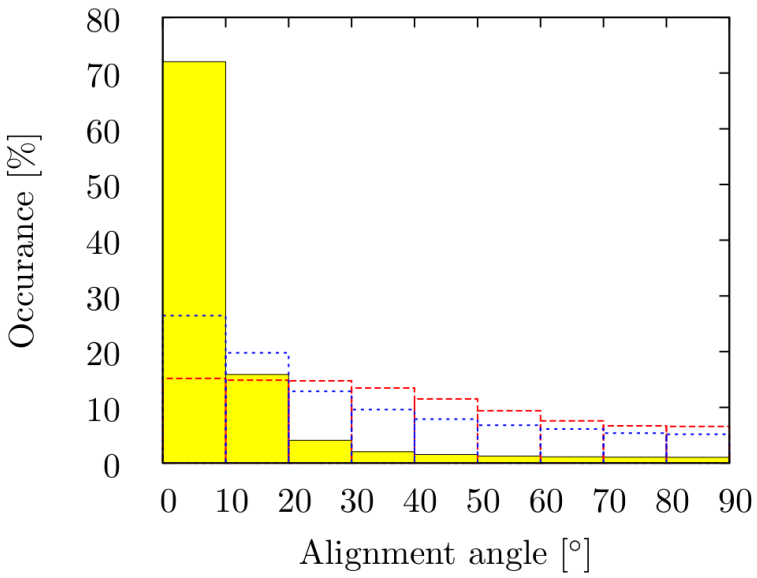

Figure 4.2 *Histograms of director angle relative to the interface for a flow-tumbling nematic with extensile activity. The solid yellow bars give the results for the full simulation. The blue and red dotted bars correspond to simulations where the advection and back-flow terms respectively have been 'turned off'.*

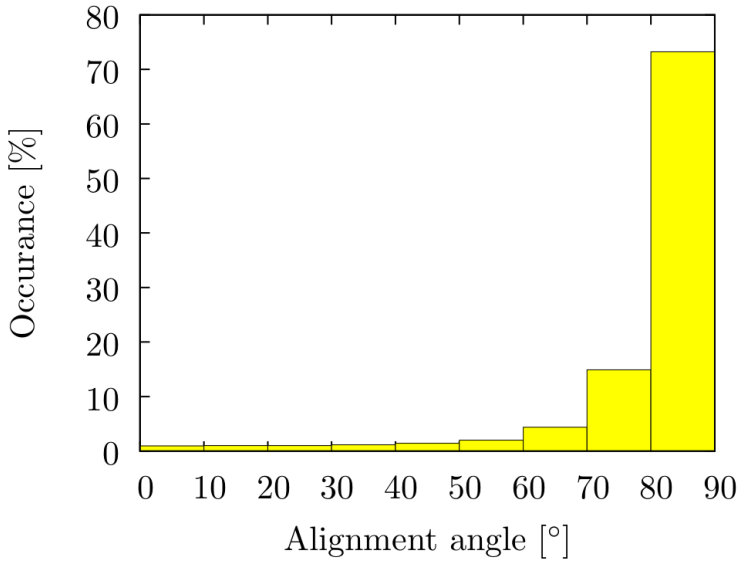

Figure 4.3 *Histograms of director angle relative to the interface for a flow-tumbling nematic with contractile activity.*

Two causes lead to this effective active anchoring, reflected in the two components of the active force in the directions perpendicular and parallel to the interface. Under the assumption that the coupling C in equation (4.1) is large enough so

that $\phi \simeq S$, this can be written as:

$$\mathbf{F}^{\text{act}} = \zeta(|\nabla S|(2(\mathbf{m}\cdot\mathbf{n})\mathbf{n} - \mathbf{m}) - 2S((\nabla\cdot\mathbf{n})\mathbf{n} + \mathbf{n}\cdot\nabla\mathbf{n})), \tag{4.6}$$

where $\mathbf{m}$ is the normal to the interface (pointing out of the nematic region), *i.e.* the unit vector $\frac{1}{|\nabla\phi|}(-\partial_y\phi, \partial_x\phi)$. Assuming that interfaces curve smoothly, one can neglect the second term in equation (4.6); we can then write the projections of $\mathbf{F}^{\text{act}}$ along $\mathbf{m}$ and the interface as:

$$F_{\perp}^{\text{act}} = -\zeta|\nabla S|\cos 2\theta, \tag{4.7}$$

$$F_{//}^{\text{act}} = \zeta|\nabla S|\sin 2\theta. \tag{4.8}$$

Examining first $F_{\perp}^{\text{act}}$, we note that, in the case of extensile activity, the active force points outwards from the nematic region when $\theta = \pi/2$, but inwards when $\theta = 0$. Thus an active drop will be stretched along the director and compressed perpendicular to it, which will tend to increase the length of interface where the director orientation is planar, and decrease the length of those regions where alignment is homeotropic, thus producing predominantly planar anchoring. For contractile activity, the forces operate the opposite way, leading to predominantly homeotropic alignment. This morphological effect is one of the two causes of active anchoring. The schematics of this mechanism have been sketched in figure (4.4).

The other mechanism of active anchoring, illustrated in the lower part of figure (4.4), is due to the tangential component of the active force. This component induces a shear in the nematic region[1], which produces a torque that rotates the director. The direction of the shear, and hence the sense of the rotation, changes with the orientation of the director, leading to certain orientations being stationary points (stable and unstable). The active anchoring is thus the result of the director adopting a stable configuration; from equations (4.3, 4.4) in stationary conditions, one can obtain (as outlined in Appendix C) that for a flat one dimensional nematic-isotropic interface the director angle θ obeys the equation:

$$S^2\partial_t\theta = -\frac{\zeta S^3}{2\eta}\sin 2\theta + (\Gamma\eta + 2S^2)(2LS^2\partial_y\partial_y\theta + 4LS\partial_y\theta\partial_y S), \tag{4.9}$$

[1]The same force also applies a shear of opposite sense in the isotropic region, but this is not relevant to the final effect, as $\phi = 0$ in said phase.

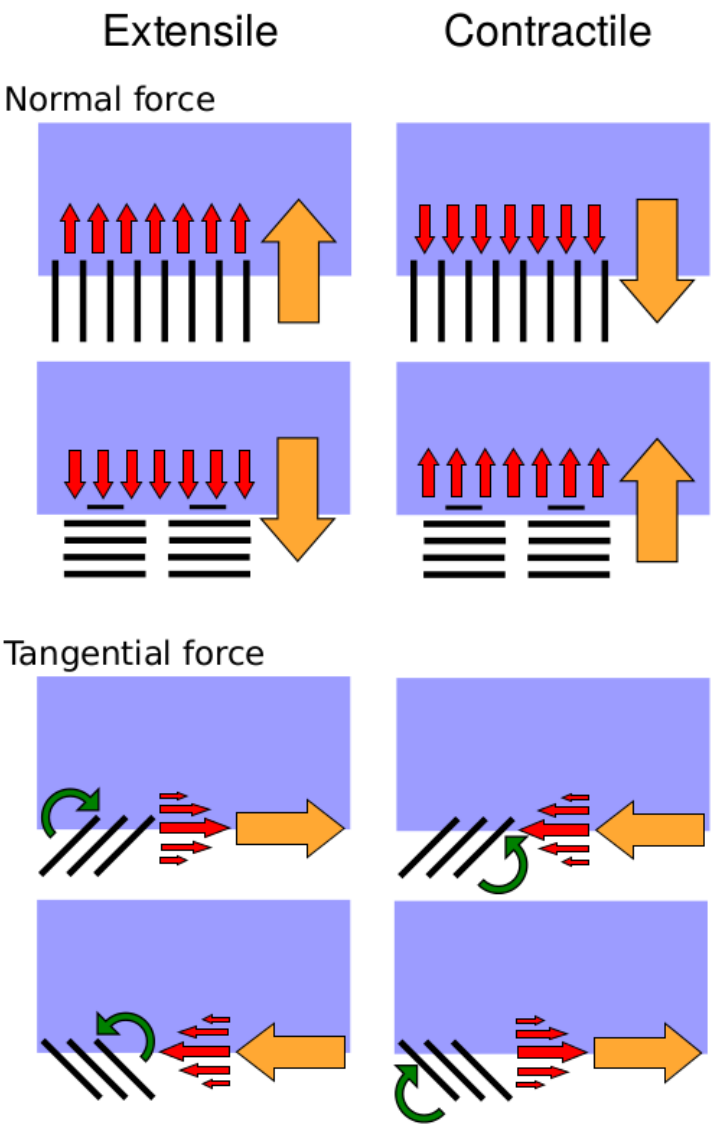

Figure 4.4 *Schematic illustration of the normal and tangential active forces at the interface (orange arrows) and the flow fields produced (red arrows). For the case of the tangential forces, the resulting shear produces a torque (green arrows) on the director.*

where y is the direction normal to the interface; from equation (4.9), it can be seen that for $\zeta > 0$ $\theta = 0$ is a stationary and stable point; while for $\zeta < 0$, the homeotropic anchoring corresponding to $\theta = \pi/2$ results stable.

We have so far determined the effects of the 'active anchoring', but not its 'strength': this presents a challenge, as the active stress in non-integrable to be included in a free energy functional. However, it is possible to compare the dynamic effects of active anchoring to those of thermodynamic anchoring.

In this vein, a thermodynamic anchoring W opposing the active anchoring can be applied: if the thermodynamic anchoring is sufficiently strong, then it will overcome the active anchoring, but if the thermodynamic anchoring is weak, the active anchoring will prevail. We can enquire what is the value of W at which this crossover occurs, thus providing an effective strength for active anchoring.

The thermodynamic anchoring term can be expressed in the free energy density by a cross terms of gradient of the nematic fields such as $\frac{J}{2}\partial_i Q_{ij}\partial_j\phi$; details are discussed in Appendix D. It can be obtained then that the active anchoring has an effective tension that can be expressed as:

$$|W| = \frac{16\sqrt{2}\zeta h}{3(\Gamma\eta + 2)}, \tag{4.10}$$

where h is the lengthscale over which the orientational order persists in the nematic phase; the nature of this length can vary significantly: for nematic phases where elastic effects dominate over the surface tension, the relevant lengthscale is the size of the nematic domain itself, l_{dom}; if the ratio K/L is higher, corresponding to weaker elastic forces compared to the surface tension, the appropriate lengthscale is $\sim \sqrt{L/\zeta}$, this being the dominant scaling of active turbulence in bulk nematics. It is then important to understand the dynamics in these two different scenarios, and how the structure of the phases is influenced by activity.

4.3 Arrested phase separation

In the absence of activity, the surface tension will drive an initially homogeneous mixture to complete phase separation. Domains of $\phi = 0$ and $\phi = 1$ will form, merge and grow without limit, such that the characteristic domain lengthscale $l_{\mathrm{dom}} \to \infty$. As we shall confirm and quantify in this section, the presence of sufficient activity can cause l_{dom} to saturate, with fluctuations around a finite value. There are various quantitative definitions of l_{dom}: here we use the inverse first moment of the circularly averaged structure factor of ϕ, which is shown to correctly capture the dynamics of phase separation [128], namely:

$$l_{\mathrm{dom}} = (\langle \boldsymbol{k} \cdot \boldsymbol{k} \rangle)^{-\frac{1}{2}}, \tag{4.11}$$

where the average denoted by the brackets $\langle\cdot\rangle$ is to be intended over the allowed wave numbers $\boldsymbol{k}$:

$$(\langle \boldsymbol{k}\cdot\boldsymbol{k}\rangle) = \int_\Omega (\boldsymbol{k}\cdot\boldsymbol{k})\mathrm{d}^2\boldsymbol{k}\int \mathrm{d}^2\boldsymbol{r}\phi(\boldsymbol{r})\mathrm{e}^{i\boldsymbol{k}\cdot\boldsymbol{r}}. \tag{4.12}$$

The scaling of l_{dom} on activity, along with the qualitative morphology of the domains, depends on whether bulk elasticity dominates over surface tension or vice versa. We investigated with numerical simulations the two regimes[2] $\gamma\xi_I/L \lesssim 1$ and $\gamma\xi_I/L \gtrsim 1$, where the coarsening is led by elasticity and interfacial tension respectively. In the absence of activity, both regimes are known and well studied at early times [39, 60, 129, 130], and are characterised by a scaling coarsening regime, where domains grow as t^α. For surface tension driven systems, $\alpha = 1/3$ at early times when diffusion dominates, and $\alpha = 1$ at late times when hydrodynamic effects become prevalent.

In isotropic-nematic quenching, numerical studies in elasticity dominaed systems have shown that in the diffusive regime, α is closer to $1/4$ [131], as we shall confirm here. However, the presence of activity significantly alters the coarsening dynamics, as the active flow competes with the coalescing forces; the extensile/contractile stresses stretch the phases along/perpendicularly to the director profile, eventually disrupting the integrity of nematic domains.

4.3.1 Scaling hypotheses

We approximate the evolution of this lengthscale using scaling arguments based on the hydrodynamic and diffusive equations. First taking (4.4), we disregard the left-hand side, assuming stationary conditions and advection being negligible compared to viscosity. On the right-hand side, we assume the following scalings for the terms from the stress tensor:

$$\nu\nabla^2\boldsymbol{u} \sim \nu\frac{\dot{l}_{\mathrm{dom}}}{l_{\mathrm{dom}}^2}, \tag{4.13}$$

$$p \sim \frac{\gamma}{l_{\mathrm{dom}}}, \tag{4.14}$$

[2]Once again: γ is the interfacial tension between the two phases; $\xi_I \sim \sqrt{K/A}$ is the thickness of the diffuse interface, with K the surface tension constant; L is the elastic constant.

$$\sigma_{ij}^{\text{pass}} \sim \frac{L}{l_{\text{dom}}}, \tag{4.15}$$

$$\zeta Q_{ij} \sim \zeta, \tag{4.16}$$

where we assumed that the time derivative $\dot{l}_{\text{dom}}$ follows the velocity field in (4.13), and that the hydrodynamic pressure (4.14) respects Laplace's law. The momentum balance equation then becomes:

$$\dot{l}_{\text{dom}} \sim b\frac{\gamma}{\nu} + d\frac{L}{\nu l_{\text{dom}}} - e\frac{|\zeta| l_{\text{dom}}}{\nu}, \tag{4.17}$$

where b, d and e are dimensionless positive constants left undetermined, whose value won't change the nature of the scaling behaviour. The minus sign has been chosen for the active term in ζ as we anticipate that the active flow opposes domain growth, while the other terms are known to promote it from coarsening theory.

Similarly, we can obtain the scaling for the contributions to the coarsening due to the diffusive effects, descending from equation (4.2,4.3):

$$\dot{l}_{\text{dom}} \sim a\frac{M\gamma}{l_{\text{dom}}^2} + c\frac{ML}{l_{\text{dom}}^3}, \tag{4.18}$$

where a and c are again positive dimensionless constants left undetermined.

Thus the full phenomenological scaling equations will read:

$$\dot{l}_{\text{dom}} \sim a\frac{M\gamma}{l_{\text{dom}}^2} + \sim b\frac{\gamma}{\nu} + c\frac{ML}{l_{\text{dom}}^3} + d\frac{L}{\nu l_{\text{dom}}} - e\frac{|\zeta| l_{\text{dom}}}{\nu}, \tag{4.19}$$

The first two terms quantifies the coarsening effects of the surface tension contribution at late times and early times, following the standard approach in isotropic passive binary fluids [39]; similarly, the third and fourth terms account from the growth in size of nematically aligned domains. The fifth term is proportional to the activity ζ, and it can be justified by replacing the phase-ordering stresses with the active stress, disrupting the phase separation.

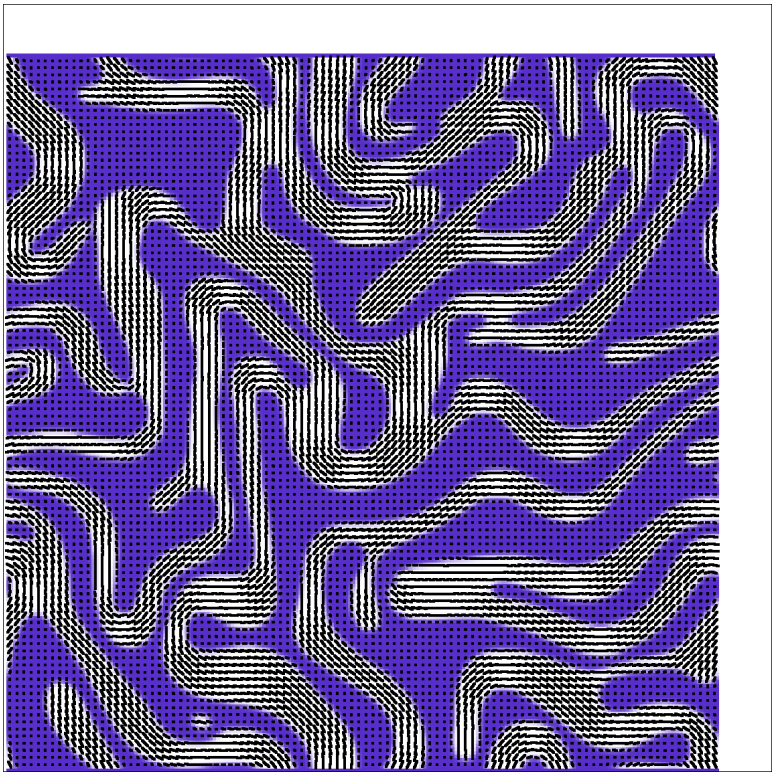

Figure 4.5 *Binary mixture with extensile activity, $L = 1 \cdot 10^{-2}$, $K = 1 \cdot 10^{-2}$, $\zeta = 10^{-3}$. The nematic phase (black bars on white) is characterized by elongated structures, with the director profile following the shape of the domains.*

4.3.2 Laminar coarsening

When elastic effects dominate, the typical lengthscale of the distortions matches the size of the domains l_{dom}; in this case, we can neglect the first two terms in equation (4.19), thus obtaining

$$\dot{l}_{\mathrm{dom}} \sim c\frac{ML}{l_{\mathrm{dom}}^3} + d\frac{L}{\eta l_{\mathrm{dom}}} - e\frac{\zeta l_{\mathrm{dom}}}{\eta}. \tag{4.20}$$

While activity disrupts the aggregational tendency of the two components of the mixture, diffusion naturally lead to larger domains. By neglecting surface tension effects, the only diffusive contribution left in equation (4.20) is $\frac{ML}{l_{\mathrm{dom}}^3}$. This is reflected in the forming domains of the ordered phase, which have a high degree of order persisting over thin and elongated domains, rather than having the characteristic spinodal aggregation in droplets, as shown in figure (4.5). We will hence refer to this as laminar coarsening.

In steady states, the left-hand side of equation (4.20) vanishes, and what is left is a quartic equation in l_{dom}. Although the coefficients c, d, e are undetermined from the scaling hypothesis, we can still conclude that there is not a unique scaling for finite l_{dom}, but rather a crossover between $l_{\text{dom}} \sim \zeta^{-\frac{1}{2}}$ and $l_{\text{dom}} \sim \zeta^{-\frac{1}{4}}$ regimes, and numerical simulations confirm this behaviour, as shown in figure (4.6).

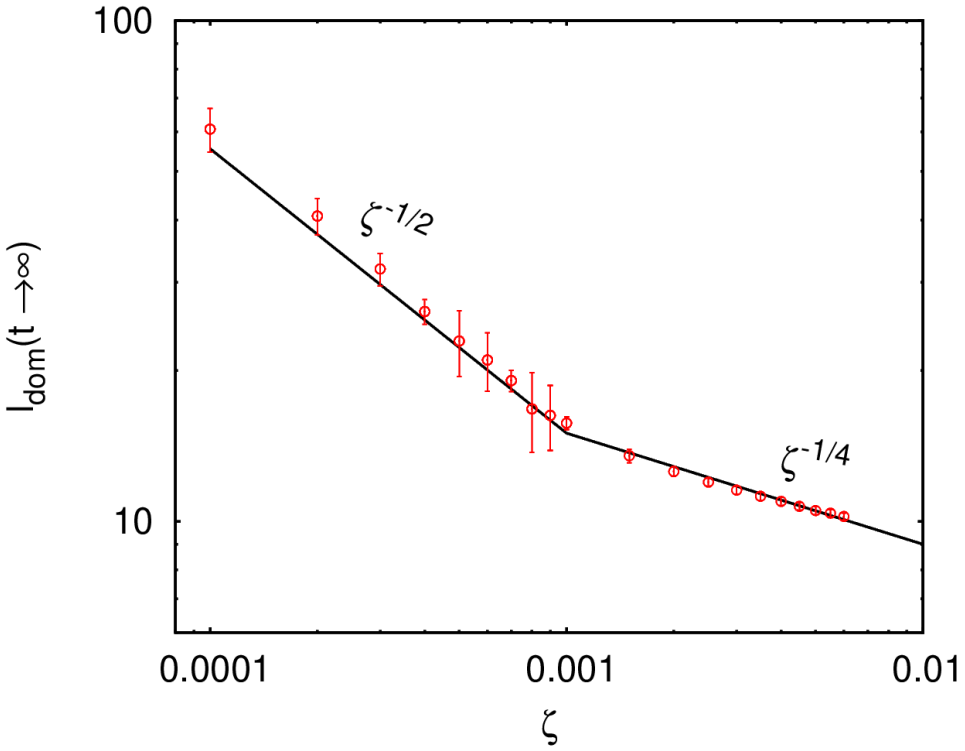

Figure 4.6 *Steady state average of l_{dom} in the laminar regime, for $\gamma\xi_I/L = 2/3$, in a 200x200 simulation box. Full phase separation occurs at $l_{\text{dom}} \sim 100$. In our simulations, even a small level of activity seems to lead to the arrest of the phase separation, with characteristic lengthscales depending on the activity ζ. Black lines outline the scalings $\zeta^{-\frac{1}{2}}$ and $\zeta^{-\frac{1}{4}}$. The average lengthscales (red dots) are taken as the time average of l_{dom} (see eqn. (4.11)) after the first 10^7 time steps of the evolution of an initially completely disordered state.*

From equation (4.20), one can also obtain a prediction on the coarsening scaling in time; in this case, one would expect to not obtain the conventional scaling $l_{\text{dom}} \sim t^{\frac{1}{3}}$ at early times predicted for surface tension led coarsening [39]; as the tension effects are negligible compared to the elastic ones, coarsening will be led by the elasticity terms in L, thus giving $t^{\frac{1}{4}}$ for the coarsening regime of the domain size at early times, from the term $\frac{ML}{l_{\text{dom}}^3}$ in (4.20). In simulations, we are indeed able to observe a coarsening close to the $t^{\frac{1}{4}}$ for small enough l_{dom}, as in figure (4.7); similar results have been observed in other numerical studies [131].

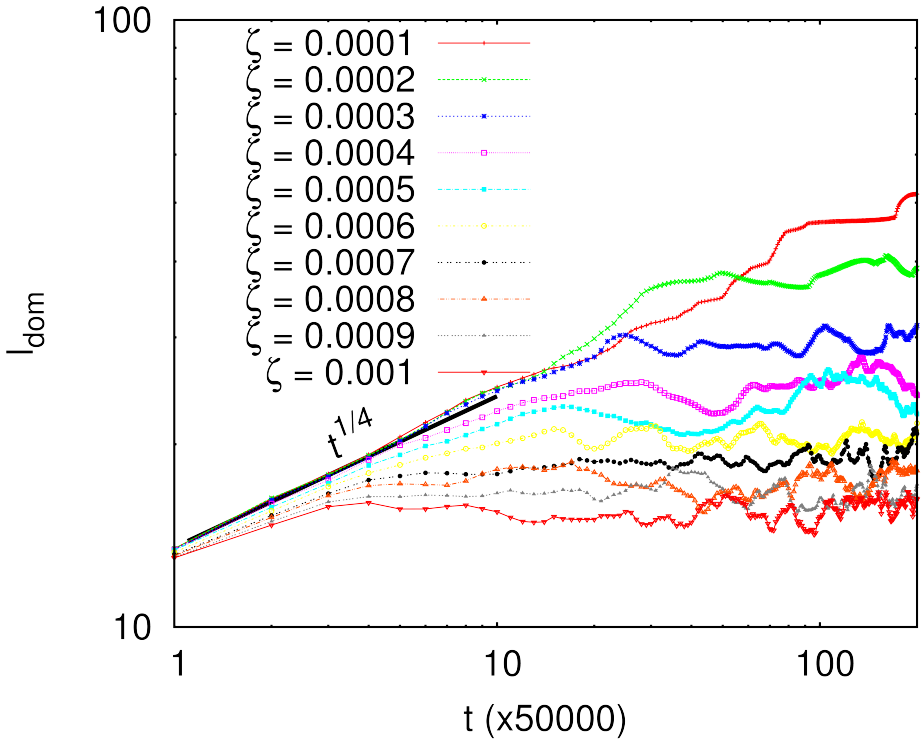

Figure 4.7 *Steady state values of l_{dom} in the laminar regime ($\gamma\xi_I/L = 2/3$) for different values of the activity ζ, in a 200x200 simulation box. Full phase separation occurs at $l_{\mathrm{dom}} \sim 100$. Black bar corresponds to a scaling in time $\sim t^{\frac{1}{4}}$.*

4.3.3 Surface-tension-led coarsening

If the value of K is increased, the surface tension will come to dominate over elasticity; in the ordered phase we observe a change from the laminar regime to the turbulent one, figure (4.8). In such a situation, a scaling analysis is more complicated because the system is no longer governed by a single lengthscale.

Most importantly, we find that the system can still undergo full phase separation for non-zero values of the activity ζ, and the size of the nematic domains keeps growing indefinitely below certain values of the activity, up to half the size of the simulation domain, where phase separation is complete, figure (4.9). However, it appears that there is a critical value of the activity ζ_c past which the phase separation is arrested; ζ_c is not independent of the parameters K, L and A, and even for fixed interfacial thickness ξ_I and tension-elasticity ratio K/L, it varies as a function of the total surface tension, $\zeta_c(\gamma)$. Below this threshold value, the presence of activity seems to have the sole effect to slightly alter the time scaling

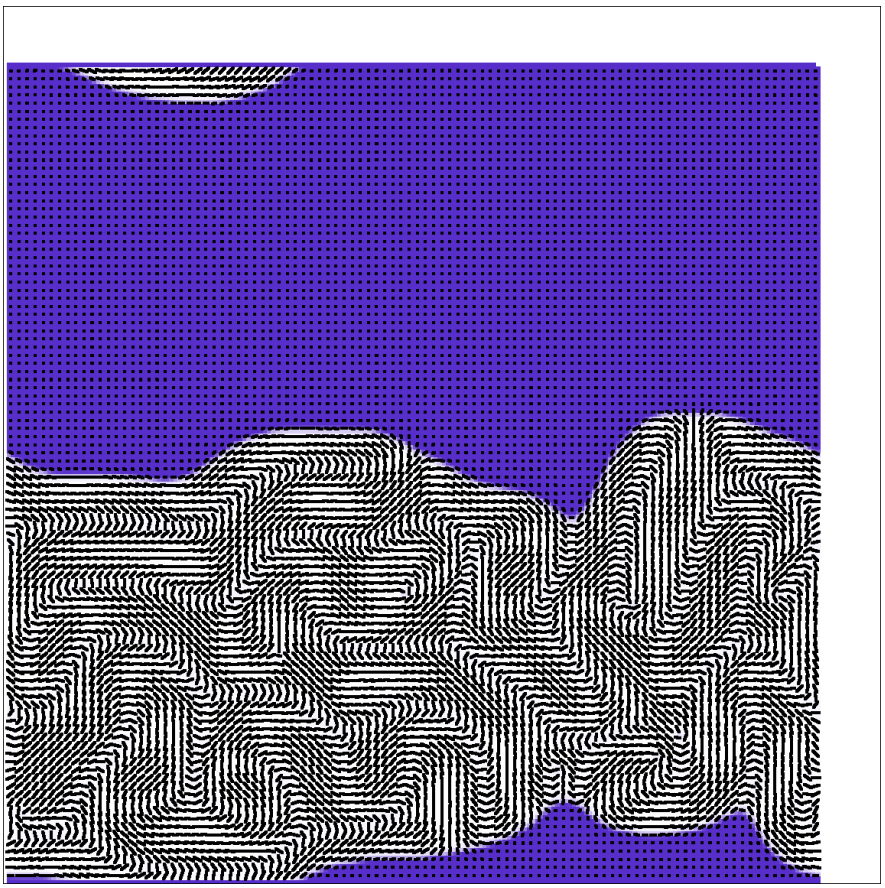

Figure 4.8 *Binary mixture with extensile activity, $L = 5 \cdot 10^{-3}$, $K = 7 \cdot 10^{-2}$, $\zeta = 10^{-3}$, 200x200 domain size. While the separation is complete, the nematic phases is characterised by a low degree of order.*

behaviour: for small enough activity and early times, we are able to observe $l_{\text{dom}} \sim t^{\alpha}$, with α close to $1/3$, as to be expected for an isotropic binary fluid separation, figure (4.10).

The existence of a threshold value for ζ seems to suggest that the interface forces are in direct competition with the activity, which, when not strong enough, does not break the continuity of the forming domains, letting the phase separation continue its course. We consider the effect of the activity at the interface, which has been quantified in the strength of the effective active anchoring in equation (4.10), and compare it to the surface tension $\gamma = \frac{2L+K}{6\xi_I}$. We then define the ratio between active anchoring and surface tension to be a capillary number Ca^{act}, and we propose it as the effective parameter to characterize the arrest of the phase

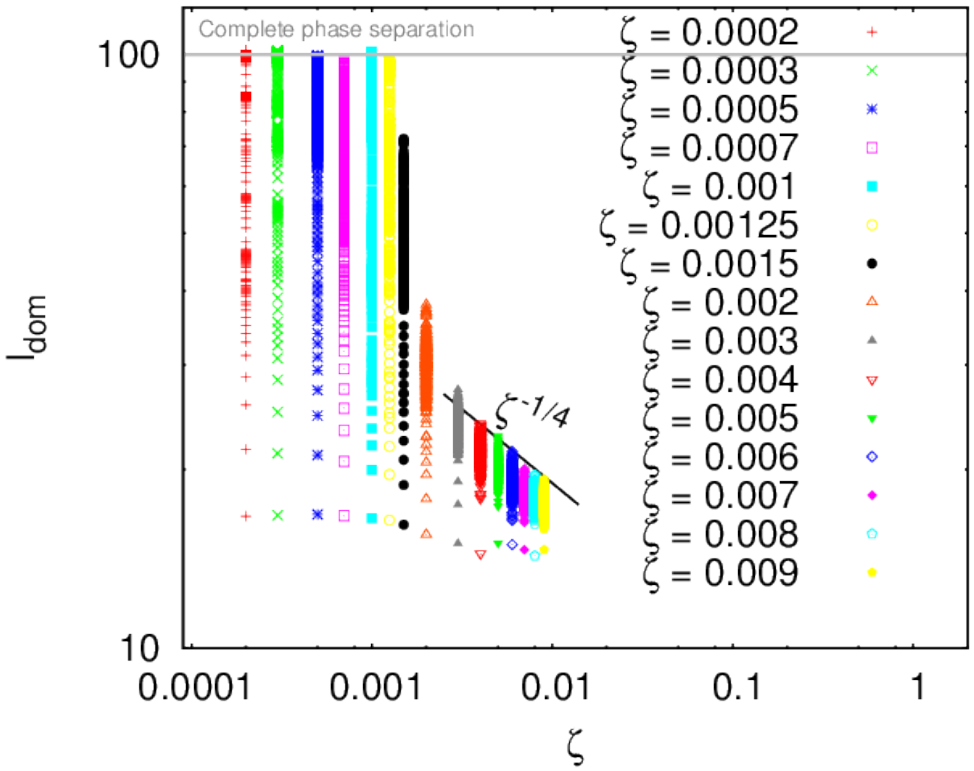

Figure 4.9 *Growth of the nematic domain size l_{dom} in the surface tension led regime ($\gamma\xi_I/K = 5$) for different strengths of the activity ζ, displaying a transition from complete to arrested phase separation around $\zeta_c \simeq 1.25{\cdot}10^{-3}$. Simulations were initialised from completely disordered states.*

separation, rather than describing the latter in terms of a threshold activity:

$$\mathrm{Ca}^{\mathrm{act}} = \frac{W}{\gamma}, \tag{4.21}$$

where W is the strength of the anchoring expressed in 4.10, and γ is once again the surface tension of the nematic/isotropic interface. Writing it out in full length leads to what seems a rather cumbersome expression:

$$\mathrm{Ca}^{\mathrm{act}} = \frac{32\sqrt{2}\xi_I}{(\Gamma\eta+2)^{\frac{1}{2}}}\sqrt{\frac{1}{\frac{K}{L}+2\frac{L}{K}+4}}\sqrt{\frac{\zeta}{K}}. \tag{4.22}$$

However, we note that for fixed K/L ratio (which is what determines whether we are in the elastic or in the surface-tension-led regime), and for fixed viscosities Γ, η and interface thickness ξ_I, the active capillary number can be summarised as

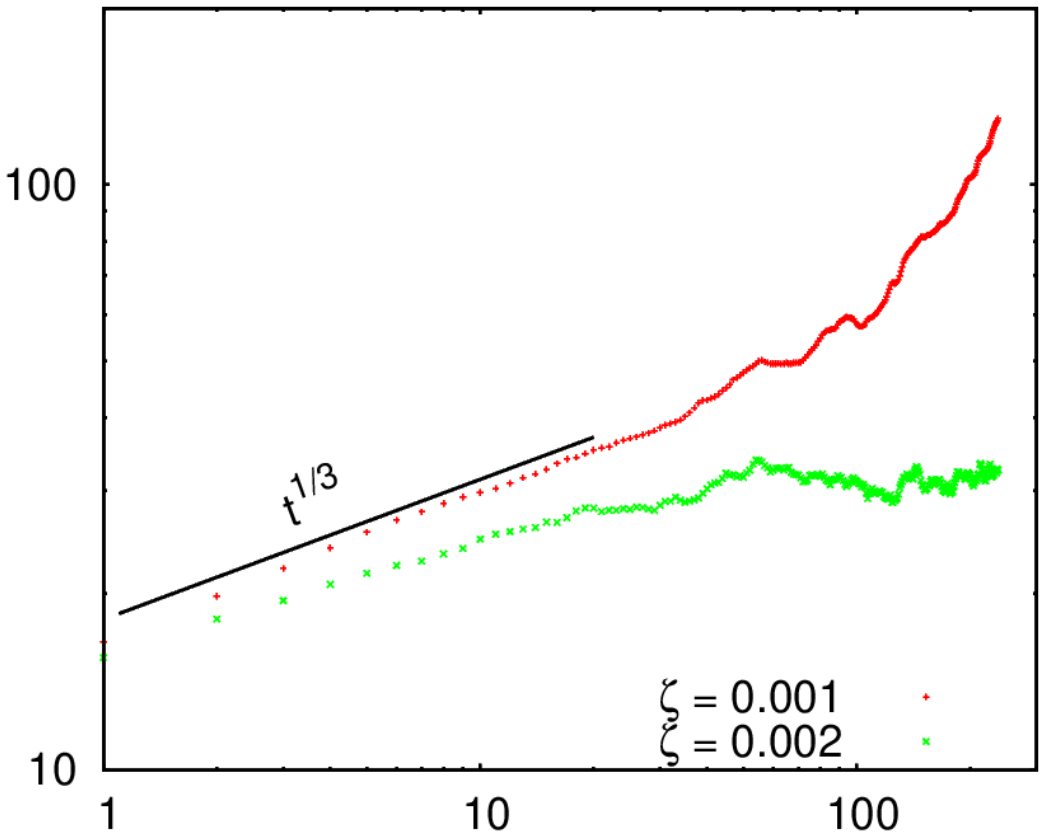

Figure 4.10 *Growth of the nematic domain size l_{dom} in the surface tension led regime ($\gamma\xi_I/K = 5$) for two values of the activity ζ; when below a critical ζ_c, the presence of activity has little effect on the coarsening dynamics, characterized by a $t^{\frac{1}{3}}$ growth regime at early times. Simulations were performed in a 400×400 box, initialised in a completely disordered state.*

it follows

$$\mathrm{Ca}^{\mathrm{act}} = f\left(\xi_I, \frac{K}{L}, \Gamma\eta\right)\sqrt{\frac{\zeta}{K}}, \tag{4.23}$$

that is, $\mathrm{Ca}^{\mathrm{act}} \propto \sqrt{\frac{\zeta}{K}}$; here f is the function encapsulating all the fixed parameters - hence a constant.

Numerical simulations seem to confirm that $\mathrm{Ca}^{\mathrm{act}}$ captures properly the arrest of the phase separation dynamics, as shown in figure (4.11); while for different surface tensions γ the domain growth stops past different values of $\zeta_c = \zeta_c(\gamma)$, there seems to be a single value $\mathrm{Ca}^{\mathrm{act}}$ that marks the passage to a finite lengthscale of the sytem. While the actual value at which l_{dom} saturates is still not unique for a given $\mathrm{Ca}^{\mathrm{act}}$, we argue that the active capillary number provides a useful criterion for predicting whether the effect of the activity at interfaces will halt

the phase separation.

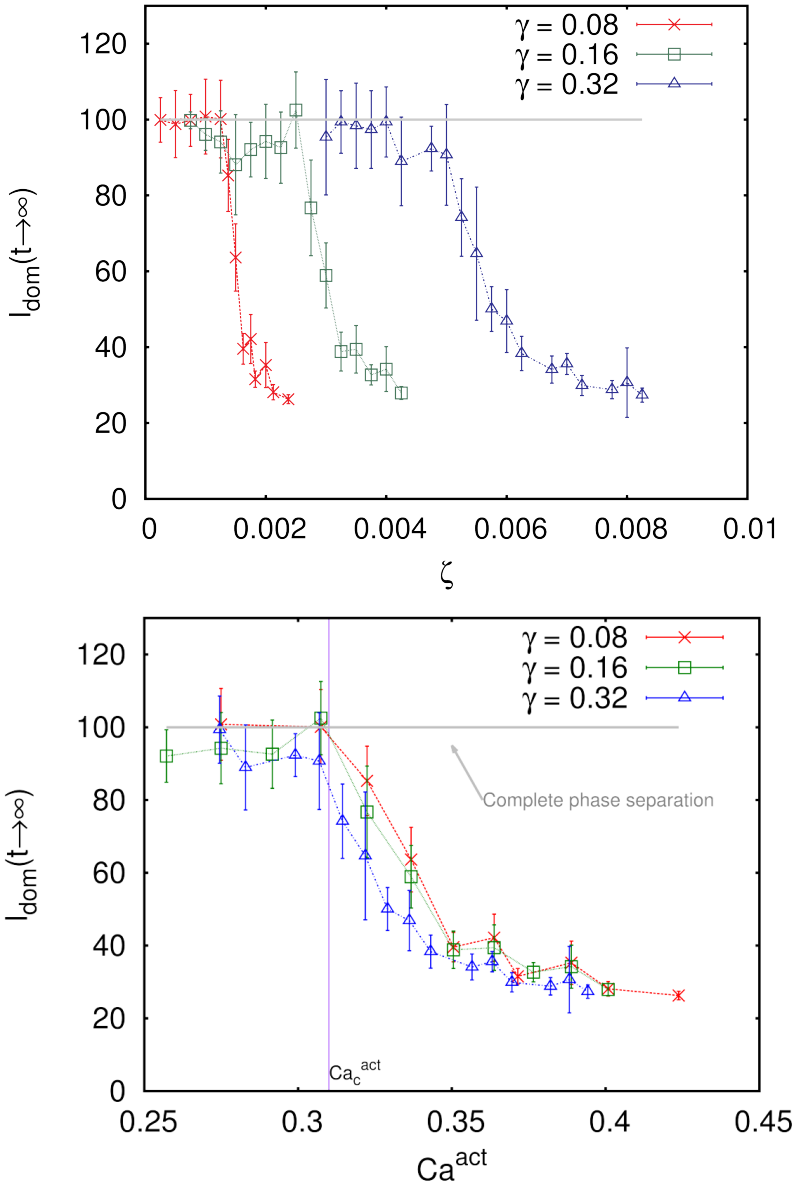

Figure 4.11 *Stationary value of* l_{dom} *in the surface tension led regime* ($\gamma\xi_I/L = 5$) *for* $\gamma = 0.08$, $\gamma = 0.16$, $\gamma = 0.32$ *as a function of the activity* ζ *(top), and the same data as a function of the capillary number* $\mathrm{Ca}^{\mathrm{act}}$ *(bottom). The data was obtained from averaging over twenty simulations of quenches for each value of the activity or capillary number, in a* 200×200 *domain. The three different curves for* l_{dom} *as a function of* ζ *seem to collapse onto a single curve when* l_{dom} *is expressed as a function of* $\mathrm{Ca}^{\mathrm{act}}$ *instead, with the arrested phase separation starting from a single critical value of the capillary number,* $\mathrm{Ca}_c^{\mathrm{act}}$

4.4 Summary

We have investigated a class of systems in two dimensions, consisting of a binary mixture of an isotropic and a nematic fluid in the same proportions. In the presence of activity, these systems present non-trivial dynamics and interface properties that cannot be quantified as a thermodynamic effect, but rather are a genuinely non-equilibrium property of the system.

In the ordered phase, we observed the nematic director profile preferentially aligning tangentially or perpendicularly to interfaces, in the cases of extensile or contractile activity respectively. This effective alignment persist even in the absence of an anchoring term in the thermodynamic free energy, and it is a direct consequence of the active stresses; these operate via a dual mechanism: the component of the active forces perpendicular to the interface tend to stretch interface regions with the favoured alignment, while shrinking those with unfavoured orientation; at the same time, the active forces tangential to the interface produce a shear field that rotates the nematic field in the preferred orientation.

While the terms causing an effective active anchoring can be identified, they can't be integrated in a free energy approach, and thus need to be considered as a genuinely out-of-equilibrium effect. However, the strength of the active anchoring can be estimated by opposing it to an actual opposing thermodynamic anchoring, so to evaluate at which point a crossover between the two regimes occurs.

We further considered the implications of the active anchoring, by analysing the coarsening dynamics of the mixture. While for a standard binary fluid model one would eventually expect complete phase separation of the two components, the presence of the activity can disrupt the structural integrity of the phases, resulting in the existence of well defined domains, but with finite size. Starting from initially completely disordered states, ordering naturally occurs, driven by diffusive, elastic and hydrodynamic contributions. We derived a phenomenological equation for the average lengthscale of the ordered domains, justified by scaling arguments descending from the equations governing the dynamics of the mixture. We then identified two distinct regimes: one where elastic stresses prevail over the surface tension, characterised by highly ordered and elongated nematic phases; and one where surface tension is the driving force of the phase separation, with weaker elastic forces, characterised by a

more disordered nematic phase and a coarsening reminiscent of the traditional isotropic binary fluid phase separation. In the first of the two regimes, we found that the elastic diffusive terms in the phenomenological equation can account for the scaling of the average domain size, giving a crossover between $l_{\mathrm{dom}} \sim \zeta^{-\frac{1}{2}}$ and $l_{\mathrm{dom}} \sim \zeta^{-\frac{1}{4}}$ in steady states; and a scaling in time close to $l_{\mathrm{dom}} \sim t^{\frac{1}{4}}$ at early times. In the second regime, activity does not necessarily arrest the phase separation: contrarily to the laminar-elastic regime, for small enough activities, the system still separates completely. Phase separation in the mixture is arrested when the activity reaches a a certain threshold value ζ_c which is dependent on the magnitude of the surface tension $\gamma = \frac{K+2L}{6\xi_I}$. For this reason we decided to introduce a capillary number to characterize the competition between the tension and the activity at the interface, defined as the ratio of γ and W, the effective strength of the active anchoring. Interestingly, we observe that, while phase separation arrest occurs for different values of the activity ζ, the coarsening begins to saturate at a finite domain lengthscale l_{dom} at the same value of the active capillary number $\mathrm{Ca}^{\mathrm{act}}$.

Chapter 5

Conclusions

In this thesis we have studied, by means of computer simulations and theory, the dynamics of active fluids. The motivation for this investigation is that many features of active fluids are currently poorly understood, whilst these systems are both of fundamental interest (due to their nonequilibrium nature) and ubiquituous in living systems and nature in general. We have focussed in particular on the cases of mixtures of passive (isotropic) and active fluids, which can be realised in the lab, for instance, as aqueous suspensions of molecular motors and cytoskeletal filaments.

Because the elementary constituents of active fluids – cytoskeletal filaments or microbial swimmers – are typically elongated, or rod-like, they can acquire orientational order, so that the natural language within which to describe them is that of liquid crystals. Additionally, because active particles typically exert dipolar forces on their surrounding, even if the microscopic constituents were spherically symmetric, they would still be generically associated with a local orientation (this case may be relevant for spherical swimmers such as synthetic self-phoretic particles). Orientational order can either be polar or apolar, according to the microscopic nature of the interactions between the constituents. As argued in Chapters 3 and 4, the polar case is relevant to actin and microtubules *in vivo*, as these filaments are not symmetric, and their two ends are distinct (they normally grow at the plus end and de-polymerise at the minus end). On the other hand, the apolar case of nematic order applies to active matter self-assembled *in vitro* from microtubule bundles and kinesin motors.

In particular, in Chapter 3 we studied the dynamics of a mixture of a passive fluid droplet immersed in a polar active nematic. This case is to some extent similar to that of a passive colloidal spheres, although unlike this the droplet can deform and change its shape. We have found several dynamical regimes, according to the nature of the active force (whether extensile or contractile) and to the anchoring of the orientational order at the droplet-bulk interface. Most notably, if the active host is extensile, and the anchoring is tangential, we found a non-equilibrium transition between a regime where the droplet is stationary but constantly sheared by the flow arising from the activity in the bulk, and another one where the droplet deforms and becomes motile. Motility occurs along a direction perpendicular to the bulk polarisation (orientation). This non-equilibrium phase transition is discontinuous in nature, and it would be of interest to look for this phenomenon experimentally. A candidate model to achieve this is the hierarchical self-assembled matter in Ref. [5]. Although the order there is nematic rather than polar, we expect that a similar transition should occur there as well as the self-motile regime is defect-free and we included no terms violating the $\boldsymbol{p} \to -\boldsymbol{p}$ symmetry.

In Chapter 3 we have also studied the case of normal anchoring, and found that the hyperbolic hedgehog defect which arises (of topological charge -1) breaks the symmetry of the polarisation pattern and leads to motion without any threshold. Intriguingly, we found that contractile and extensile hosts lead to motion which are not mirror-symmetric for equal and opposite values of the activity. This is because bend and splay, which feature in different ratios and at different places in the liquid crystal patterns, couple differently to the two kinds of activity.

Taken together, the results in Chapter 3 show that the study of even a single passive droplet in an active polar fluid yield very rich dynamics and phenomenology, which all depends on the far-from-equilibrium nature of active matter. Besides a possible experimental realisations, our results could also stimulate further theoretical work to predict analytically the flow and polarisation patterns in the non-linear regime (*e.g.*, corresponding to the transition between rotating and motile droplet in the extensile and tangential anchoring case). It may also be fruitful to characterise more in detail the turbulent regime of high activity which we have not explored in our work.

In Chapter 4, we have instead considered a 50 : 50 mixture of passive isotropic and active nematic fluids, which yields a rich phase separation dynamics. We

have found that depending on the relative strength of active and elastic effects, the mixture either phase separates to completion or is arrested in a configuration where domains reach a self-limiting size. The size in this latter phase is dictated by the balance between active and elastic forces.

For the regime where phase separation proceeds to completion, we found different growth laws, with exponents compatible with those found in the literature for binary mixtures of either isotropic or isotropic-nematic fluids. The arrested phase is unique to the case of active fluids, and we have shown that a key feature in determining the final morphology is an effective active anchoring which arises due to the contractile and extensile forcing, and is purely non-equilibrium in origin. The morphology in the arrested regime therefore depends on the orientational order, hence is fundamentally different from that observed in other spontaneously phase-separating active matter systems, such as a suspension of self-propelled particles which is known to undergo motility-induced phase separation, which can be arrested due to hydrodynamic interactions [132].

Appendix A

Inverse droplets in large geometries

Here we show one snapshot for a simulation of the same inverse droplet as in Section 3.3 but in a larger 'box', to verify the absence of confinement effects. Similarly to what seen for the rectangular box, the droplet acquires motility and the flow pushes it along the positive x-direction, with a defect located on the left side of the surface of the droplet. The flow and polarisation are qualitatively similar to the ones presented in Chapter 3 in smaller geometries, and the measured drift velocity is $v_d \simeq 2.58 \cdot 10^{-4}$ (lattice units), very close to the case with a 'narrower' channel. We therefore ruled out the presence of finite size effects due to the periodic boundary conditions.

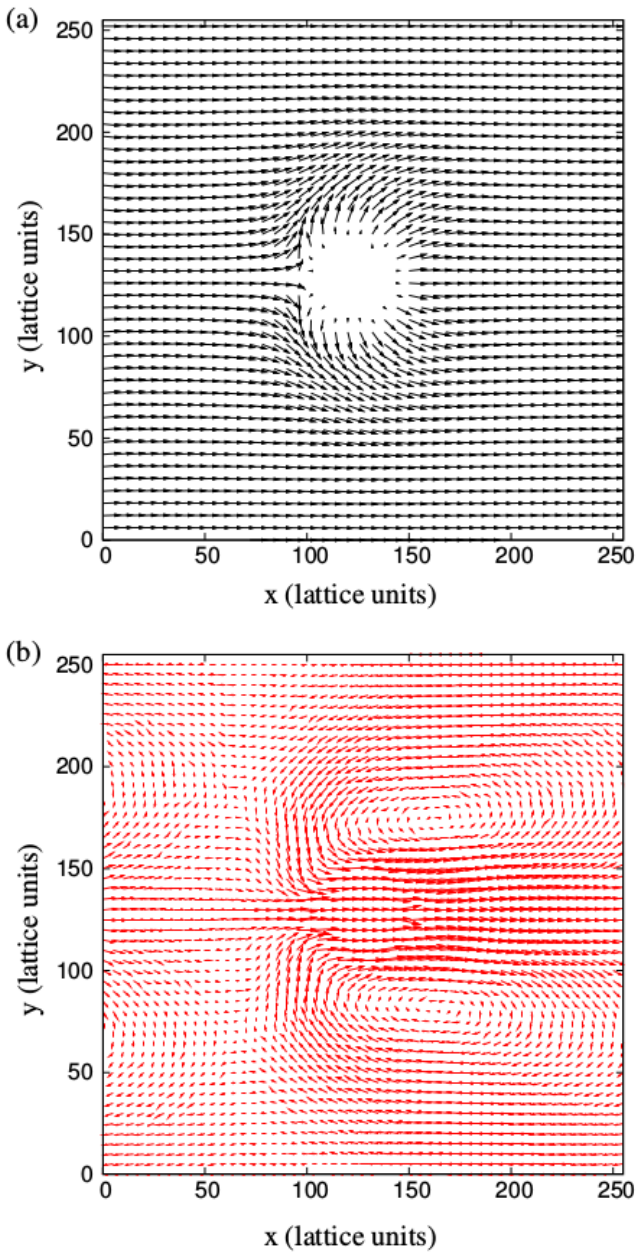

Figure A.1 *The polarisation field outside an isotropic droplet with homeotropic anchoring on its surface is reported in (a) for the contractile case, with* $\zeta = -0.0001$, $\kappa = 0.02$, $k = 0.14$. *The lattice size is* $L_x = L_y = 256$. *The other parameters are as in Chapter 3 in the main text. The corresponding velocity field profile is shown in (b).*

Appendix B

Active stress in the linear regime

The polarisation field around a static isotropic droplet embedded in a polar medium with homeotropic anchoring can be expressed as a function of an angle field $\alpha(\boldsymbol{x})$ as $p_x = \cos(\alpha)$, $p_y = \sin(\alpha)$. In polar coordinates the angle field reads:

$$\alpha(r,\theta) = 2\theta - \tan^{-1}\left(\frac{r\sin\theta}{Rc_0 + r\cos\theta}\right) - \tan^{-1}\left(\frac{r\sin\theta}{R/c_0 + r\cos\theta}\right). \tag{B.1}$$

When the activity ζ is finite, the droplet is propelled forward in the x-direction by the defect that emerges at its rear as a consequence of the homeotropic anchoring. For small enough activity, the droplets reaches a steady state velocity scaling linearly with the activity; this regime is characterized by a small Ericksen number $\mathrm{Er} = \frac{\Gamma v R}{\kappa}$ and $\zeta \ll \Gamma/\kappa$, meaning that the elastic stresses (related to k, κ, β) dominate over viscous and active effects. We assume that in this regime the polar configuration defined by α in the static limit persist unaltered, as confirmed by our simulations, see figure (3.2,3.7).

In this quasi-static limit, we assume that the polarisation field translates 'rigidly' in the direction of the droplet motion, namely $\boldsymbol{p} = \boldsymbol{p}(\alpha(\boldsymbol{x} - \hat{x}v_{drift}t))$. We can then explicitly calculate the active force density on the droplet, which reads:

$$f_x^{\mathrm{act}} = \frac{1}{2\pi}\int_{-\pi}^{\pi} \partial_i \sigma_{ij}^{\mathrm{act}} \hat{x}_j \Big|_{r=R} \mathrm{d}\theta = -\frac{1}{2\pi}\int_{-\pi}^{\pi} \partial_i(\phi\zeta p_i p_j)\hat{x}_j \Big|_{r=R} \mathrm{d}\theta. \tag{B.2}$$

Explicitly, this reads:

$$f_x^{\mathrm{act}} = -\frac{\zeta\phi_0}{4\pi}\int_{-\pi}^{\pi} (\partial_x(p_x p_x) + \partial_y(p_x p_y))_{r=R}\mathrm{d}\theta, \tag{B.3}$$

where the term in $\nabla\phi$ has been omitted, as it averages to zero by symmetry. Using the definition of $\boldsymbol{p} = \boldsymbol{p}(\alpha)$, we obtain:

$$f_x^{\text{act}} = -\frac{\zeta\phi_0}{4\pi}\int_{-\pi}^{\pi}\left(-\sin(2\alpha)\partial_x\alpha + \cos(2\alpha)\partial_y\alpha\right)_{r=R}\mathrm{d}\theta. \tag{B.4}$$

Writing now the derivatives in polar coordinates leads to:

$$\begin{aligned} f_x^{\text{act}} = -\frac{\zeta\phi_0}{4\pi}\int_{-\pi}^{\pi}\Bigg(&\cos(2\alpha)\left(\sin\theta\partial_r\alpha + \frac{\cos\theta}{r}\partial_\theta\alpha\right) \\ &- \sin(2\alpha)\left(\cos\theta\partial_r\alpha + \frac{\sin\theta}{r}\partial_\theta\alpha\right)\Bigg)_{r=R}\mathrm{d}\theta. \end{aligned} \tag{B.5}$$

By noting that $\alpha(r = R, \theta) = \theta$, and through a few trigonometry identities, equation (B.5) can be further simplified to:

$$\begin{aligned} f_x^{\text{act}} &= -\frac{\zeta\phi_0}{4\pi}\int_{-\pi}^{\pi}\left(\sin(\theta - 2\alpha)\partial_r\alpha + \frac{\cos(2\alpha - \theta)}{R}\right)_{r=R}\mathrm{d}\theta \\ &= -\frac{\zeta\phi_0}{2\pi R}\int_{-\pi}^{\pi}\sin(\theta)\frac{\sin\theta}{\left(c_0 + \frac{1}{c_0}\right) + 2c_0\cos\theta}\mathrm{d}\theta. \end{aligned} \tag{B.6}$$

In the last equality, we used again $\alpha(r = R, \theta) = \theta$, and dropped the second term in the first line of equation (B.6), as it averages to zero. The integral can now be evaluated immediately, giving:

$$f_x^{\text{act}} = -\frac{\zeta\phi_0}{Rc_0}. \tag{B.7}$$

Appendix C

Boundary conditions for the alignment angle at a nematic - isotropic interface

We consider a flat interface approximation for the following calculations, assuming that the interface lies along the x direction, with the isotropic phase on top of the nematic, as sketched in figure (4.4).

In the pure tumbling regime, corresponding to the shear alignment coupling parameter $\xi = 0$, the momentum equation for a nematic fluid (4.4)

$$\partial_t u_i + u_k \partial_k u_i = \partial_k \sigma_{ki}, \tag{C.1}$$

where the stress tensor can be expressed in the following form:

$$\sigma_{ij} = 2\eta\Lambda_{ij} - p\delta_{ij} + [Q,H]\epsilon_{ij} - \zeta Q_{ij} + (f - \mu\phi)\delta_{ij} - \frac{\partial f}{\partial(\partial\phi)}\partial_j\phi - \frac{\partial f}{\partial(\partial_i Q_{kl})}\partial_j Q_{kl}, \tag{C.2}$$

where ϵ_{ij} is the Levi-Civita antisymmetric symbol, and $[Q,H]$ is:

$$[Q,H] = Q_{xk}Hky - H_{xk}Q_{ky} \tag{C.3}$$

We make the assumption that there is no flow across the interface ($u_y = 0$), and that the ∂_x derivatives vanish because of the symmetry. We then consider the system to be overdamped, as it is usually the case for the active fluids considered,

characterized by small Reynolds number. Equation (C.1) is then reduced to:

$$\eta \partial_y u_x = \zeta Q_{xy} - [Q, H] = \zeta \sin(2\theta) - [Q, H] \tag{C.4}$$

Under the same assumptions, the nematic profile reads:

$$\partial_t Q_{ij} = Q_{ik}\epsilon_{ij}\partial_y u_x + \Gamma H_{ij}, \tag{C.5}$$

It is then useful to note that $Q_{xx}\partial_t Q_{xy} - Q_{xy}\partial_t Q_{xx}$ reads

$$2S^2 \partial_t \theta = -S^2 \partial_y u_x + \frac{\Gamma}{2}[Q, H]. \tag{C.6}$$

We can now use equation (C.1) to eliminate $\partial_y u_x$ from (C.6), which finally leads to

$$S^2 \partial_t \theta = -\frac{\zeta S^3}{2\eta} \sin(2\theta) + \frac{\Gamma\eta + 2S^2}{4\eta}[Q, H]. \tag{C.7}$$

Applying the definition of the molecular field H_{ij} for the free energy from equation (4.1), and assuming strong coupling C - corresponding to $\phi \simeq S$, equation (C.7) reduces to (4.9):

$$S^2 \partial_t \theta = -\frac{\zeta S^3}{2\eta} \sin 2\theta + (\Gamma\eta + 2S^2)(2LS^2 \partial_y \partial_y \theta + 4LS \partial_y \theta \partial_y S). \tag{C.8}$$

Appendix D

Effective active anchoring

We extend the free energy density given in equation (4.1) so to include a thermodynamic anchoring term:

$$\mathcal{F} = \int \left\{ \frac{A}{2}\phi^2(\phi-1)^2 + \frac{K}{2}(\partial_k\phi)^2 + \frac{L}{2}(\partial_k Q_{ij})^2 + \frac{C}{2}\left(\phi^2 - \frac{Q_{ij}Q_{ij}}{2}\right)^2 + \frac{J}{2}\partial_i Q_{ij}\partial_j\phi \right\}, \tag{D.1}$$

where the sign of J defines the type of anchoring: $J > 0$ will favour the nematic phase aligning to the interface (tangential), while $J < 0$ corresponds to a homeotropic anchoring. The corresponding surface tension is then

$$\gamma = \frac{K + 2L - J\cos(2\theta)}{6\xi_I}, \tag{D.2}$$

where $\xi_I = \sqrt{\frac{K+2L-J\cos(2\theta)}{A}}$ is the 'thickness' of the diffuse interface. One can then define the strength of the thermodynamic anchoring as the difference between the interfacial tensions in the homeotropic and tangential states, namely

$$W = |\gamma - \gamma\perp| \simeq \frac{|J|}{3\xi_I} \tag{D.3}$$

By including the thermodynamic anchoring term, equation (C.8) changes to:

$$S^2\partial_t\theta = -\frac{\zeta S^3}{2\eta}\sin 2\theta + (\Gamma\eta + 2S^2)\left(2LS^2\partial_y\partial_y\theta + 4LS\partial_y\theta\partial_y S - \frac{JS}{4}\sin(2\theta)(\partial_y S)^2\right). \tag{D.4}$$

The order parameter is constant in the bulk, and sharply increases at the interface over the lengthscale $\xi_I = \sqrt{\frac{2L+K-J\cos(2\theta)}{A}}$, as from equation (3.13):

$$\phi(y) \simeq S(y) \simeq \frac{1}{2} + \frac{1}{2}\tanh\left(\frac{y}{2\xi_I}\right). \tag{D.5}$$

In stationary conditions, the left hand side of equation (D.4) vanishes; as for the right hand side, terms in $\partial_y S$ will dominate over the others; by dropping all but the highest orders in the gradients of S, we obtain the boundary condition:

$$L\partial_y\theta = \frac{J\partial_y S}{16}\sin(2\theta) = \frac{3|W|}{64}\sin(2\theta), \tag{D.6}$$

where we used equation (D.5) to evaluate $\partial_y S$ in the mid-point of the interface, and equation (D.3). We also assumed that $J < 0$, so as to produce homeotropic anchoring to oppose a planar active anchoring for $\zeta > 0$.

In the bulk of the nematic region, equation (D.4) reduces to:

$$\partial_y\partial_y\theta = \frac{1}{2}\lambda^{-2}\sin(2\theta), \tag{D.7}$$

where $\lambda = \sqrt{L(\Gamma\eta + 2)/\zeta}$. It has been noted [133] that such an equation is analogous to hat for the Freedericksz transition the phenomenon by which an applied electric field causes an an- chored layer of dielectric liquid crystal to distort above a critical thickness with activity playing the role of the electric field. But unlike in [133], the anchoring is 'weak' (i.e. finite). For such anchoring conditions, it can be shown that there are two transition points [134]: one where the director becomes uniform and horizontal (active anchoring dominates over thermodynamic anchoring) and one where the director becomes uniform and vertical (thermodynamic anchoring dominates). Between these points, there is a continuous set of deformed textures marking the crossover of the two anchoring regimes.

To determine the point where the uniform horizontal texture starts to deform, we solve equation (D.7) in the limit of small θ. Assuming the solution is symmetrical across the interface, we obtain:

$$\frac{\theta(y)}{\theta(h)} = \frac{\cosh(y/\lambda)}{\cosh(h/\lambda)}, \tag{D.8}$$

where h is the relevant lengthscale over which the order persists inside of the

nematic phase. When combining (D.8) with the boundary condition (D.6), we provide a self-consistency relation for the anchoring strength:

$$|W^{\text{horiz}}| = \frac{32L}{3\lambda} \tanh\left(\frac{h}{\lambda}\right). \tag{D.9}$$

Following a similar procedure, we can solve (D.8) around $\theta = \frac{\pi}{2}$ for $\zeta < 0, J > 0$, yeilding for the vertical transition:

$$|W^{\text{vert}}| = \frac{32L}{3\lambda} \tan\left(\frac{h}{\lambda}\right). \tag{D.10}$$

In the limit of small $\frac{h}{\lambda}$, these transition points converge upon a common value

$$|W| = \frac{32Lh}{3\lambda^2} = \frac{16\sqrt{2}\zeta h}{3(\Gamma\eta + 2)} \tag{D.11}$$

which can thus be taken as the effective strength of the active anchoring. We see that this depends not only on the magnitude of the active ζ, but also on the lengthscale h. For systems that we defined as 'laminar' in Chapter 4, this lengthscale is l_{dom} , the characteristic lengthscale of the domains, as shall be defined in the next section. However, if the ratio K/L is higher, as will be quantified in the next section, the bulk nematic will show distortions within the domains, as illustrated in figure (4.10). In this turbulent regime, the appropriate lengthscale the dominant scaling of active turbulence in bulk nematics, $h \sim \sqrt{L/\zeta}$ [31, 32, 99, 133]. The active anchoring strength follows

$$|W| \sim \frac{16}{3}\sqrt{\frac{2L\zeta}{\Gamma\eta + 2}}. \tag{D.12}$$

Bibliography

[1] G De Magistris, A Tiribocchi, CA Whitfield, RJ Hawkins, ME Cates, and D Marenduzzo. Spontaneous motility of passive emulsion droplets in polar active gels. *Soft matter*, 10(39):7826–7837, 2014.

[2] G. De Magistris and D. Marenduzzo. An introduction to the physics of active matter. *Physica A: Statistical Mechanics and its Applications*, 418:65–77, 2015.

[3] Tamás Vicsek and Anna Zafeiris. Collective motion. *Physics reports*, 517(3-4):71–140, 2012.

[4] R Kemkemer, D Kling, D Kaufmann, and H Gruler. Elastic properties of nematoid arrangements formed by amoeboid cells. *The European Physical Journal E*, 1(2-3):215–225, 2000.

[5] Tim Sanchez, Daniel T. N. Chen, Stephen J. DeCamp, Michael Heymann, and Zvonimir Dogic. Spontaneous motion in hierarchically assembled active matter. *Nature*, 491:431,434, 2012.

[6] Tamás Vicsek, András Czirók, Eshel Ben-Jacob, Inon Cohen, and Ofer Shochet. Novel type of phase transition in a system of self-driven particles. *Phys. Rev. Lett.*, 75:1226–1229, 1995.

[7] G Foffano, JS Lintuvuori, A Tiribocchi, and D Marenduzzo. The dynamics of colloidal intrusions in liquid crystals: A simulation perspective. *Liquid Crystals Reviews*, 2(1):1–27, 2014.

[8] Paul M Chaikin and Tom C Lubensky. *Principles of condensed matter physics*. Cambridge university press, 2000.

[9] Boris Rubinstein, Maxime F Fournier, Ken Jacobson, Alexander B Verkhovsky, and Alex Mogilner. Actin-myosin viscoelastic flow in the keratocyte lamellipod. *Biophysical journal*, 97(7):1853–1863, 2009.

[10] Erin L Barnhart, Kun-Chun Lee, Kinneret Keren, Alex Mogilner, and Julie A Theriot. An adhesion-dependent switch between mechanisms that determine motile cell shape. *PLoS biology*, 9(5):e1001059, 2011.

[11] R Golestanian, TB Liverpool, and A Ajdari. Designing phoretic micro-and nano-swimmers. *New Journal of Physics*, 9(5):126, 2007.

[12] R Aditi Simha and Sriram Ramaswamy. Hydrodynamic fluctuations and instabilities in ordered suspensions of self-propelled particles. *Physical review letters*, 89(5):058101, 2002.

[13] Sriram Ramaswamy, R Aditi Simha, and John Toner. Active nematics on a substrate: Giant number fluctuations and long-time tails. *EPL (Europhysics Letters)*, 62(2):196, 2003.

[14] Frank Schweitzer. Brownian agents and active particles. on the emergence of complex behavior in the natural and social sciences. *Springer Series in Synergetics. Berlin, Germany, Springer*, 2003.

[15] Walter F Paxton, Kevin C Kistler, Christine C Olmeda, Ayusman Sen, Sarah K St. Angelo, Yanyan Cao, Thomas E Mallouk, Paul E Lammert, and Vincent H Crespi. Catalytic nanomotors: autonomous movement of striped nanorods. *Journal of the American Chemical Society*, 126(41):13424–13431, 2004.

[16] Yashodhan Hatwalne, Sriram Ramaswamy, Madan Rao, and R. Simha. Rheology of Active-Particle Suspensions. *Physical Review Letters*, 92(11):118101, 2004.

[17] John Toner, Yuhai Tu, and Sriram Ramaswamy. Hydrodynamics and phases of flocks. *Annals of Physics*, 318(1):170 – 244, 2005. Special Issue.

[18] Frank Juelicher, Karsten Kruse, Jacques Prost, and J-F Joanny. Active behavior of the cytoskeleton. *Physics Reports*, 449(1-3):3–28, 2007.

[19] Vijay Narayan, Sriram Ramaswamy, and Narayanan Menon. Long-lived giant number fluctuations in a swarming granular nematic. *Science*, 317(5834):105–108, 2007.

[20] Jean-François Joanny and Jacques Prost. Active gels as a description of the actin-myosin cytoskeleton. *HFSP journal*, 3(2):94–104, 2009.

[21] Sriram Ramaswamy. The mechanics and statistics of active matter. *Annual Review of Condensed Matter Physics*, 1(1):323–345, 2010.

[22] M. C. Marchetti, J. F. Joanny, S. Ramaswamy, T. B. Liverpool, J. Prost, Madan Rao, and R. Aditi Simha. Hydrodynamics of soft active matter. *Rev. Mod. Phys.*, 85:1143–1189, 2013.

[23] John Toner and Yuhai Tu. Long-range order in a two-dimensional dynamical xy model: how birds fly together. *Physical review letters*, 75(23):4326, 1995.

[24] John Toner and Yuhai Tu. Flocks, herds, and schools: A quantitative theory of flocking. *Physical review E*, 58(4):4828, 1998.

[25] Karsten Kruse, Jean-Francois Joanny, Frank Jülicher, Jacques Prost, and Ken Sekimoto. Generic theory of active polar gels: a paradigm for cytoskeletal dynamics. *The European Physical Journal E*, 16(1):5–16, 2005.

[26] Tanniemola B Liverpool and M Cristina Marchetti. Rheology of active filament solutions. *Physical review letters*, 97(26):268101, 2006.

[27] ME Cates, SM Fielding, D Marenduzzo, E Orlandini, and JM Yeomans. Shearing active gels close to the isotropic-nematic transition. *Physical review letters*, 101(6):068102, 2008.

[28] R Phillips, J Kondev, J Theriot, and H Garcia. *Physical Biology of the Cell*. 2009.

[29] ME Cates, D Marenduzzo, I Pagonabarraga, and J Tailleur. Arrested phase separation in reproducing bacteria creates a generic route to pattern formation. *Proceedings of the National Academy of Sciences*, 107(26):11715–11720, 2010.

[30] Sumesh P. Thampi, Ramin Golestanian, and Julia M. Yeomans. Velocity correlations in an active nematic. *Phys. Rev. Lett.*, 111:118101, 2013.

[31] Sumesh P Thampi, Ramin Golestanian, and Julia M Yeomans. Vorticity, defects and correlations in active turbulence. *Phil. Trans. R. Soc. A*, 372(2029):20130366, 2014.

[32] Luca Giomi. Geometry and topology of turbulence in active nematics. *Physical Review X*, 5(3):031003, 2015.

[33] Sumesh P Thampi, Amin Doostmohammadi, Tyler N Shendruk, Ramin Golestanian, and Julia M Yeomans. Active micromachines: Microfluidics powered by mesoscale turbulence. *Science advances*, 2(7):e1501854, 2016.

[34] Amin Doostmohammadi, Tyler N Shendruk, Kristian Thijssen, and Julia M Yeomans. Onset of meso-scale turbulence in active nematics. *Nature communications*, 8:15326, 2017.

[35] S. Chapman and T.G. Cowling. *The Mathematical Theory of Non-uniform Gases: An Account of the Kinetic Theory of Viscosity, Thermal Conduction and Diffusion in Gases*. Cambridge Mathematical Library. Cambridge University Press, 1970.

[36] T. B. Liverpool and M. C. Marchetti. Bridging the microscopic and the hydrodynamic in active filament solutions. *EPL (Europhysics Letters)*, 69(5):846, 2005.

[37] Eric Bertin, Michel Droz, and Guillaume Grégoire. Boltzmann and hydrodynamic description for self-propelled particles. *Phys. Rev. E*, 74:022101, Aug 2006.

[38] Eric Bertin, Hugues Chaté, Francesco Ginelli, Shradha Mishra, Anton Peshkov, and Sriram Ramaswamy. Mesoscopic theory for fluctuating active nematics. *New journal of physics*, 15(8):085032, 2013.

[39] A J Bray. Theory of phase-ordering kinetics. *Advances in Physics*, 43(3):357–459, 1994.

[40] Marco Polin, Idan Tuval, Knut Drescher, Jerry P Gollub, and Raymond E Goldstein. Chlamydomonas swims with two gears in a eukaryotic version of run-and-tumble locomotion. *Science*, 325(5939):487–490, 2009.

[41] Martin Lenz. Geometrical origins of contractility in disordered actomyosin networks. *Phys. Rev. X*, 4:041002, 2014.

[42] Daniel S Seara, Vikrant Yadav, Ian Linsmeier, A Pasha Tabatabai, Patrick W Oakes, SM Ali Tabei, Shiladitya Banerjee, and Michael P Murrell. Entropy production rate is maximized in non-contractile actomyosin. *Nature communications*, 9(1):4948, 2018.

[43] Aparna Baskaran and M Cristina Marchetti. Hydrodynamics of self-propelled hard rods. *Physical Review E*, 77(1):011920, 2008.

[44] K. Kruse, J. F. Joanny, F. Jülicher, J. Prost, and K. Sekimoto. Asters, vortices, and rotating spirals in active gels of polar filaments. *Phys. Rev. Lett.*, 92:078101, 2004.

[45] R. Voituriez, J. F. Joanny, and J. Prost. Generic phase diagram of active polar films. *Phys. Rev. Lett.*, 96:028102, Jan 2006.

[46] D. Marenduzzo, E. Orlandini, M. E. Cates, and J. M. Yeomans. Steady-state hydrodynamic instabilities of active liquid crystals: Hybrid lattice Boltzmann simulations. *Physical Review E - Statistical, Nonlinear, and Soft Matter Physics*, 76(3):1–18, 2007.

[47] David Saintillan and Michael J. Shelley. Instabilities and pattern formation in active particle suspensions: Kinetic theory and continuum simulations. *Phys. Rev. Lett.*, 100:178103, Apr 2008.

[48] S. M. Fielding, D. Marenduzzo, and M. E. Cates. Nonlinear dynamics and rheology of active fluids: Simulations in two dimensions. *Phys. Rev. E*, 83:041910, Apr 2011.

[49] L. Giomi, L. Mahadevan, B. Chakraborty, and M. F. Hagan. Excitable patterns in active nematics. *Phys. Rev. Lett.*, 106:218101, 2011.

[50] Howard C. Berg and Richard M. Berry. *E. Coli in motion*. Springer, 2005.

[51] Hugues Chaté, Francesco Ginelli, Guillaume Grégoire, and Franck Raynaud. Collective motion of self-propelled particles interacting without cohesion. *Phys. Rev. E*, 77:046113, 2008.

[52] Ramin Golestanian. Anomalous diffusion of symmetric and asymmetric active colloids. *Phys. Rev. Lett.*, 102:188305, May 2009.

[53] Silke Henkes, Yaouen Fily, and M. Cristina Marchetti. Active jamming: Self-propelled soft particles at high density. *Phys. Rev. E*, 84:040301, 2011.

[54] A. B. Slowman, M. R. Evans, and R. A. Blythe. Jamming and attraction of interacting run-and-tumble random walkers. *Phys. Rev. Lett.*, 116:218101, 2016.

[55] D. Marenduzzo, E. Orlandini, and J. M. Yeomans. Hydrodynamics and rheology of active liquid crystals: A numerical investigation. *Phys. Rev. Lett.*, 98:118102, 2007.

[56] Luca Giomi, M. Cristina Marchetti, and Tanniemola B. Liverpool. Complex spontaneous flows and concentration banding in active polar films. *Phys. Rev. Lett.*, 101:198101, 2008.

[57] J. Tailleur and M. E. Cates. Statistical mechanics of interacting run-and-tumble bacteria. *Phys. Rev. Lett.*, 100:218103, 2008.

[58] Ewan J Hemingway, Prashant Mishra, M Cristina Marchetti, and Suzanne M Fielding. Correlation lengths in hydrodynamic models of active nematics. *Soft Matter*, 12(38):7943–7952, 2016.

[59] Pierre C Hohenberg and Bertrand I Halperin. Theory of dynamic critical phenomena. *Reviews of Modern Physics*, 49(3):435, 1977.

[60] Akira Onuki. *Phase transition dynamics*. Cambridge University Press, 2002.

[61] L.D Landau and E.M. Lifshitz. *Fluid Mechanics*. Elsevier, 1987.

[62] F. M. Leslie. Some constitutive equations for liquid crystals. *Archive for Rational Mechanics and Analysis*, 28(4):265–283, 1968.

[63] Ronald G Larson. *The structure and rheology of complex fluids*, volume 150. Oxford University Press, 1999.

[64] Brett L. Van Horn and H. Henning Winter. Dynamics of shear aligning of nematic liquid crystal monodomains. *Rheologica Acta*, 39(3):294–300, 2000.

[65] C Dombrowski. C. dombrowski, l. cisneros, s. chatkaew, re goldstein, and jo kessler, phys. rev. lett. 93, 098103 (2004). *Phys. Rev. Lett.*, 93:098103, 2004.

[66] Poul M Bendix, Gijsje H Koenderink, Damien Cuvelier, Zvonimir Dogic, Bernard N Koeleman, William M Brieher, Christine M Field, L Mahadevan, and David A Weitz. A quantitative analysis of contractility in active cytoskeletal protein networks. *Biophysical journal*, 94(8):3126–3136, 2008.

[67] Antony N. Beris and Brian J. Edwards. *Thermodynamics of Flowing Systems: with Internal Microstructure*. Oxford University Press, 1994.

[68] P.G. de Gennes. *The Physics of Liquid Crystals*. Clarendon Press, 1995.

[69] C. Blanc, D. Svenšek, S. Žumer, and M. Nobili. Dynamics of nematic liquid crystal disclinations: The role of the backflow. *Phys. Rev. Lett.*, 95:097802, Aug 2005.

[70] Elsen Tjhung, Michael E Cates, and Davide Marenduzzo. Nonequilibrium steady states in polar active fluids. *Soft Matter*, 7(16):7453–7464, 2011.

[71] Matthew L Blow, Sumesh P Thampi, and Julia M Yeomans. Biphasic, lyotropic, active nematics. *Physical review letters*, 113(24):248303, 2014.

[72] Alexandre P. Solon, Joakim Stenhammar, Raphael Wittkowski, Mehran Kardar, Yariv Kafri, Michael E. Cates, and Julien Tailleur. Pressure and phase equilibria in interacting active brownian spheres. *Phys. Rev. Lett.*, 114:198301, May 2015.

[73] F. M. Leslie. Continuum theory for nematic liquid crystals. *Continuum Mechanics Thermodynamics*, 4:167–175, 1992.

[74] J. S. Rowlinson and B. Widom. *Molecular Theory of Capillarity*, volume 88. Clarendon Press, 1984.

[75] H.K. Versteeg and W. Malalaseker. *An Introduction to Computational Fluid Dynamics: The Finite Volume Method*. Pearson, 2007.

[76] M. Sbragaglia. *Private communication*.

[77] Michael R. Swift, W. R. Osborn, and J. M. Yeomans. Lattice boltzmann simulation of nonideal fluids. *Phys. Rev. Lett.*, 75:830–833, 1995.

[78] Michael R. Swift, E. Orlandini, W. R. Osborn, and J. M. Yeomans. Lattice boltzmann simulations of liquid-gas and binary fluid systems. *Phys. Rev. E*, 54:5041–5052, 1996.

[79] D. A. Wolf-Gladrow. *Lattice-Gas Cellular Automata and Lattice Boltzmann Models*. Springer-Verlag, 2000.

[80] Shiyi Chen and Gary D. Doolen. Lattice boltzmann method for fluid flows. *Annual Review of Fluid Mechanics*, 30(1):329–364, 1998.

[81] Sauro Succi. *The lattice Boltzmann equation: for fluid dynamics and beyond*. Oxford university press, 2001.

[82] Cyrus K. Aidun and Jonathan R. Clausen. Lattice-boltzmann method for complex flows. *Annual Review of Fluid Mechanics*, 42(1):439–472, 2010.

[83] K. Huang. *Statistical mechanics*. Wiley, 1987.

[84] Dominique d'Humières. Multiple–relaxation–time lattice boltzmann models in three dimensions. *Philosophical Transactions of the Royal Society of London A: Mathematical, Physical and Engineering Sciences*, 360(1792):437–451, 2002.

[85] Xiaowen Shan, Xue-Feng Yuan, and Hudong Chen. Kinetic theory representation of hydrodynamics: a way beyond the navier–stokes equation. *Journal of Fluid Mechanics*, 550:413–441, 2006.

[86] YH Qian, Dominique d'Humières, and Pierre Lallemand. Lattice bgk models for navier-stokes equation. *EPL (Europhysics Letters)*, 17(6):479, 1992.

[87] Guy R. McNamara, Alejandro L. Garcia, and Berni J. Alder. A hydrodynamically correct thermal lattice boltzmann model. *Journal of Statistical Physics*, 87(5):1111–1121, 1997.

[88] M Sbragaglia, R Benzi, M Bernaschi, and S Succi. The emergence of supramolecular forces from lattice kinetic models of non-ideal fluids: applications to the rheology of soft glassy materials. *Soft Matter*, 8(41):10773–10782, 2012.

[89] Zhaoli Guo, Chuguang Zheng, and Baochang Shi. Discrete lattice effects on the forcing term in the lattice boltzmann method. *Physical Review E*, 65(4):046308, 2002.

[90] Andrew K. Gunstensen, Daniel H. Rothman, Stéphane Zaleski, and Gianluigi Zanetti. Lattice boltzmann model of immiscible fluids. *Phys. Rev. A*, 43:4320–4327, Apr 1991.

[91] Xiaowen Shan and Hudong Chen. Lattice boltzmann model for simulating flows with multiple phases and components. *Phys. Rev. E*, 47:1815–1819, Mar 1993.

[92] Xiaowen Shan and Gary Doolen. Multicomponent lattice-boltzmann model with interparticle interaction. *Journal of Statistical Physics*, 81(1):379–393, 1995.

[93] E. Orlandini, M.R. Swift, and J. Yeomans. A Lattice Boltzmann model of binary-fluid mixtures. *Europhys. Lett.*, 32:463–468, 1995.

[94] A. Tiribocchi, N. Stella, G. Gonnella, and A. Lamura. Hybrid lattice boltzmann model for binary fluid mixtures. *Phys. Rev. E*, 80:026701, Aug 2009.

[95] Xiaoyi He, Shiyi Chen, and Gary D Doolen. A novel thermal model for the lattice boltzmann method in incompressible limit. *Journal of Computational Physics*, 146(1):282–300, 1998.

[96] C. M. Pooley and K. Furtado. Eliminating spurious velocities in the free-energy lattice boltzmann method. *Phys. Rev. E*, 77:046702, Apr 2008.

[97] Charles Hirsch. *Numerical computation of internal and external flows: The fundamentals of computational fluid dynamics*. Elsevier, 2007.

[98] Tim Sanchez, Daniel T N Chen, Stephen J DeCamp, Michael Heymann, and Zvonimir Dogic. Spontaneous motion in hierarchically assembled active matter. *Nature*, 491(7424):431–4, 2012.

[99] Luca Giomi, Mark J Bowick, Prashant Mishra, Rastko Sknepnek, and M Cristina Marchetti. Defect dynamics in active nematics. *Phil. Trans. R. Soc. A*, 372(2029):20130365, 2014.

[100] Amin Doostmohammadi, Michael F Adamer, Sumesh P Thampi, and Julia M Yeomans. Stabilization of active matter by flow-vortex lattices and defect ordering. *Nature communications*, 7, 2016.

[101] Henricus H Wensink, Jörn Dunkel, Sebastian Heidenreich, Knut Drescher, Raymond E Goldstein, Hartmut Löwen, and Julia M Yeomans. Meso-scale turbulence in living fluids. *Proceedings of the National Academy of Sciences*, 109(36):14308–14313, 2012.

[102] Dmitri Volfson, Scott Cookson, Jeff Hasty, and Lev S Tsimring. Biomechanical ordering of dense cell populations. *Proceedings of the National Academy of Sciences*, 105(40):15346–15351, 2008.

[103] Thomas D Pollard and Gary G Borisy. Cellular motility driven by assembly and disassembly of actin filaments. *Cell*, 112(4):453–465, 2003.

[104] Patricia T Yam, Cyrus A Wilson, Lin Ji, Benedict Hebert, Erin L Barnhart, Natalie A Dye, Paul W Wiseman, Gaudenz Danuser, and Julie A Theriot. Actin–myosin network reorganization breaks symmetry at the cell rear to spontaneously initiate polarized cell motility. *J Cell Biol*, 178(7):1207–1221, 2007.

[105] Francis G. Woodhouse and Raymond E. Goldstein. Spontaneous circulation of confined active suspensions. *Phys. Rev. Lett.*, 109:168105, Oct 2012.

[106] Elsen Tjhung, Davide Marenduzzo, and Michael E Cates. Spontaneous symmetry breaking in active droplets provides a generic route to motility. *Proceedings of the National Academy of Sciences*, 109(31):12381–12386, 2012.

[107] Shuang Zhou. *Living Liquid Crystals*, pages 77–92. Springer International Publishing, Cham, 2017.

[108] Pau Guillamat, Jordi Ignés-Mullol, and Francesc Sagués. Control of active liquid crystals with a magnetic field. *Proceedings of the National Academy of Sciences*, 113(20):5498–5502, 2016.

[109] Chenhui Peng, Taras Turiv, Yubing Guo, Qi-Huo Wei, and Oleg D Lavrentovich. Command of active matter by topological defects and patterns. *Science*, 354(6314):882–885, 2016.

[110] Daniel A Fletcher and Phillip L Geissler. Active biological materials. *Annual review of physical chemistry*, 60:469–486, 2009.

[111] Yu-Li Wang. Exchange of actin subunits at the leading edge of living fibroblasts: possible role of treadmilling. *The Journal of cell biology*, 101(2):597–602, 1985.

[112] A. R. Fialho, M. L. Blow, and D. Marenduzzo. Anchoring-driven spontaneous rotations in active gel droplets. *Soft Matter*, pages –, 2017.

[113] Ana S DePina and George M Langford. Vesicle transport: the role of actin filaments and myosin motors. *Microscopy research and technique*, 47(2):93–106, 1999.

[114] Huang Jian-Dong, Scott T Brady, Bruce W Richards, David Stenoien, et al. Direct interaction of microtubule-and actin-based transport motors. *Nature*, 397(6716):267, 1999.

[115] Steven P Gross. Hither and yon: a review of bi-directional microtubule-based transport. *Physical biology*, 1(2):R1, 2004.

[116] David Jacqmin. Calculation of two-phase navier–stokes flows using phase-field modeling. *Journal of Computational Physics*, 155(1):96–127, 1999.

[117] Philippe Poulin, Holger Stark, TC Lubensky, and DA Weitz. Novel colloidal interactions in anisotropic fluids. *Science*, 275(5307):1770–1773, 1997.

[118] TC Lubensky, David Pettey, Nathan Currier, and Holger Stark. Topological defects and interactions in nematic emulsions. *Physical Review E*, 57(1):610, 1998.

[119] Ph Poulin and DA Weitz. Inverted and multiple nematic emulsions. *Physical Review E*, 57(1):626, 1998.

[120] Sriram Ramaswamy and Madan Rao. Active-filament hydrodynamics: instabilities, boundary conditions and rheology. *New Journal of Physics*, 9(11):423, 2007.

[121] Luca Giomi and Antonio DeSimone. Spontaneous division and motility in active nematic droplets. *Phys. Rev. Lett.*, 112:147802, Apr 2014.

[122] Luca Giomi, Mark J Bowick, Xu Ma, and M Cristina Marchetti. Defect annihilation and proliferation in active nematics. *Physical review letters*, 110(22):228101, 2013.

[123] G Foffano, JS Lintuvuori, AN Morozov, K Stratford, ME Cates, and D Marenduzzo. Bulk rheology and microrheology of active fluids. *The European Physical Journal E: Soft Matter and Biological Physics*, 35(10):1–11, 2012.

[124] Allen T. Chwang and T. Yao-Tsu Wu. Hydromechanics of low-reynolds-number flow. part 2. singularity method for stokes flows. *Journal of Fluid Mechanics*, 67(4):787815, 1975.

[125] Kevin Connington and Taehun Lee. A review of spurious currents in the lattice boltzmann method for multiphase flows. *Journal of mechanical science and technology*, 26(12):3857, 2012.

[126] Israel Lazo, Chenhui Peng, Jie Xiang, Sergij V Shiyanovskii, and Oleg D Lavrentovich. Liquid crystal-enabled electro-osmosis through spatial charge separation in distorted regions as a novel mechanism of electrokinetics. *Nature communications*, 5:5033, 2014.

[127] Matthew Blow, Giulio De Magistris, and Davide Marenduzzo. Active anchoring and arrested phase separation in biphasic active nematics. *to be published*.

[128] Alexander Wagner. *Theory and Applications of the Lattice Boltzmann Method*. Ph.D. thesis, University of Oxford, 1997.

[129] B. Yurke, A. N. Pargellis, and N. Turok. Coarsening dynamics in nematic liquid crystals. *Molecular Crystals and Liquid Crystals Science and Technology. Section A. Molecular Crystals and Liquid Crystals*, 222(1):195–203, 1992.

[130] Z Bradač, Samo Kralj, and S Žumer. Early stage domain coarsening of the isotropic-nematic phase transition. *The Journal of chemical physics*, 135(2):024506, 2011.

[131] Matthew Mata, Carlos J García-Cervera, and Hector D Ceniceros. Ordering kinetics of a conserved binary mixture with a nematic liquid crystal component. *Journal of Non-Newtonian Fluid Mechanics*, 212:18–27, 2014.

[132] Adriano Tiribocchi, Raphael Wittkowski, Davide Marenduzzo, and Michael E Cates. Active model h: scalar active matter in a momentum-conserving fluid. *Physical review letters*, 115(18):188302, 2015.

[133] R Voituriez, Jean-François Joanny, and Jacques Prost. Spontaneous flow transition in active polar gels. *EPL (Europhysics Letters)*, 70(3):404, 2005.

[134] J Nehring, AR Kmetz, and TJ Scheffer. Analysis of weak-boundary-coupling effects in liquid-crystal displays. *Journal of Applied Physics*, 47(3):850–857, 1976.